

**STRUCTURAL, PHYSICAL AND OPTICAL
PROPERTIES OF RARE EARTH OXIDES
DOPED CALCIUM PHOSPHATE GLASSES
WITH AND WITHOUT SILVER
NANOPARTICLES**

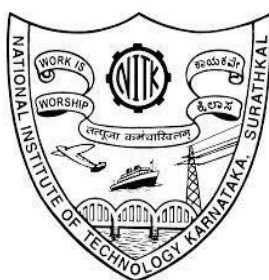
Thesis

Submitted in partial fulfilment of the requirements for the degree of

DOCTOR OF PHILOSOPHY

by

MATHEWOS TULORE DUTEBO



DEPARTMENT OF PHYSICS

**NATIONAL INSTITUTE OF TECHNOLOGY KARNATAKA
SURATHKAL, MANGALORE -575025**

MAY, 2023

**STRUCTURAL, PHYSICAL AND OPTICAL
PROPERTIES OF RARE EARTH OXIDES
DOPED CALCIUM PHOSPHATE GLASSES
WITH AND WITHOUT SILVER
NANOPARTICLES**

Thesis

Submitted in partial fulfilment of the requirements for the degree of

DOCTOR OF PHILOSOPHY

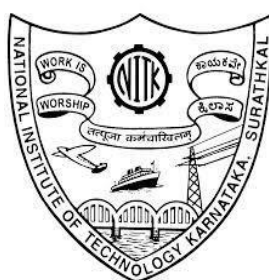
by

MATHEWOS TULORE DUTEBO

(Roll No. 187PH001)

Under the guidance of

Prof. H. D SHASHIKALA



DEPARTMENT OF PHYSICS

**NATIONAL INSTITUTE OF TECHNOLOGY KARNATAKA
SURATHKAL, MANGALORE -575025**

MAY, 2023

DECLARATION

by the Ph.D. Research Scholar

*I hereby declare that the Research Thesis/Synopsis entitled “**STRUCTURAL, PHYSICAL AND OPTICAL PROPERTIES OF RARE EARTH OXIDES DOPED CALCIUM PHOSPHATE GLASSES WITH AND WITHOUT SILVER NANOPARTICLES**”, which is being submitted to the National Institute of Technology Karnataka, Surathkal in partial fulfilment of the requirements for the award of the Degree of Doctor of Philosophy in PHYSICS is a bonafide report of the research work carried out by me. The material contained in this Research Thesis has not been submitted to any University or Institution for the award of any degree.*



Mathewos Tulore Dutebo

(Roll. No.: 187PH001)

Department of Physics

National Institute of Technology Karnataka, Surathkal

Place: NITK – Surathkal

Date: 01-06-2023

CERTIFICATE

This is to certify that the Research Thesis entitled “**STRUCTURAL, PHYSICAL AND OPTICAL PROPERTIES OF RARE EARTH OXIDES DOPED CALCIUM PHOSPHATE GLASSES WITH AND WITHOUT SILVER NANOPARTICLES**” submitted by Mathewos Tulore Dutebo (Register Number:187106PH001) as the record of the research work carried out by him, is accepted as the Research Thesis submission in partial fulfillment of the requirements for the award of the degree of Doctor of Philosophy.

H.D. Shashikala

Prof. H. D. Shashikala

(Research Guide)

Department of Physics

NITK Surathkal - 575025

(Signature)
Chairman – DRPC 21/6/2023

(Signature with Date and Seal)

Dr. N.K. UDAYASHANKAR
PROFESSOR & HEAD
DEPARTMENT OF PHYSICS
NITK SURATHKAL, SRINIVASNAGAR
MANGALORE - 575 025, INDIA

ACKNOWLEDGMENT

I am incredibly grateful to the Almighty God for His kindness, blessing, and provision of the strength, knowledge, health, wisdom, time, and patience necessary for me to complete this research successfully.

I would like to thank my supervisor, Prof. H. D. Shashikala, Department of Physics, NITK Surathkal, for her guidance, suggestions, helpful criticism, and critical examination of this thesis. I also want to thank her for her inspirational leadership, invaluable recommendations, on-going support, and continual encouragement during the research time, all of which have contributed to the success of my research effort.

I would like to use this opportunity to convey my sincere gratitude to my RPAC members, Dr. Partha Pratim Das, Department of Physics, and Dr. Udaya Kumar D., Department of Chemistry, NITK Surathkal, for all the motivation and advice given by them, which filled me with hope in times of hardship during my research life.

I want to extend my sincere gratitude to all the faculty at the Department of Physics at NITK Surathkal, including Prof. Kasturi V. Bangera, Prof. N. K. Udayashankar, Prof. M. N. Satyanarayan, Dr. H. S. Nagaraja, Dr. Ajith K. M, Dr. Deepak Vaid, Dr. T. K. Shajahan, Dr. Kartick Tarafder, and Dr. V. Shreenath, for their insightful discussions and all the assistance for my research and daily activities in the department to be completed successfully, I sincerely appreciate the help and cooperation of the non-teaching staff members of the Department of Physics, Mrs. Ashalatha, Mr. Harshith, Mr. Pradeep S, Mr. Dhanraj, Ms. Namisha, Mrs. Veena, and Mr. Karthik. I express sincere thanks to Prof. Sib Sankar Mal, chemistry Dept for providing FTIR facility.

I especially want to thank my friends and colleagues, Dr. Soumalya B., Dr. Manoj K M, and Dr. Amudha A. Mr. Avinash I. Ms. Rashmi I, Ms. Vasundhara Raghuvanshi, Mr. Mukesh P., Mr. Lakshmi S.G., Mr. Manmohan D., General Temesgen Abose, Dejene Gizaw, Dr. Deselegn Girma., Dr. Utino Worabo, Mr. Kebede Hadaro, Aba W/Meskel G/Yohannis, Mr. Asalif Habtegiyorgis, Dr. Adane Haile, Mr. Birhanu Achamo, Mr. Birhanu Hemure, Mr. Tagese Sawo, Mr. Lombiso Markos, Mr. Temesgen Teshome, and Mr. Temesgen Bafo for all their support and assistance over the years.

I appreciate the financial aid and facilities provided by the Ministry of Education, FDRE, and Wachemo University.

Last but not least, I sincerely want to express my gratitude to my family, especially my parents, Mr. Tulore Dutebo Baje and Mrs. Hundame Achiso Awono, our kids Kalkidan Mathewos and Maereg Mathewos, my dear brothers Abayneh Tulore, Yacob Tulore, and Amanuel Tulore and my sisters Selamawit Tulore and Ayane Tulore for their love and sacrifice, which inspired me to accomplish this goal.

Above all, I owe tremendous gratitude to my beloved wife, Lydia Mathewos Laloto (Lola), for her support, selfless efforts, and inspiration, all of which enabled me to achieve my objectives and become the person I am today. Her whole-hearted support has been the invisible strength that held me together in every challenge of my research and daily life.

Finally, there are too many to list individually, and I would like to thank them for their support and help to all who directly or indirectly contributed to my research and made this happen.

MATHEWOS TULORE DUTEBO

ABSTRACT

This thesis describes the synthesis, optimization and systematic characterization of rare earth (La, Ce, Er, and Eu) doped Calcium phosphate glasses as well as these glasses' incorporation with silver nanoparticles. The high-purity raw ingredients were weighed and mixed according to the molar composition. A series of glass samples in the composition of $50\text{P}_2\text{O}_5-(50-x)\text{CaO}-x\text{REI}$ ($0.0 \leq x \leq 5.0$ mol% and rare earth ions (REI) = La, Ce, and Er), $50\text{P}_2\text{O}_5-(50-x)\text{CaO}-x\text{Er}_2\text{O}_3-4\text{Ag}_2\text{O}-\text{SnO}$ ($0.0 \leq x \leq 5$ mol%) and $50\text{P}_2\text{O}_5-49\text{CaO}-1\text{REI}-4\text{Ag}_2\text{O}-\text{SnO}$ (REI= Eu^{3+} and Er^{3+}) were synthesized using melt-quenching technique and subsequent heat treatment applications. The Taguchi approach of DOE with orthogonal array was used to optimize the process parameters of glass preparation utilizing the melt quenching technique. The impact of rare earth ion addition and co-doping of Silver nanoparticles on the structural, physical, and optical characteristics of calcium phosphate glass were analysed using different techniques. The samples were thoroughly characterized using X-ray diffraction, Density measurements, Transmission electron microscopy (TEM) and SAED, Fourier transform infrared, ultraviolet-visible (UV-Vis) absorption, photoluminescence (PL), FESEM, and EDAX. XRD confirmed the samples' amorphous nature. Utilizing TEM image micrographs and ImageJ software, the average size of AgNPs was estimated to be about 12nm. Its images manifested the nucleation of homogeneously distributed spherical silver (Ag) nanoparticles in the glass matrix. Using Fourier transform infrared (FTIR) spectroscopy, the vibrational mode of these glasses was examined. FTIR spectra revealed the bonding vibrations for P-O bonds, P-O-P linkages, and PO_2 units. The primary metaphosphate glass structure had not been affected by the production or development of silver nanoparticles, according to Fourier-infrared (FTIR) spectroscopy. The absorption spectrum of rare earth oxides doped P_2O_5 -CaO glasses with and without incorporating Ag nanoparticles was analysed for band gap and Urbach energy. The optical properties of glasses containing rare-earth ions and noble-metal nanoparticles were examined to determine whether there were any ways to increase the luminescence efficiency of rare-earth ions.

Keywords: Phosphate glass, Rare earth ions, AgNPs, Melt-quenching technique, Physical, Structural, Optical, Heat treatment, Taguchi method, DOE, optimization

TABLE OF CONTENTS

TABLE OF CONTENTS	i
LIST OF FIGURES	v
LIST OF TABLES	vii
NOMENCLATURE	ix
CHAPTER 1	1
INTRODUCTION	1
1.1 Introduction to glass	1
1.2 Glass Transitions	2
1.3 Glass Formation	4
1.4 Glass components	5
1.5 Types of Glasses	6
1.6 Structure of Phosphate Glasses	7
1.7 Glass Preparation Techniques	10
1.8 Optimization using design of experiments	12
1.9 Special properties of Phosphate glasses	13
1.10 Rare-earth ion-doped glasses containing noble metals	15
1.11 Scope and objective of the research	18
1.11.1 Scope	18
1.11.2 Objectives	20
1.12 Thesis Structure	20
CHAPTER 2	22
MATERIALS AND METHODS	22
Overview	22
2.1 Materials used for glass synthesis in the present study	23
2.2 Experimental procedure	25
2.3 Preparation of CPAS, CPEAS1 and CPASEu1 glasses	28
2.4 Polishing of the Glass samples	29
2.5 Design of experiments for optimization	30
2.5.1 Taguchi Method	32

2.6 Techniques for Glass characterization.....	33
2.6.1 X-ray diffraction study	34
2.6.2 Density and Molar volume	35
2.6.3 Fourier transform infra-red (FTIR) spectroscopy.....	37
2.6.4 Field Effect Scanning electron microscope (FESEM)	38
2.6.5 High Resolution Transmission Electron Microscope (HRTEM)	39
2.6.6 Index of Refraction (n) measurements	40
2.6.7 UV-Vis-NIR/UV-Vis spectrometer	42
2.6.8 Photoluminescence (PL) study	44
2.7 Error Analysis.....	45
2.7.1 Standard Deviation of the Mean (SDOM) Calculation	46
CHAPTER 3	48
INFLUENCE OF (Er ³⁺ , La ³⁺ , Ce ⁴⁺) ADDITIONS ON PHYSICAL AND OPTICAL PROPERTIES OF 50CaO-50P ₂ O ₅ GLASSES	48
Overview	48
3.1 Introduction	49
3.2 Results and discussion	49
3.2.1 XRD Analysis.....	49
3.2.2 Density and Molar volume	51
3.2.3 Refractive Index and Metallization Criteria	55
3.2.4 Physical Parameters.....	56
3.2.5 FTIR studies	57
3.2.6 UV-Vis spectroscopy study	62
3.3 Conclusions	64
CHAPTER 4	65
STATISTICAL OPTIMIZATION OF MELT-QUENCHING PROCESS PARAMETERS OF RARE-EARTH IONS DOPED CALCIUM PHOSPHATE GLASSES USING TAGUCHI METHOD	65
Overview	65
4.1 Introduction	65
4.2 Results and discussion	66
4.2.1 X-ray Diffraction study	66

4.2.2 Application of Design of experiment (DOE) Taguchi Method to glasses synthesized as L ₉ orthogonal array	67
4.2.3 Melt-quenching process parameter statistical optimization	69
4.3 Conclusions	76
CHAPTER 5	77
EFFECT OF RARE EARTH ION DOPING ON THE PHYSICAL, STRUCTURAL AND OPTICAL PROPERTIES OF SILVER OXIDE-CONTAINING CALCIUM PHOSPHATE GLASSES	77
Overview	77
5.1 Introduction	78
5.2 Results and discussion	78
5.2.1 X-ray diffraction study	78
5.2.2 Density and molar volume.....	79
5.2.2.2 Physical Parameters	80
5.2.3 Refractive index and Metallization criterion	83
5.2.4 Metallization criterion	84
5.2.5 FTIR Analysis.....	84
5.2.6 UV–Vis spectroscopy	87
5.2.6.1 Optical band gap and Urbach energy	89
5.2.7 EDAX analysis	91
5.3 Conclusion	92
CHAPTER 6	93
THE EFFECT OF HEAT TREATMENT ON THE STRUCTURAL AND OPTICAL CHARACTERIZATION OF SILVER NANOPARTICLES EMBEDDED IN RARE EARTH (ERBIUM, EUROPIUM) ION DOPED CALCIUM PHOSPHATE GLASSES	93
Overview	93
6.1 Introduction	93
6.2 Results and discussion	94
6.2.1 X-ray diffraction study	94
6.2.2 Energy Dispersive X-ray analysis (EDAX) of heat treated samples.....	95
6.2.3 Physical Properties	96
6.2.4 The impact of various heat treatment times on structural investigations	97

6.2.4.1 FTIR Analysis.....	97
6.2.4.2 HRTEM Analysis	100
6.2.4.3 Particle Size of CPEAS1 as a function of duration of heat treatment	101
6.2.5 Photoluminescence (PL) studies.....	102
6.3 Conclusion	104
CHAPTER 7	106
SUMMARY AND CONCLUSIONS	106
7.1 Summary and conclusions	106
7.2 Future work's scope	108
Lists of Publications, International conferences, and Workshop attended	110
Bibliography.....	111

LIST OF FIGURES

1.1	<i>Temperature effect on the Enthalpy of glass-forming melt (Shelby 2020)</i>	3
1.2	<i>Phosphate glass formations with a basic phosphate tetrahedron(Brauer 2012)</i>	8
1.3	<i>Polymerisation of the phosphate anion giving rise to various polyphosphate anions linked via (a) oxygen bridges which may be linear or branched (b) a combination of the both (Brow 2000)</i>	9
1.4	<i>The corresponding structure of a phosphate glass network is typically classified under the Q^n terminology(Brauer 2012; Brow 2000)</i>	10
2.1	<i>Flow chart of the preparation and characterization of CPRE and CPEAS glasses</i>	26
2.2	<i>Furnace used for glass preparation</i>	27
2.3	<i>Images of synthesized glasses of CPEAS system</i>	27
2.4	<i>Flow chart of sample Preparation of heat treatment and characterization of CPAS, CPEAS1, and CPASEu1</i>	29
2.5	<i>The image of the synthesized CPASEu1 series</i>	29
2.6	<i>Polishing machine employed in the polishing of glass samples</i>	30
2.7	<i>Raigaku Miniflex 600 X-ray diffractometer</i>	35
2.8	<i>Microbalance with density kit</i>	36
2.9	<i>FTIR Spectrometer (Bruker ALPHA-200952 Spectrometer)</i>	38
2.10	<i>FESEM [7610FPLUS, Jeol, Japan] microscope, CRF-NITK</i>	39
2.11	<i>Abbe refractometer</i>	41
2.12	<i>UV-Vis-NIR spectrometer (from Central research Facility, NITK) [Lambda 950, Perkin Elmer, Singapore]</i>	44
2.13	<i>Fluoromax-4 Photoluminescence spectrometer (PL)</i>	45
3.1(a)	<i>XRD pattern of the prepared samples of $50P_2O_5 - (50 - x) CaO-xLa_2O_3$ ($x = 0, 1, 2, 3,$ and 5 mol. %)</i>	49
3.1(b)	<i>XRD pattern of the prepared samples of $50P_2O_5 - (50 - x) CaO-xCeO_2$ ($x = 0, 1, 2, 3,$ and 5 mol. %)</i>	50
3.1(c)	<i>XRD pattern of the prepared samples of $50P_2O_5 - (50 - x) CaO-xEr_2O_3$ ($x = 0, 1, 2, 3,$ and 5 mol. %)</i>	50
3.2(a)	<i>Variation of the density and molar volume of glasses in relation to the amount of La_2O_3</i>	54
3.2(b)	<i>Variation of the density and molar volume of glasses in relation to the amount of CeO_2</i>	54
3.2(c)	<i>Variation of the density and molar volume of glasses in relation to the amount of Er_2O_3</i>	55
3.3(a)	<i>The FTIR spectra of $50P_2O_5- (50-x)CaO-xLa_2O_3$ glasses</i>	59
3.3(b)	<i>The FTIR spectra of $50P_2O_5- (50-x)CaO-xCeO_2$ glasses</i>	59
3.3(c)	<i>The FTIR spectra of $50P_2O_5- (50-x)CaO-xEr_2O_3$ glasses</i>	60
3.4	<i>The UV-Vis spectra of $50P_2O_5- (50-x)CaO-xLa_2O_3$ glasses (a) absorbance and (b) optical band gap energy obtained from Tauc plots</i>	63
3.5	<i>The UV-Vis spectra of $50P_2O_5-(50-x)CaO-xCeO_2$ glasses (a) absorbance and (b) optical band gap energy obtained from Tauc plots</i>	63

3.6	<i>The UV-Vis spectra of 50P₂O₅- (50-x)CaO-xEr₂O₃ glasses (a) absorbance and (b) optical band gap energy obtained from Tauc plots</i>	64
4.1	<i>Patterns of X-ray diffraction in (a) La³⁺ doped and (b) Ce⁴⁺ doped samples prepared for optimization</i>	67
4.2(a)	<i>Main effects plots for Signal-Noise ratio of the density of Lanthanum oxide doped glass</i>	72
4.2(b)	<i>Main effects plots for Signal-Noise ratio of the density of Cerium oxide doped glasses</i>	73
5.1	<i>e Patterns of X-ray diffraction in samples 50P₂O₅-(50-x) CaO-xEr₂O₃-4Ag₂O-4SnO where x=0, 0.5, 1, 1.5, 2.5 and 5mol%</i>	78
5.2	<i>Density and Molar volume of the 50P₂O₅-(50-x) CaO-xEr₂O₃-4Ag₂O-4SnO where x=0, 0.5, 1, 1.5, 2.5 and 5mol%</i>	80
5.3	<i>Inter-ionic distance and field strength variations in glasses as a function of Er₂O₃ concentration</i>	82
5.4	<i>FTIR (Fourier Transform Infrared) spectra of the investigated glass system 50P₂O₅-(50-x) CaO-xEr₂O₃-4Ag₂O-4SnO with (x=0 to 5mol%)</i>	86
5.5	<i>UV-Vis Absorbance of Erbium oxide doped CPAS system</i>	89
5.6	<i>Tauc plot of direct bandgap energy of CPAS, CPEAS.5, CPEAS1, CPEAS1.5, CPEAS2.5, and CPEAS5.</i>	90
5.7	<i>The urbach energy diagram of investigated glass system system 50P₂O₅-(50-x) CaO-xEr₂O₃-4Ag₂O-4SnO with (x=0 to 5mol%)</i>	91
5.8	<i>The EDAX spectrum of CPEAS1 glass</i>	92
6.1	<i>X-ray diffraction patterns of samples CPAS, CPEAS1, and CPASEu1 without heat treatment</i>	95
6.2	<i>The EDAX spectrum of CPEAS1-3 glass</i>	95
6.3(a)	<i>Fourier transforms infrared (FTIR) transmittance spectra of the CPE1, CPEAS1-0, CPEAS1-10, and CPEAS1-25 glasses</i>	98
6.3(b)	<i>Fourier transforms infrared (FTIR) transmittance spectra of the CPEu1, CPASEu1-0, CPASEu1-10, and CPASEu1-25 glasses</i>	98
6.4	<i>The CPEAS-50 (a) TEM micrograph (b) Different silver nanoparticle planes are shown in the SAED pattern (c) average particle distribution histogram (d) high crystallinity of the silver nanoparticles as shown by a magnified image.</i>	101
6.5	<i>HRTEM images of of CPEAS1-3 (b) Histogram of nano particle distribution of CPEAS1-3 (c) TEM image of CPEAS1-10, (d) Particle size distribution of nanoparticles in CPEAS1-10, (e) HRTEM image of CPEAS1-50, (f) shows the size distribution of nanoparticles, of CPEAS1-50 glass samples.</i>	102
6.6	<i>Photoluminescence (PL) spectra of the CPE1, CPEAS1-3, CPEAS1-25, and CPEAS1-50 glasses</i>	103
6.7	<i>Photoluminescence (PL) spectra of the CPEu, CPASEu1-0, CPASEu1-3, CPASEu1-10, CPASEu1-25, and CPASEu1-50 glasses</i>	104

LIST OF TABLES

1.1	<i>A summary of Rare earth elements selected for the current work</i>	16
2.1	<i>Chemicals used in the present study</i>	23
2.2	<i>Batch composition of 50P₂O₅-(50-x) CaO- xREI (REI = La³⁺, Ce⁴⁺, and Er³⁺) glasses</i>	24
2.3	<i>Effect of Erbium Concentrations on Calcium Phosphate glasses with Silver and Tin oxide</i>	24
2.4	<i>Effects of heat treatment on rare earth ion (Eu³⁺, Er³⁺) doped Calcium Phosphate glasses with Silver and Tin oxide</i>	25
2.5	<i>Process parameters used in the experiment</i>	32
2.6	<i>Taguchi L₉ Orthogonal arrays of (La³⁺, Ce⁴⁺) doped Phosphate glass samples</i>	33
3.1(a)	<i>Density (ρ), Molar volume (V_m), Band gap Energy (E_{opt}) and Refractive Index (n) of 50P₂O₅ - (50 - x) CaO-xLa₂O₃ (x = 0, 1, 2, 3, and 5 mol. %)</i>	52
3.1(b)	<i>Density (ρ), Molar volume (V_m), Band gap Energy (E_{opt}) and Refractive Index (n) of 50P₂O₅ - (50 - x) CaO-xCeO₂ (x = 0, 1, 2, 3, and 5 mol. %)</i>	53
3.1(c)	<i>Density (ρ), Molar volume (V_m), Band gap Energy (E_{opt}) and Refractive Index (n) of 50P₂O₅ - (50 - x) CaO-xEr₂O₃ (x = 0, 1, 2, 3, and 5 mol. %)</i>	53
3.2	<i>Ion Concentration (N), Inter-nuclear distance (r_i), Polaron radius (r_p), Field Strength (F), and Metallicity Factor (M) of sample 50P₂O₅ - CaO-REI (where REI= La, Ce, Er)</i>	57
3.3	<i>The FTIR spectra peaks of CP, La-doped, Ce-doped, and Er-doped glass samples with band assignments</i>	61
4.1	<i>Melt-quenching Process parameters used in the experiment</i>	68
4.2	<i>S/N ratio and mean values of a measured density of (La³⁺, Ce⁴⁺) doped Phosphate glass</i>	70
4.3(a)	<i>Response table for Signal- to- Noise(S/N) ratio for larger is better characteristics of Lanthanum oxide doped sample</i>	70
4.3(b)	<i>Response table for Signal- to- Noise(S/N) ratio for larger is better characteristics of Cerium oxide doped sample</i>	71
4.4(a)	<i>Response table for means of density of Lanthanum oxide doped</i>	72
4.4(b)	<i>Response tables for means of density of Cerium oxide doped</i>	72
4.5	<i>Analysis of Variance (ANOVA) for Transformed Response</i>	74
	<i>a) Lanthanum oxide doped glasses and</i>	
	<i>b) Cerium oxide doped glasses</i>	75
4.6	<i>optimized process parameters and the corresponding density values</i>	76
5.1	<i>Molecular mass, Density (ρ), Molar Volume, Ion Concentration(N_{Er}), Polaron radius (r_p), Inter ionic distance (r_i), Field Strength(F), Index of refraction, and Metallicity Factor (M_c) of the investigated glasses</i>	81
5.2	<i>The FTIR spectra bands of CP, CPAS, CPEAS1, CPEAS2.5, and CPEAS5 glass samples with band assignments</i>	87
5.3	<i>Absorption Transitions (From the Ground State, ⁴I_{15/2}) in CPEAS5</i>	88
5.4	<i>Indirect Band gap Energy and urbach energy of synthesized glasses</i>	90
6.1	<i>The sample code and composition of Erbium oxide and Europium oxide doped glasses</i>	94
6.2(a)	<i>Density (ρ) and Refractive Index (n) of 50P₂O₅ - 49 CaO-1Er₂O₃-</i>	96

	<i>4Ag₂O-4SnO (heat treated at 0, 3, 10, 25, and 50hr)</i>	
6.2(b)	<i>Density (ρ) and Refractive Index (n) of 50P₂O₅ - 49 CaO-1Eu₂O₃- 4Ag₂O-4SnO (heat treated at 0, 3, 10, 25, and 50hrs)</i>	97
6.3(a)	<i>The FTIR spectra peaks of CPE1, CPEAS1-0, CPEAS1-10, and CPEAS1-25 glass samples with band assignments</i>	99
6.3(b)	<i>The FTIR bands of CPE1u, CPASEu1-0, CPASEu1-10, and CPASEu1-25 glass samples with band assignments</i>	99

NOMENCLATURE

A°	Angstrom
$^\circ\text{C}$	Degree Celsius
h	Planck's constant
Ag	Silver
Ag_2O	Silver(I) oxide
Al_2O_3	Aluminum oxide
ANOVA	Analysis of variance
As	Arsenic
As_2O_3	Arsenic trioxide
B_2O_3	Boron trioxide
Ba	Barium
BaO	Barium oxide
Bi_2O_3	Bismuth(III) oxide
Ca	Calcium
CaF_2	Calcium fluoride
CaO	Calcium oxide
CaCO_3	calcium carbonate
Cc	cubic centimeter
DOE	Design of experiments
DOF	Degree of freedom
DTA	Differential thermal analysis
EDAX	Energy dispersive analysis of X-ray spectroscopy
etc.	et cetera
FTIR spectroscopy	Fourier transform infrared spectroscopy
FWHM	Full-width at half-maximum
gm	Gram
Ga_2O_3	Gallium(III) oxide

Ge	Germanium
GeO ₂	Germanium dioxide
h	Hour
r _p	Polaron radius
F	Field Strength
r _i	Inter-nuclear distance
N _{Er}	Erbium ion Concentration
ρ _s	Density of Sample
M _c	Metallicity Factor
N	Ion Concentration
α	electronic polarizability
ASTM	The American Society for Testing and Materials
IR	Infrared
KBr	Potassium bromide
m	Meter
Min	Minute
N	Newton
N _A	Avogadro's number
NH ₄ H ₂ PO ₄	Ammonium dihydrogen phosphate
P ₂ O ₅	Phosphorus pentoxide
PL	Photoluminescence spectroscopy
s	Second
SAED	Selected area electron diffraction
Sb	Antimony
Sb ₂ O ₃	Antimony trioxide
SDOM	Standard deviation of the mean
SEM	Scanning electron microscopy
SeO ₂	Selenium dioxide
Si	Silicon
SiO ₂	Silicon dioxide

SnO	Tin(II) oxide
SPR	Surface plasmon resonance
T_g	Glass transition temperature
T_m	Melting temperature
T_x	Onset crystallization temperature
TEM	Transmission electron microscopy
TeO_2	Tellurium dioxide
TGA	Thermogravimetric analysis
UV	Ultraviolet
V	Volt
V_2O_5	Vanadium(V) oxide
V- P_2O_5	Vitreous phosphorus pentoxide
Er_2O_3	Erbium Oxide
La_2O_3	Lanthanum Oxide
Eu_2O_3	Europium Oxide
CeO_2	Cerium Oxide
DF	Degree of Freedom
REI	Rare earth ions

CHAPTER 1

INTRODUCTION

1.1 Introduction to glass

Glass is an amorphous substance that has existed in many forms for thousands of years and has been made for human use since 12,000 BC (Shelby 2020; Varshneya and Mauro 2019b; Zanotto and Mauro 2017a). The American Society for Testing and Materials (ASTM) defines 'Glass as an inorganic fusion product cooled to a rigid state without crystallization' (Yamane and Asahara 2000).

Glass is a substance that may be produced in various ways and can be inorganic, organic, or metallic. Although not all amorphous solids are glasses, they are all amorphous solids. Glasses frequently have an unstable structural environment that lacks long-range order. Even though a liquid's atoms or molecules might undergo considerable displacements, glass only experiences thermal vibrations at an average constant position (Shelby 2020; Varshneya and Mauro 2019d).

Glass belongs to the oldest artificial material in the history of humankind. From glass windows and containers to lenses and optical fiber, glass has been proven to be essential material for developing modern human civilization. It has also been the focus of intensive current research since the positive influence of glass on our world continues to grow as new glass products and processes developed to address global challenges in energy, the environment, health care, information/communication technology, etc. (Varshneya and Mauro 2019b). Glasses now play an increasingly important role in modern technology, which enters into increasingly sophisticated applications in high-tech devices that include lasers, optical fiber communications, energy conversions, optoelectronics, medicine, etc., due to the indelible impact of glass on modern society (Morse and Evenson 2016).

Optically transparent composite materials research has grown in importance due to modern technological applications (Shelby 2020; Venkateswara Rao and Shashikala 2015; Yamane and Asahara 2000). Optical materials such as glasses, which have excellent optical transmission range from visible to infrared wavelength areas, have

aroused a lot of interest in the disciplines of lasers, optoelectronics, telecommunication, remote sensing, and wave guiding. They surpass other materials due to several unique features, including excellent optical transparency, compositional flexibility, structural rigidity, and adaptability to property tailoring. These characteristics of glasses enable the incorporation of nanoparticles of various crystals, metals, semiconductors, oxides, and other materials into glass matrices, resulting in a wide range of glass composites with novel yet unknown properties(Varshneya 2013).

Glasses have significant properties such as the ability to accommodate various types of dopants, such as rare earth ions, transition metal ions, metal nanoparticles, etc. A foreign atom can easily find a place to occupy inside the glass because of its random network structure. Glass can be made with excellent homogeneity in various forms and sizes, from tiny fibers to meter-sized pieces. Furthermore, it can be doped with rare-earth ions and micro crystallites, and a wide range of properties can be chosen to meet the needs of various applications(Yamane and Asahara 2000).

Despite its long history, glass continues to be one of the most intriguing inorganic materials science topics to research. Glass has a long and distinguished past and a promising future. It is a significant material in many applications due to its remarkable characteristics and adaptability(Kohli et al. 2022).

1.2 Glass Transitions

The progressive and reversible change in an amorphous material's condition as the temperature rises from a rigid, somewhat brittle "glassy" state to a fluid or rubbery one is known as the glass transition(Shelby 2020; Varshneya and Mauro 2019c). Glass is an amorphous substance that shows the glass transition. Vitrification is the reverse transition, accomplished by super-cooling a viscous liquid into the glass state. Alternatively, the glass transition (or transformation) range is the temperature range during which a given system gradually converts from a supercooled liquid state to a glassy one as it cools(Varshneya 2013; Zanotto and Mauro 2017b). A glass with an irregular atomic arrangement over a long distance has higher configuration entropy and thus more free energy than a crystalline material of the same composition. In other words, glass is a thermodynamically metastable material that cannot be changed

to its most stable state because of atomic rearrangement impediment during the glass formation process. As the temperature is raised, amorphous materials gradually shift from a complex and moderately brittle "glassy" state to a viscous or rubbery state (Shelby 2020; Varshneya and Mauro 2019d; Yamane and Asahara 2000). Figure 1.1 shows the dependence of Enthalpy on temperature. Metals are crystalline, so they have a well-defined melting temperature, but amorphous substances like glass don't have a sharp melting temperature. Instead, they have a range of temperatures (from glass transition temperature, T_g to melting temperature, T_m) over which they melt. The range of temperatures at which this glass transition takes place is defined by the material's glass-transition temperature T_g . If a crystalline form of the material exists, it is always lower than the melting point, T_m . The reversible transformation from a glass to a viscous liquid also takes place if the glass is heated to a temperature above T_g (Yamane and Asahara 2000).

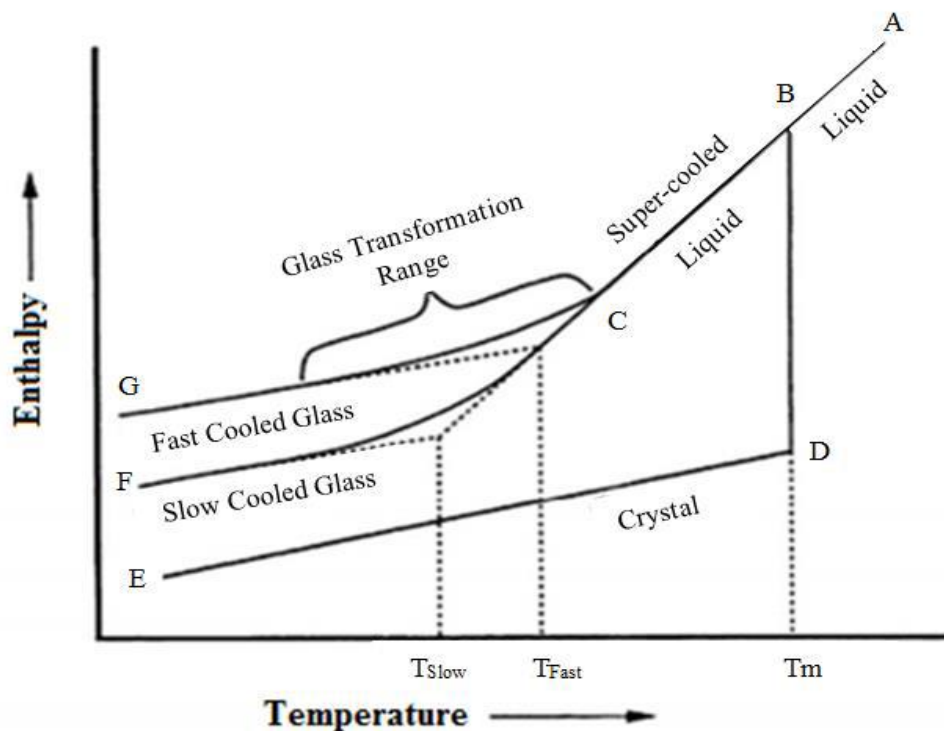


Figure 1.1 Temperature effect on the Enthalpy of glass-forming melt (Shelby 2020)

The effect of cooling rate on glass formation is illustrated in this enthalpy-temperature diagram depicting the creation of crystalline and glassy materials. The glass transition occurs due to an increase in viscosity, and the growth rate in viscosity

depends on the cooling rate, so T_g is not the same for the glass of the same chemical composition. Rather it depends on the cooling rate, too (Shelby 2020; Varshneya and Mauro 2019d). So rapid cooling causes a quick increase in viscosity and results in a glass transition at a higher temperature.

Compared to silicate and borate based glasses, alkaline earth phosphate glasses have better thermal expansion coefficients, lower glass transition temperatures, and higher electrical conductivities, making them significant materials for technology (Velli et al. 2005). Liang and his colleagues synthesized glasses containing calcium metaphosphate and lanthanum using the traditional melt quench technique and found that glass transition temperature T_g of the samples in the region 540°C – 557°C (Liang et al. 2011). Similarly in another research work the glass transition temperature measured by using differential scanning calorimeter (DSC), T_g values of alkaline earth metaphosphate glasses were reported to be in the region of 470 to 540°C (Parsons 2021).

1.3 Glass Formation

Oxides were divided into glass formers and non-glass formers by Zachariasen (1932). Glass production necessitates the creation of a vitreous network. As a result, Zachariasen studied the structural configurations that could result in such a network. Structural Theories of Glass Formation are lumped together theories based on the type of chemical bonding and the shape of the structural unit (Shelby 2020). Random network theory was proposed by Zachariasen and consisted of four fundamental laws that an oxide must follow to create a glass.

- i) An oxygen atom can only be connected to two cations at a time.
- ii) Cations must be surrounded by a limited number of oxygen atoms (3 or 4).
- iii) The oxygen polyhedra share corners, not edges or faces, with one another.
- iv) If the network is three-dimensional, at least three corners in each oxygen polyhedron must be shared.

The formation of complicated oxide glasses defied the criteria mentioned above. As a result, Zachariasen tweaked the original principles to account for the creation of glasses containing non-glass producing oxides. The following are the updated rules:

- i) A large fraction of cations surrounded by oxygen triangles or tetrahedral should be present in the material.
- ii) Only the corners of polyhedra connect them.
- iii) Some oxygen atoms establish just two bonds with these cations and do not create further connections with other cations.

According to the above statements, sufficient network cations must be present to build a continuous structure. Because a network is an open structure, there must be enough bonds connecting the network polyhedra to make a continuous network structure. Glass-forming cations or other cations that can substitute isomorphically may be present. Any cation that isn't glass-producing is referred to as a network modifier. They introduce non-bridging oxygen into the completely connected continuous random network structure. Zachariassen's model was well-received and helped to explain the formation of oxide glasses. However, the discovery of glasses with no oxygen, such as chalcogenide glasses, glassy metals, and heavy metal fluoride glasses, changed the information about how glass was formed. Because processing techniques were used to control the formation of these glasses, kinetics of formation became crucial. As a result, the Kinetic Theory of Glass Formation was used to explain the formation of non-oxide glasses (Shelby 2020; Yamane and Asahara 2000).

1.4 Glass components

Commonly studied oxides in glasses are classified as

- i) Glass former
- ii) Network modifiers
- iii) Intermediate

Glass formers

SiO_2 , P_2O_5 , GeO_2 , B_2O_3 , and As_2O_3 are all oxides that can easily form glasses on their own. These oxides form the interconnected backbone of the glass network. They are known as network formers (Brow 2000; Shelby 2020; Yamane and Asahara 2000). They have random networks with well-defined oxygen coordination polyhedral.

Network modifiers

They are present as ions to alter the glass network and are compensated by non-bridging oxygen (NBO) in oxide glasses, and usually reduce glass network connectivity(Brauer and Möncke 2016). The oxides BaO, CaO, MgO, ZnO, Al₂O₃, and B₂O₃ are examples of modifiers.

Intermediate

The oxides such as TeO₂, SeO₂, MoO₃, WO₃, Bi₂O₃, Al₂O₃, Ga₂O₃, and V₂O₅ can function as network formers or modifiers depending on glass composition and are known as intermediates or conditional glass formers, as they do not form glasses on their own(Yamane and Asahara 2000). Still, they can be made into glasses by melting with a suitable oxide.

1.5 Types of Glasses

Depending on the network former used, glasses can be classified as silicate, borosilicate, aluminosilicate, borate, phosphate glasses, chalcogenide glasses, etc. Large varieties of glasses are obtained by varying the composition of the batch. They are

i) Chalcogenide glasses, ii) Halide and oxy-Halide glasses, iii) Oxide glasses(Shelby 2020; Yamane and Asahara 2000)

Oxide Glasses

Silicate Glasses

Silicate glasses are commercially essential and extensively studied in oxide glass systems. In silicate glasses, SiO₂ is the glass former(Brauer and Möncke 2016). Due to their chemical and weathering stability, these glasses have plenty of applications in the semiconductor industry, photolithography, and optoelectronic devices.

Borate Glasses

Borate glasses consist of BO₃ triangles and BO₄ tetrahedra, which are formed by combining alkali, alkaline earth oxides, etc.(Brauer and Möncke 2016; Varshneya

2013). They show high compatibility with rare-earth elements, the most crucial feature of borate glasses for application in optical and optoelectronic fields. Borate glasses have also been used widely as solder glasses for glass-to-glass and glass-to-ceramic bonding because of their low softening point.

Phosphate Glasses

The network former in phosphate glass is P_2O_5 (Brow 2000; Huang and Jiang 2022:2). Phosphate glasses consist of P-O-P chains of four-fold coordinated phosphorous (Brauer and Möncke 2016; Hoppe 1996). Crystalline P_2O_5 exists in sheet form at low temperatures and in molecular form P_4O_{10} at high temperatures.

Phosphorous oxide (P_2O_5) is a glass-forming oxide free of additives. P_2O_5 is, however, a very hygroscopic molecule, which has historically hampered the manufacturing of phosphate glasses (Brow 2000; Mountjoy 2022; Shelby 2007). The ability to produce stable phosphate glasses requires the proper addition of either a network modifier or another network former. Certain cations find the phosphate network an excellent host, resulting in great consequences. Phosphate glasses can have significant rare earth concentrations, which gives them unique feature.

Phosphate glasses are one of the most common types of oxide glasses, and the cation P^{5+} forms them. Even though the silicate and borosilicate glass families are the most studied and produced, the phosphate glass family is of tremendous scientific and technical importance for specific applications. Phosphate glasses for lasers, biological applications, and nuclear waste vitrification are just a few examples (Mountjoy 2022).

The phosphate glass network is dominated by a pattern of the linkages between the PO_4 tetrahedra (Brow 2000). In the case of vitreous P_2O_5 , these groups are connected to adjacent units by three of their four vertices; one place is occupied by a terminal, double-bonded oxygen atom (DBO). Adding metal oxide leads to depolymerization of the network with oxygen atoms breaking the P-O-P links. The present work will be on Phosphate glasses.

1.6 Structure of Phosphate Glasses

Glasses and other noncrystalline solids differ structurally from crystalline solids in that they lack the periodicity, symmetry, and long-range order that constitute

crystalline solids(Presti et al. 2022). Phosphate glasses, like silicate glasses, have no long-range order or substantial symmetry in their atomic arrangement but exhibit short-range order(Brauer 2012; Hoppe 1996; Varshneya 2013). As figure 1.2 shows, P_2O_5 is the glass-forming component in phosphate glasses. The orthophosphate (PO_4^{3-}) tetrahedron, a phosphorus atom surrounded by four oxygen atoms, is the basic unit in the phosphate glass structure. Only the three other oxygen atoms can operate as 'bridges' to other orthophosphate tetrahedra because one of the oxygen atoms is connected to the phosphorus atom by a double bond. Covalent P-O-P bonds can connect individual orthophosphate tetrahedra by building such bridges. Bridging oxygens are the oxygens found in these P-O-P connections. As a result, orthophosphate tetrahedra can be organized into chains, rings, or networks.

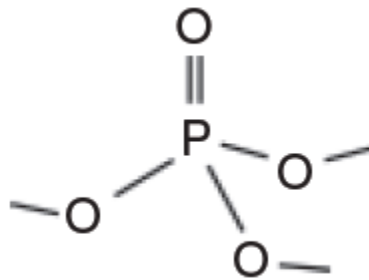


Figure 1.2 Phosphate glass formations with a basic phosphate tetrahedron(Brauer 2012)

Phosphate glasses are cross-linked and chain-like structures similar to a network of polymer chains. They are generally considered to be polymeric. However, these chains are much shorter than those of organic polymers. Furthermore, an alkali metal cation aids in network formation(Brow 2000; Zachariasen 1932).

A fundamental work by Zachariasen (1932) introduced the theory of phosphate glass structure. This study describes phosphate glasses as composed of a three-dimensional structural network produced by the reaction of glass-forming phosphorus pentoxide (P_2O_5) compounds.

Figure 1.3 Represents a three-dimensional random network of covalently bonded P-tetrahedrons for a simple vitreous P_2O_5 glass (v- P_2O_5) as described by Zachariasen(Zachariasen 1932)

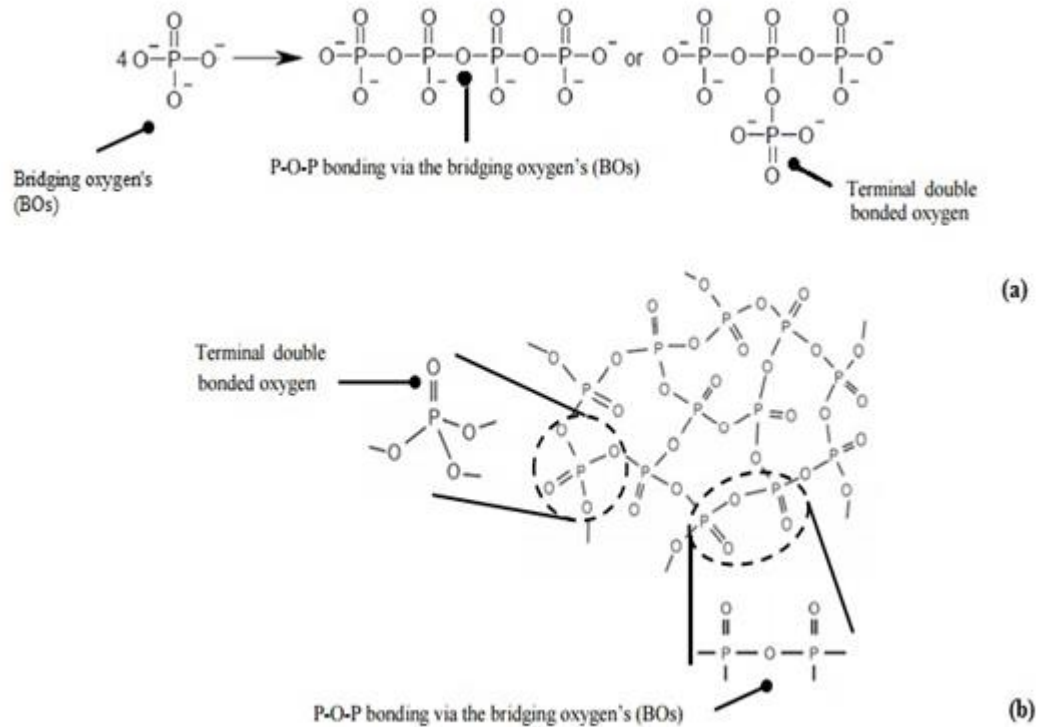


Figure 1.3 Polymerisation of the phosphate anion giving rise to various polyphosphate anions linked via (a) oxygen bridges which may be linear or branched (b) a combination of the both (Brow 2000).

The corresponding structure of a phosphate glass network is typically classified under the Q^n terminology, where n represents the number of bridging oxygens (BOs) per tetrahedron (Figure 1.4). This terminology was initially devised for silicon glasses but has been applied to phosphates.

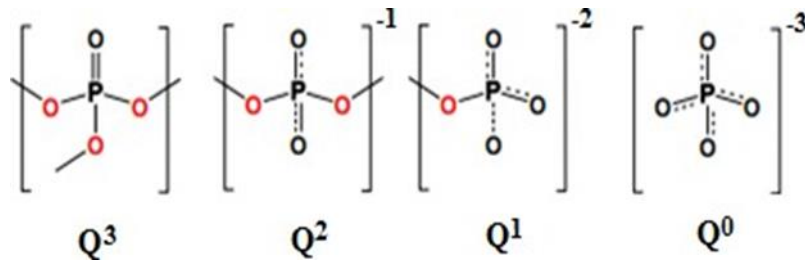


Figure 1.4 The corresponding structure of a phosphate glass network is typically classified under the Q^n terminology (Brauer 2012; Brow 2000)

Depending on the $[O]/[P]$ ratio set by glass composition, phosphate glasses can have a variety of structures ranging from a cross-linked network of Q^3 tetrahedra (vitreous P_2O_5) to polymer-like metaphosphate chains of Q^2 tetrahedra to invert glasses based on small pyro- Q^1 and orthophosphate (Q^0) anions (Brow 2000).

In a pure P_2O_5 system, the glass is a 3-dimensional network of branching Q^3 units with three bridging oxygen atoms and one doubly bonded oxygen per tetrahedral unit. The addition of modifying alkali or alkaline earth cations replaces Q^3 units with Q^2 units, the cations creating ionic cross-links between the phosphate units. At a P_2O_5 concentration of approximately 50 mol%, the Q^3 units disappear, and the structure consists of only Q^2 units in the form of linear phosphate chains. Further addition of modifying cations at concentrations greater than 50 mol% begins to convert Q^2 units to Q^1 units and finally Q^0 units (Brow 2000; Hoppe 1996).

1.7 Glass Preparation Techniques

There are different techniques used to prepare materials in an amorphous state. Three commonly used methods are:

- i) **melt quenching**
- ii) chemical vapor depositions (CPD), and
- iii) sol-gel process

Melt-quenching process

The melting-quenching technique is a standard glass preparation technology. More than 90% of practical glasses in both volume and number of types are prepared by the melt-quenching process (Murugasen, Sagadevan, and Shajan 2015; Shelby 2020; Varshneya and Mauro 2019d).

A batch mixture is prepared by precisely weighing and thoroughly mixing calculated amounts of fine powdered crystalline raw materials to get glasses with the desired property. After that, the initial powders are melted in a high-temperature furnace under room temperature in a suitable crucible (silica, alumina or platinum, etc.) and then quenched in hot metal moulds in air or water. The formed glass sample is then annealed near the glass transition temperature to remove any thermal stresses developed during the formation due to the low thermal conductivity of the glass. The advantages of the melt–quenching technique compared to the other methods are:

- i) The high flexibility of the geometry of a glass - It is advantageous in obtaining material of large size required for the preparation of glasses with unique properties
- ii) The large flexibility of composition- Preparation of glasses with a wide variety of compositions consisting of several constituents at various ratios is possible because simple melt quenching does not require stoichiometry among constituents. The doping or co-doping of active ions like rare-earth or transition metal at a few percent or less is possible, which is essential for producing glasses with unique properties.
- iii) The production process is simple, the technology is relatively mature and reliable, the cost is low, the types of noble metal introduced into the glass are varied (salt, acid, oxidate, halide, sulfide, etc.), and the prospect of industrialization is very bright(Shelby 2020; Yamane and Asahara 2000).

The melt-quenching method has some disadvantages, like difficulty in preparing glasses of ultra-high purity. Phosphate glasses often melt at lower temperatures than bioactive silicate glasses, between 800°C to 1300°C, depending on the glass's composition. When the material has completely melted, it is immediately quenched between two metal plates or poured into water to cool(Brauer 2012; Murugasen et al. 2015).

Recently, a large number of researchers(Alqarni et al. 2020; A.V. et al. 2018a, 2019a; Bhattacharya and Shashikala 2018; Du et al. 2022; Jiménez 2016; Lysenko et

al. 2006; Mrabet, Cherbib, and Khattech 2020:22202; Narayanan and Shashikala 2015a; Shakhgildyan et al. 2022) have synthesised oxide glasses (phosphate, silicate, and borate) utilising the melt-quenching approach for a variety of applications.

1.8 Optimization using design of experiments

Optimizing process factors that directly or indirectly affect material properties can lead to the development of outstanding material properties (Montgomery 2017). Taguchi's Design of Experiment (DOE) is a statistical approach created by Genichi Taguchi (1980s) (Narayanan and Shashikala 2014; Narayanan, Shashikala, and Manjaiah 2015) to improve product quality by reducing variation in a process through a robust design. Design of Experiment is a statistically-based method for analyzing the relationship between various controllable process parameters, which aids in determining the contribution of each process parameter to the desired properties and identifying the most critical factor influencing the response parameter (Narayanan et al. 2015). The Taguchi technique relies on process parameter optimization to obtain the highest quality material without raising costs (Narayanan et al. 2015). This is because optimizing process parameters can enhance performance, and the Taguchi method's optimal process parameters are resistant to changes in the environment and other noise sources. In essence, traditional process parameter design is challenging to use (Narayanan and Shashikala 2014). The flowchart of the Taguchi Process is depicted in figure 1.5.

A critical stage in the experiment design is deciding which parameters impact the product's attributes. Taguchi's experimental design includes orthogonal arrays to organize the process's influencing parameters and the levels at which they should be altered and a robust test design to limit process volatility (Narayanan and Shashikala 2014).

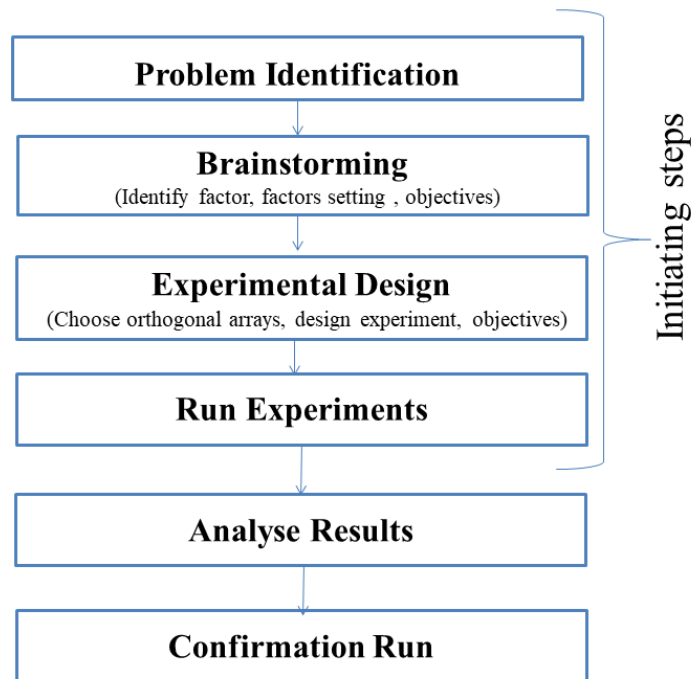


Figure 1.5: The flowchart of the Taguchi Process

Using orthogonal arrays, the Taguchi technique determines the parameters that affect the process and the levels at which they should be modified. Before optimizing a design to reach mean objective values for output characteristics, the Taguchi method is one of the most influential experimental procedures for decreasing variance in design parameters. It uses orthogonal arrays to evaluate all design issues with the fewest possible experiments. As three process parameters and three levels are selected for optimizations, the L_9 orthogonal array is chosen in the current work.

Taguchi's method converts the acquired values of the response parameters' signal-to-noise (S/N) ratios at various levels of process parameters. The (S/N) ratios describe the variation in response characteristics across several experimental levels of process parameters' circumstances. The optimal situation for testing is at the process parameter level when the response parameter has the highest S/N ratio and lowest variable features (Mandal et al. 2011; Narayanan and Shashikala 2014).

1.9 Special properties of Phosphate glasses

Unlike other oxide glasses, Phosphate glasses exhibit unique thermal and optical features, such as a low melting temperature, a low glass transition temperature, a low

softening temperature, a high thermal expansion coefficient, a high refractive index, and a high ultraviolet (UV) transmission. Optical fibres, solid-state lasers, nuclear waste disposal, solid-state batteries, solar energy concentrators, glass-to-metal sealing, and biomedical applications are all possible. Their wide range of technological applications is limited by their hygroscopic nature, poor chemical durability, and inferior thermal stability (Brow 2000; Dutebo and Shashikala 2020; Edathazhe and Shashikala 2018a; Shelby 2007).

The addition of oxides like alkali and Alkaline earth oxides to phosphate glasses may result in the formation of new bonds, linking PO_4 structural units with covalent bonding oxygens, and condensation of the phosphate network, improving the chemical durability, thermal stability, and water resistance of the glass network on the one hand, and increasing the water-resistance of phosphate glasses on the other (Liu et al. 2016a; Saddeek et al. 2017).

The chemical composition flexibility of glass allows for the doping of specific ions or active elements for the development of special colors, emission of fluorescent light, strong nonlinear susceptibility, photochromism, and other properties. Doping transition metal ions, rare-earth elements, noble metals, and semiconductor compounds into glasses produce a variety of colors and properties (Kreibig and Vollmer 2010; Shelby 2020; Yamane and Asahara 2000).

Inorganic glass systems have received much attention recently due to their exciting features and potential uses as fibers and optical broadband amplifiers, lasers, optical temperature sensors, and white light generators. The structural, optical, and physical properties of glass systems are all influenced by the composition of the glass host matrices.

Phosphate glasses have been researched among the various inorganic glass systems for a variety of industrial applications as well as a wide range of optical applications in the visible and infrared luminescence ranges. Glass materials containing rare-earth ions due to their superior luminescent characteristics have potential uses as fibers and optical broadband amplifiers, high power lasers system,

optical temperature sensors, and white light generators(Kuwik, Pisarska, and Pisarski 2020; Othman, Arzumanyan, and Möncke 2016).

Phosphate glasses are technically and structurally crucial due to their unique properties compared to silicate and borate glasses: They have the following properties(Brow 2000; Cramer et al. 2013; Jiménez and Sendova 2014; Shelby 2020; Shi et al. 2019; Wen et al. 2019; Yamane and Asahara 2000).

- Low melting and low softening temperature,
- The large glass-forming region
- Low glass transition temperatures,
- High optical characteristics,
- High transparency from the deep ultraviolet to the near-infrared,
- High Thermal expansion,
- High metal solubility,
- Potential to accommodate large concentrations of active ions, Rare earth ions, metal nanoparticles, etc.,

1.10 Rare-earth ion-doped glasses containing noble metals

Lanthanum and the f-block elements, cerium through lutetium, are examples of Rare earth elements (REE)(Atwood 2013). Scandium and yttrium are included in this group because their ionic radii are close to those of the lighter f-block elements and occur in the same ores. Compared to other metals in the periodic table, where two neighbouring elements in a period usually have dramatically different chemical properties, the 17 REE are unique due to their chemical similarities. This makes it difficult to separate the REE from one another, while there are minerals that concentrate the lighter (La–Eu) and heavier (Y and Gd–Lu) REE(Atwood 2013). However, this commonality has aided REE research because compounds and materials made with one REE may typically be duplicated with one or more REEs. A summary of Rare earth elements selected for the current work is shown in table 1.1.

Table 1.1 a summary of Rare earth elements selected for the current work

Rare Earth Elements	Symbol	Atomic number(Z)	Ground state configuration	Atomic weight
Lanthanum	La	57	[Xe]5d ¹ 6s ²	138.905
Cerium	Ce	58	[Xe]4f ¹ 5d ¹ 6s ²	140.116
Europium	Eu	63	[Xe]4f ⁷ 6s ²	151.964
Erbium	Er	68	[Xe]4f ¹² 6s ²	167.259

Rare earth ions (REIs) have 4fⁿ electronic configurations, resulting in multiple electronic levels and excited state levels with long lifetimes (10⁻⁶-10⁻² s), allowing them to produce absorbing transition and radiation throughout a broad spectrum range from Ultraviolet to Infrared (UV-VIS-IR). Furthermore, the outer 5s and 5p electrons of RE ions protect the 4f electrons, decreasing the outside effect from electric, magnetic, and ligand fields, resulting in spectra of RE ions doped in host materials that are identical to those of a free ion or atom (Hu et al. 2013).

The most prominent active ion in the RE family, trivalent erbium (Er³⁺), has been utilized in many glasses for applications in solid-state lasers and optical amplifiers due to its favorable energy level structure (Soltani, Hraiech, Horchani-Naifer, Elhouichet, et al. 2016). The interest in erbium as a RE doping ion in a host glass medium stems from the fact that its radiative transition (⁴I_{13/2} → ⁴I_{15/2}) at 1530nm coincides with the third optical communication window, which corresponds to minimal attenuation (0.2 dB/km) in silica glass, and is located in an eye-safe spectral region (Pugliese et al. 2016).

When Er³⁺ ions are optically pumped at roughly 980 or 1480 nm and then radiate light at 1530 nm in stimulated emission, Erbium-doped glasses or crystals can be employed as optical amplification media. This approach produces an unusually mechanically easy laser optical amplifier for fibre optic signals. Because conventional single-mode optical fibres have little loss at this wavelength, the 1530 nm wavelength is essential for optical communications.

Crystal matrix and glass matrix are the most common solid host materials nowadays. Although crystal is the first solid material to realize laser output, it has

some drawbacks, including difficulty in preparing optically uniform and large-size crystals, narrow absorption spectrum lines, and low doping concentration and optical parameters of RE ions in the crystal, among others. These have severely hampered the development of crystal substrate conversion materials. Although it cannot completely replace the crystal in some ways, glass matrix luminescent materials have the potential to overcome the flaws mentioned earlier and become a hotspot for research. Due to the possible uses in fields like lasers, optical fibers and amplifiers, the Up-conversion of infrared to visible by rare earth ions(REIs) doped glasses have been intensively explored over the past decades(Hu et al. 2013).

Regarding matrix selection, phosphate-based glass hosts are gaining popularity due to their high REIs solubility, making them promising photonic materials(Jiménez et al. 2011).Phosphate glasses are the oxide glasses used to develop noble metal nanoparticles without oxidation or contamination from the environment. The size, shape, and distribution of nanoparticles in a cluster and the dielectric properties of the surrounding matrix all impact the optical, physical, and structural properties of glasses. Photonics, optical limiting, optical switching, nonlinear optics, and other fields have benefited from developing composite materials like these.

Calcium-based phosphate glasses have attracted the curiosity of materials scientists for various applications ranging from biomaterials to optics. Adding noble metals (Au, Ag, Cu) to a glass matrix is particularly interesting in this study because the amorphous materials that develop can have unique features. Depending on the nature of the noble metal and its oxidation and aggregation states, these glasses can be antibacterial, luminous, or nonlinear optical materials(Jiménez 2016; Venkateswara Rao and Shashikala 2015). Because of its importance in developing optoelectronic devices like lasers, light converters, sensors, high-density memory, optical fibers, and amplifiers, Rare earth Ions(REIs) doped crystals and glasses have been extensively studied(Ahmadi, Hussin, and Ghoshal 2018).

In an era of photonics and integrated optics difficulties, research and development in novel optical materials are becoming increasingly vital(Shakhgildyan et al. 2022). Rare earth (RE) ion-containing glasses exhibit sound optical emission

and fluorescence capabilities, making them a good choice for glass lasers, optical amplification, photonic devices, and solid-state illumination (Du et al. 2022).

The following work is being undertaken in response to a growing demand for robust materials and a better knowledge of the characteristics and structure of metal nanoparticles and rare earth oxide inside phosphate glasses. Rare-earth ions doped binary calcium phosphate glasses with and without silver and tin oxide are prepared. Their physical, structural, and optical properties are investigated in this study.

1.11 Scope and objective of the research

1.11.1 Scope

The necessity to develop noble materials for various applications – from decorative objects, optoelectronic devices, and military facilities, to medical interferences such as drug- deliverers and artificial bones – has motivated the materials engineers and scientists to demand new materials with low cost, high efficiency, long durability, and recyclability. In this regard, glasses are one of the crucial candidates of materials.

The study and synthesis of glasses with special properties are active research areas because of the need for technological developments in photonics, optical telecommunications, green renewable energy, information processing, nuclear waste management, etc. These studies depend critically on the development of improved glass materials. They have essential advantages like optical transparency, mechanical strength, chemical durability, dimensional stability, and low product cost. These glasses can accommodate various dopants such as rare earth ions, transition metals ions, and metal nanoparticles (Au, Ag, Cu, Pt...).

Since the positive impact of glass has grown, new glass products and methods have been developed to meet global concerns in energy, the environment, health care, information and communication technology, and other fields.

Among all oxide-based glasses, Phosphate glass has attracted significant attention in the last few decades due to its unique structural and optical properties such as low melting temperature, high transparency from UV to NIR, and good

thermal and mechanical stability. Structurally, they also have tremendous importance because they accept many dopants like rare-earth ions, transition elements, and metal nanoparticles without losing their main properties. This makes them suitable for high-power solid-state batteries, solar energy concentrators, data transmission, nuclear waste vitrification, glass metal seals, etc.

The disadvantage of Phosphate glasses, like poor chemical durability and hygroscopic nature, are challenging to extensive practical applications. Still, efforts were made over the last decades by adding different metal oxides and a small amount of fluorine-containing components to the starting batch materials.

Calcium and Barium metaphosphate glasses are optically transparent dielectric materials usually used to prepare noble metal nanoparticle-embedded glasses due to their high metal solubility(Kreibig and Vollmer 2010; Uchida et al. 1994). Rare earth (RE) ions, called Lanthanides, are the active constituents of many optical materials. The REI's unique properties and interdependence with the embedding glass matrix enable much of today's optical technology and emerging innovations.

Incorporating metallic nanoparticles in rare-earth-doped oxide glasses has been an exciting method to enhance optical properties. Controlling the size and shape of metallic nanoparticles is a challenging issue that depends strongly and ambiguously on the concentration, time, and temperature of heat treatments(Amjad, M. R. Sahar, et al. 2012; Dousti and Amjad 2016). The effects of metals on REIs remain controversial, and several problems related to these effects remain unaddressed(Jiao et al. 2015).

Detail knowledge regarding the structural, physical, and optical properties of solid-state lasers, waveguides, optical amplifiers, and light-emitting materials is required to obtain insight into their properties.

Therefore, further study is necessary to investigate the properties of the co-doping effects of rare-earth ions and metal nanoparticles in Phosphate glasses for different applications. The main objective of this research is to “Synthesize and

characterize rare earth doped alkaline earth Phosphate glasses with metal nanoparticles and study their different properties.”

1.11.2 Objectives

- To synthesize rare-earth ions doped alkaline earth phosphate glasses using melt quenching technique
- To synthesize metal nanoparticles embedded in alkaline earth Phosphate glasses using melt quenching technique and subsequent heat treatment
- To synthesize rare earth doped alkaline earth Phosphate glasses with noble metal particles using melt quenching technique and subsequent heat treatment
- To study the structural characterization of synthesized glass system using XRD, SEM, TEM, and FTIR
- To study the physical, optical, structural, and luminescence properties of the synthesized glasses

1.12 Thesis Structure

The following is a breakdown of the current thesis

Chapter1 provides an overview of oxide glasses and glasses with unique features. This chapter also contains an overview of glass formation principles, glass preparation procedures, glass system classification, and optimization techniques. This chapter also includes a synopsis of research on the structure and behavior of phosphate-based glasses doped by rare-earth ions and noble metal nanoparticles. Furthermore, at the end of this chapter, the scope and objectives of the current research activity and the organization of the present thesis are provided.

Chapter2 gives details on the materials and synthesis procedures employed for the fabrication of Phosphate glasses, Rare-earth doped glass, and glass-metal nanoparticle composites in the current research. It also contains a summary of the various characterization techniques utilized to investigate the structure and properties of prepared samples at different phases of study. The methods and ideas for analyzing

sample qualities and optimizing rare-earth doped Calcium phosphate glasses' numerous performance aspects are also described.

Chapter3 discusses the effects of (Er^{3+} , La^{3+} , Ce^{4+}) additions on the physical, optical, and structural aspects of binary Calcium Phosphate Glasses. Additionally, efforts are being made to correlate the examined properties with structure and compositions, which will aid in developing better glasses with superior properties.

Chapter4 illustrates the Statistical optimization of melt-quenching process parameters of rare-earth ions doped calcium phosphate glasses using the Taguchi method. Response tables and main effect plots are used to investigate the effect of process parameters such as Rare earth ion (La^{3+} , Ce^{4+}) content, melting temperature, and melting time on the response parameters of $(50-x)\text{CaO}-x\text{RE}-50\text{P}_2\text{O}_5$ ($x = 1, 2, 3$ mol%) glasses prepared according to Taguchi's standard orthogonal array experimental layout.

Chapter5 includes the effect of rare earth ion doping on the physical, structural, and optical properties of silver oxide-containing calcium phosphate glasses $50\text{P}_2\text{O}_5 - (50-x) \text{CaO}-x\text{Er}_2\text{O}_3-4\text{Ag}_2\text{O}-4\text{SnO}$ (where $x=0$ to 5mole%). In addition, data from characterization studies carried out such as X-ray diffraction (XRD), FTIR, density measurement, and UV-Vis on these glasses are discussed.

Chapter 6 details the effects of heat treatment on optical, physical, and structural properties of rare-earth (Er^{3+} , Eu^{3+}) ion doped metal nanoparticles embedded in $49\text{CaO}-1\text{REI}-50\text{P}_2\text{O}_5$ glasses at various annealing times and temperatures above the glass transition temperature. TEM and optical spectroscopy are used to examine precipitated nanoparticles' size, shape, and distribution.

Chapter7 summarizes the significant findings and conclusions of the current research activity. This chapter also discusses future research opportunities in the field of glass science.

CHAPTER 2

MATERIALS AND METHODS

Overview

In this work, a series of phosphate glasses were prepared, and an extensive analysis was carried out. This study used the Melt-quenching technique to make a series of calcium phosphate glasses with rare-earth ions (REI) and silver nanoparticles or oxide. To investigate the influence of adding REI (Lanthanum, Cerium, Erbium ions) to binary Calcium phosphate glasses, $50\text{P}_2\text{O}_5-(50-x)\text{CaO}-x\text{REI}$, where the values of x vary from 0 to 5 mol.% and $\text{REI} = \text{La}^{3+}$, Ce^{4+} , and Er^{3+} were synthesized using the melt-quenching technique. The Taguchi method of Design of Experiments (DOE) with an L_9 orthogonal array was adopted in Rare earth (La^{3+} , Ce^{4+}) ions doped glasses $50\text{P}_2\text{O}_5 - (50-x) \text{CaO}-x\text{REI}$ (where REI represents the added Rare earth ion and $x=1$ to 3mole%) to optimize the process parameters of glass preparation. Using these glasses examined the impact of process variables such as composition, melting temperature, and melting duration on the response parameter. Erbium ion-doped glasses $50\text{P}_2\text{O}_5 - (50-x) \text{CaO}-x\text{Er}_2\text{O}_3-4\text{Ag}_2\text{O}-4\text{SnO}$ (where $x=0$ to 5mol %) were synthesized using melt-quenching technique and optical, physical, structural properties were examined. In addition, glasses with the compositions $50\text{P}_2\text{O}_5-49\text{CaO}-1\text{REI}-4\text{Ag}_2\text{O}-4\text{SnO}$ (Er_2O_3 , Eu_2O_3), in which spherical silver nanoparticles (NPs) of varied sizes were embedded after heat-treatment were synthesized. Silver nanoparticle embedded Rare earth doped Calcium phosphate glasses were made by standard melt quenching with subsequent chemical reduction performed by controlled heat treatment at varying post-annealing durations above the glass transition temperature. To avoid material loss during processing due to the hygroscopic and volatile nature of P_2O_5 , ammonium dihydrogen phosphate ($\text{NH}_4\text{H}_2\text{PO}_4$) was utilized as a precursor in the synthesis of all the glasses in the present study.

2.1 Materials used for glass synthesis in the present study

Glasses of compositions $50\text{P}_2\text{O}_5-(50-x)\text{CaO}-x\text{REI}$ where $x = 0, 1, 2, 3, 5$ mol.% and $\text{REI} = \text{Er}^{3+}, \text{La}^{3+}, \text{and Ce}^{3+}$ were synthesized to study the effect of rare earth ion additions to calcium phosphate glass. Glasses with composition $50\text{P}_2\text{O}_5 - (50-X) \text{CaO}-x\text{Er}_2\text{O}_3-4\text{AgO}-4\text{SnO}$ where $x=0, 0.5, 1, 1.5, 2.5,$ and 5mol. \% were prepared to study the effect of Ag_2O addition on different Erbium oxide doped calcium phosphate glass compositions. Tin oxide (SnO) acts like a reducing agent to reduce Ag ion in AgO to Ag^0 . Among these glasses, $50\text{P}_2\text{O}_5-49\text{CaO}-1\text{Er}_2\text{O}_3-4\text{Ag}_2\text{O}-4\text{SnO}$ was selected to study the effect of heat treatment in reducing Ag^+ to the silver nanoparticle (Ag^0). Similar studies were carried out on $50\text{P}_2\text{O}_5-49\text{CaO}-1\text{Eu}_2\text{O}_3-4\text{Ag}_2\text{O}-4\text{SnO}$ also. Table 2.1 shows Chemicals/Reagents used with their purity level (%). Table 2.2, Table 2.3, and Table 2.4 show the glass compositions employed in this study, along with the sample code.

Table 2.1 Chemicals used in the present study

Sl. No.	Chemicals/Reagents	Purity (%)	Provided by
1.	$\text{NH}_4\text{H}_2\text{PO}_4$	>98.00	Alfa Aesar
2.	CaCO_3	>99.50	Alfa Aesar
3.	Er_2O_3	>99.99	Alfa Aesar
4.	La_2O_3	>99.99	Alfa Aesar
5.	CeO_2	>99.99	Alfa Aesar
6.	Eu_2O_3	>99.99	Alfa Aesar
7.	Ag_2O	>99.80	Alfa Aesar
8.	SnO	>99.00	Alfa Aesar

Table 2.2 Batch composition of 50P₂O₅-(50-x) CaO- xREI (REI = La³⁺, Ce⁴⁺, and Er³⁺) glasses.

Glass Code	Batch compositions (mol %)		
	P ₂ O ₅	CaO	REI(La ³⁺ , Ce ⁴⁺ , Er ³⁺)
CP	50	50	0
CPRE1	50	49	1
CPRE2	50	48	2
CPRE3	50	47	3
CPRE5	50	45	5

Table 2.3 Effect of Erbium Concentrations on Calcium Phosphate glasses with Silver and Tin oxide

Glass Code	Batch compositions (mol %)				
	P ₂ O ₅	CaO	Er ₂ O ₃	Ag ₂ O	SnO
CPAS	50	50	0	4	4
CPEAS.5	50	49.5	0.5	4	4
CPEAS1	50	49	1	4	4
CPEAS1.5	50	48.5	1.5	4	4
CPEAS2.5	50	47.5	2.5	4	4
CPEAS5	50	45	5	4	4

Table 2.4 Effects of heat treatment on rare earth ion (Eu^{3+} , Er^{3+}) doped Calcium Phosphate glasses with Silver and Tin oxide

Glass Code	Batch compositions (mol %)					
	P ₂ O ₅	CaO	Er ₂ O ₃	Eu ₂ O ₃	Ag ₂ O	SnO
CPAS	50	50	0	0	4	4
CPEAS1	50	49	1	0	4	4
CPASEu1	50	49	0	1	4	4

2.2 Experimental procedure

The chemicals were accurately weighed in determined molar proportions (Shelby 2020) using a Contech analytical balance with a 0.1 mg accuracy and mixed with a pestle in an agate mortar. A batch of 20gm of each mixture was weighed and thoroughly mixed. Melt quenching was used to make all the glasses. To remove the water, ammonia, and carbon dioxide molecules from NH₄H₂PO₄ and CaCO₃, the finely mixed and powdered batch was placed in a silica crucible and calcined at 400°C for 2 hours in a muffle furnace. Using a high-temperature furnace, the calcined batch was melted in silica crucibles at 1200, 1250, and 1300°C for 0.5hr, 1hr, and 1.5 hours at room temperature. The homogenized melt was poured onto copper plates. Quenched glass samples were annealed in a muffle furnace at 550°C for 3 hours to reduce thermal stresses created during quenching, then allowed cooling at ambient temperature in the furnace.

To avoid moisture attacks from the atmosphere, annealed glass samples were kept in a vacuum desiccator. XRD measurements were performed on powdered materials. To get flat surfaces suitable for testing physical and optical properties, prepared samples were ground and polished with emery sheets of various grit sizes (80–2500) and alumina powder (0.05µm) solution. Figure 2.1 depicts the preparation and characterization flowchart for CPRE and CPEAS glasses. By preparing samples according to Taguchi's orthogonal array's (OA) experimental arrangement, the performance characteristics of Rare earth doped Calcium phosphate glasses were

optimized. The glass samples were prepared using a high-temperature furnace depicted in Figure 2.2. The representative images of synthesized glasses are shown in Figure 2.3.

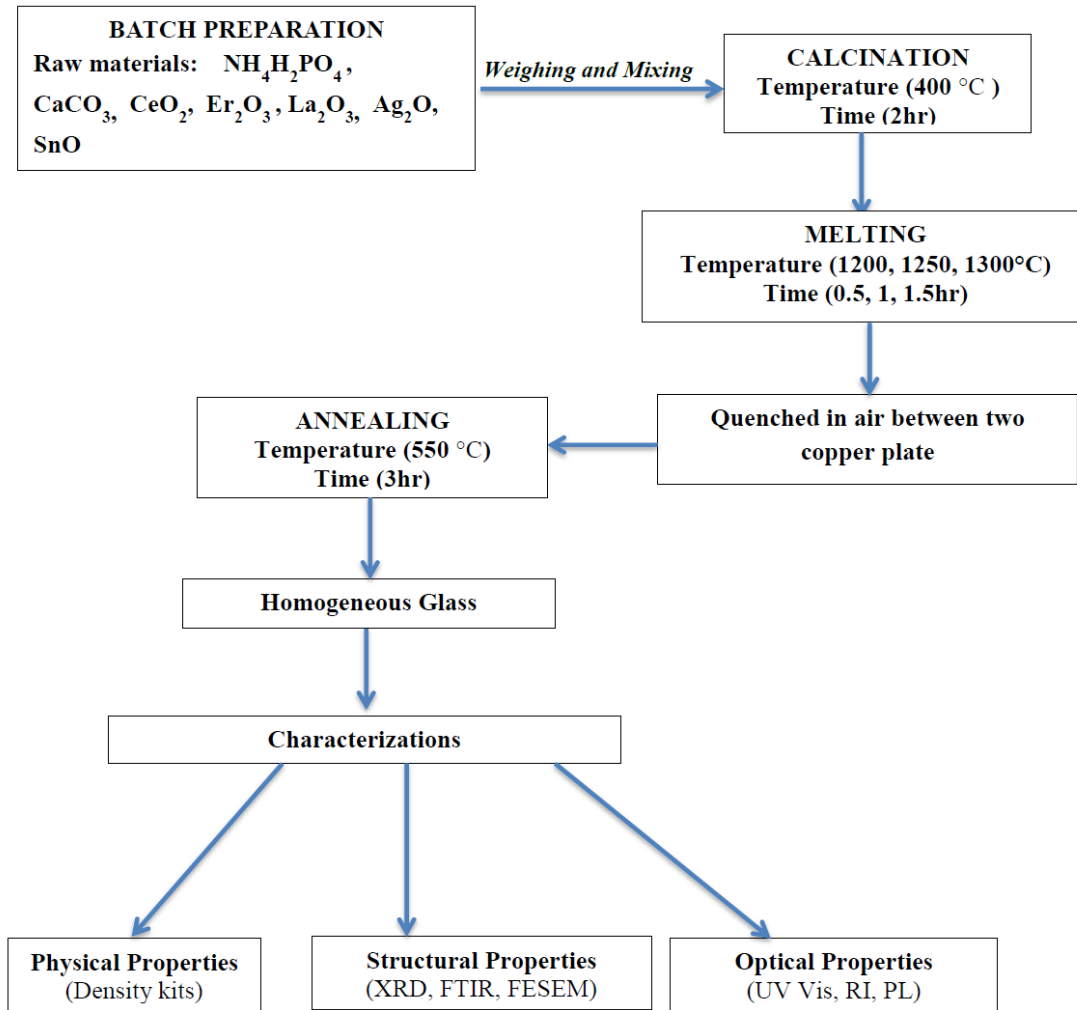


Figure 2.1 Flow chart of the preparation and characterization of CPRE and CPEAS glasses



Figure 2.2 Furnace used for glass preparation

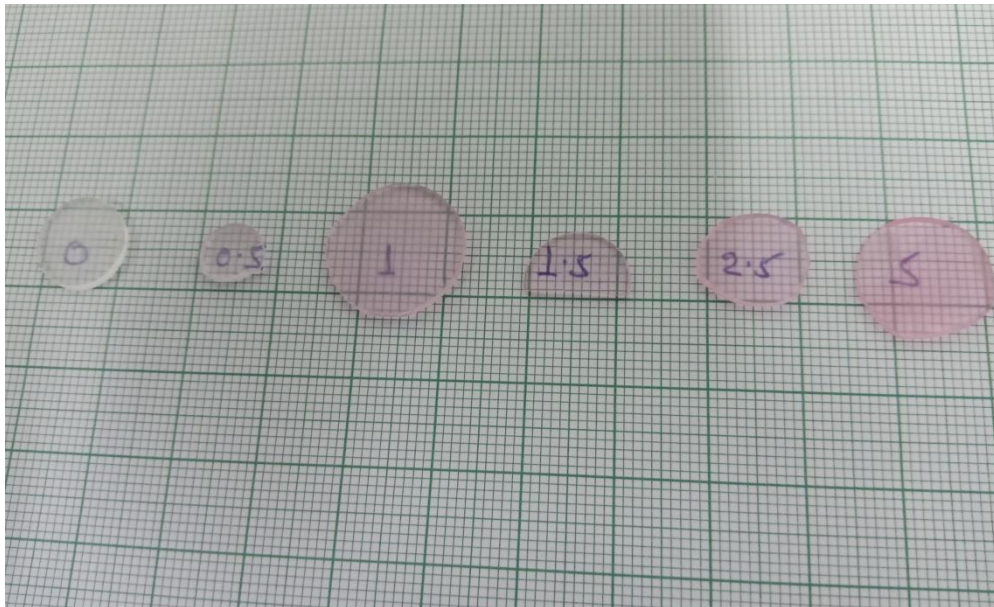


Figure 2.3 Images of synthesized glasses of CPEAS system.

2.3 Preparation of CPAS, CPEAS1 and CPASEu1 glasses

As host matrices for CPAS, CPEAS1, and CPASEu1 samples, glass powders with compositions of $50\text{P}_2\text{O}_5\text{-}50\text{CaO}$, $50\text{P}_2\text{O}_5\text{-}49\text{CaO-}1\text{Er}_2\text{O}_3$, and $50\text{P}_2\text{O}_5\text{-}49\text{CaO-}1\text{Eu}_2\text{O}_3$ were chosen. After calcination, four mol.% Ag_2O (silver nanoparticle precursor) and an equal amount of SnO (reducing agent) were added and melt-quenched to precipitate silver nanoparticles in the host matrix. A slightly modified synthesis procedure was used to prepare these glasses instead of following the standard technique of mixing all the oxides and melting them all at once, all the precursors and raw materials in the required proportions were mixed thoroughly by grinding in an agate mortar and calcined at $400^\circ\text{C}/2\text{hrs}$ in a muffle furnace. The calcined batch was finely mixed with the requisite amounts of Ag_2O and SnO in an agate mortar and melted at 1200°C in a PID-controlled high-temperature furnace. The melt was kept at that temperature for 1 hour to achieve the required homogeneity. The homogenized melt was cooled to room temperature using the same quenching technique mentioned earlier. To remove residual thermal stresses created during quenching, quenched samples were annealed at 550°C for 3 hours in a muffle furnace and then cooled to ambient temperature. As-quenched and annealed samples were transparent for CPAS, CPASEu1, and CPEAS1 glasses. To develop glass samples embedded with silver nanoparticles of variable mean particle size and distribution, annealed samples were heat-treated (post-annealed) at a fixed temperature with varying heat treatment duration.

Figure 2.4 depicts the flow charts of synthesizing and characterization process of CPAS, CPEAS1, and CPASEu1 glasses. For Erbium ion doped glass system, CPEAS1-0, CPEAS1-3, CPEAS1-10, CPEAS1-25, and CPEAS1-50 are the sample codes given to samples that were heat-treated at 550°C for 0hrs, 3hrs, 10hrs, 25hrs, and 50hrs, respectively. Similarly, for Europium ion-doped samples CPASEu1-0, CPASEu1-3, CPEAS1-10, CPASEu1-25, and CPASEu1-50 represent the glasses heat treated at 0hrs, 3hrs, 10hrs, 25hrs, and 50hrs respectively. Figure 2.5 shows the images of the synthesized glass sample CPAS, CPEAS1, and CPASEu1 heat treated for a different duration.

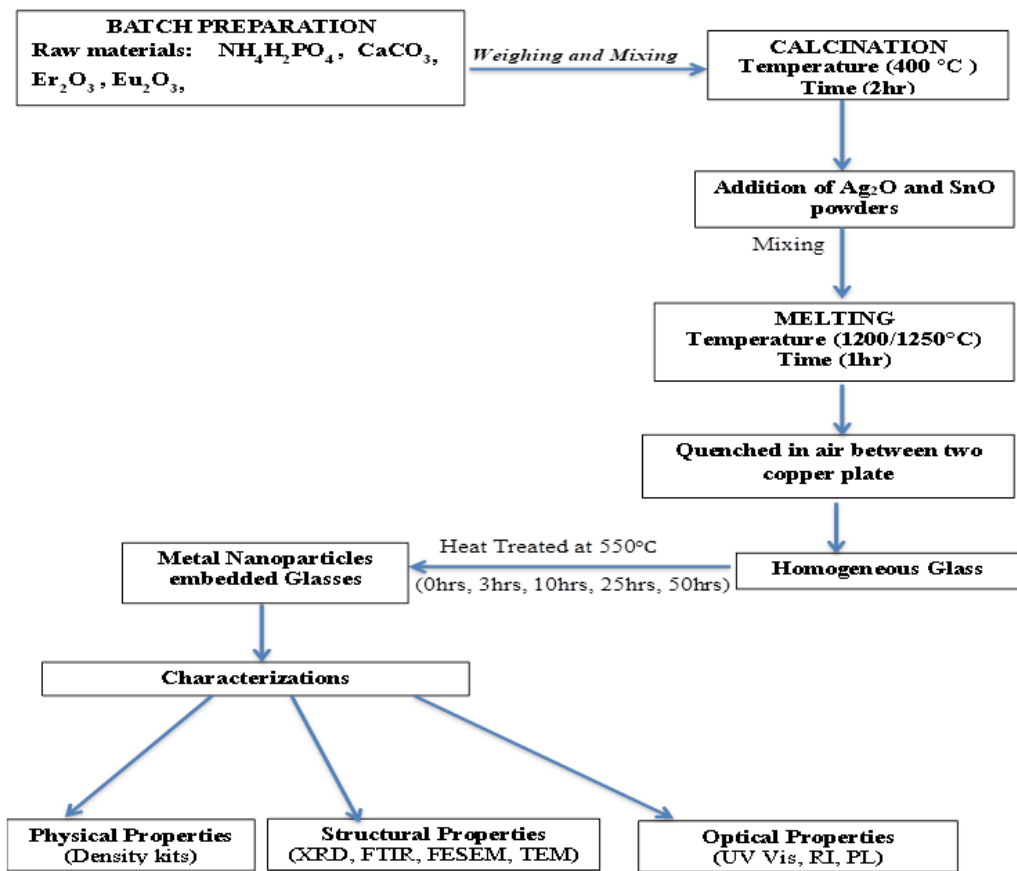


Figure 2.4 Flow chart of sample Preparation of heat treatment and characterization of CPAS, CPEAS1, and CPASEu1



Figure 2.5 The image of the synthesized CPASEu1 series

2.4 Polishing of the Glass samples

To achieve optically flat surfaces suitable for studying optical properties, prepared host glasses and nanoparticle embedded glasses were ground and polished on both sides using silicon carbide sheets of different grit sizes and alumina powder

suspension. Glasses were initially ground and polished for around five minutes per side using silicon carbide emery papers with successive grit sizes ranging from 80, 180, 320, 400, 600, 800, 1000, 1200, 1500, and finally with 2500, using distilled water as a coolant. Then, cloth polishing with alumina powder (0.05 micron) suspension gave optically smooth polished surfaces of glasses. Motorized polishing equipment was used to grind and polish the glasses (BAiNPol, Chennai Metco, Grinder-Polishing machine). To remove any remaining polishing compounds, glass surfaces were cleaned with acetone and then gently dried with a hair dryer. Samples with thicknesses of 1.5mm to 2 mm and optically smooth surfaces could be obtained by following the above mentioned steps.



Figure 2.6 Polishing machine employed in the polishing of glass samples

2.5 Design of experiments for optimization

The design of experiments is a valuable strategy for determining the best inputs and parameter levels for a high-quality product. The selection of parameters impacting the product's qualities is a crucial stage in the experiment design. To detect non-significant parameters as soon as feasible, as many parameters as possible should be incorporated into the design (Mohan, Ramachandra, and Kulkarni 2005). Previous studies in glass research have mainly focused on the effects of batch composition changes on the qualities of glass samples, using either simulation or the traditional trial and error method.

In the present work, the effect of processing parameters: melting temperature, melting time and rare-earth oxide composition on density as response characteristic has been investigated. The influence of process parameters impacting the response parameter was shown by an analysis of variance (ANOVA)(Narayanan and Shashikala 2014) directed at the signal-Noise(S/N) ratio of the response parameter. It was predicted that the best condition for the contribution of process parameters impacting the response parameter would be found. Previous studies used traditional trial and error approaches to obtain optimum glass samples, which necessitated many tests. In this study, using Taguchi's conventional L_9 orthogonal array, only nine samples of rare-earth oxide-doped calcium phosphate glasses were prepared experimentally and the processing parameters could be optimized.

The Taguchi technique relies on process parameter optimization to obtain the highest quality material without raising costs(Narayanan et al. 2015). This is because optimizing process parameters can enhance performance, and the Taguchi method's optimal process parameters are resistant to changes in the environment and other noise sources. In essence, traditional process parameter design is challenging to use.

Depending on the experimental design of Taguchi's orthogonal array, the batch materials were weighed put into a silica crucible and melted in a PID-controlled high-temperature furnace for 30–90 minutes in the temperature range 1200–1300°C. After being quenched in the air on copper plates, the homogenized melt was cooled to room temperature in the furnace and then annealed at 550°C for 3 Hours to remove thermal stresses created during the quenching.

A critical stage in the experimental design was deciding which parameters impacted the product's attributes. In the current design, there were a total of eight degrees of freedom (DOF) connected with three process parameters, each of which had three levels. The L_9 orthogonal was an excellent option since it complied with the design of experiments (DOE) guideline that the number of experimental trials in an orthogonal must be more than the sum of the degree of freedom. Taguchi's experimental design includes using L_9 orthogonal arrays to organize the process's influencing parameters and the levels at which they should be altered, as well as a

robust test design to limit process volatility. The process parameters used in this experiment, as well as their levels listed in table2.5.

Table2.5 Process parameters used in the experiment

Process Parameters	Symbol	High	medium	Low
Compositions (mol.%)	A	3	2	1
Melting temperature(T) , °C	B	1300	1250	1200
Melting time (Time), min	C	90	60	30

2.5.1 Taguchi Method

Using orthogonal arrays, the Taguchi technique determines the parameters that affect the process and the levels at which they should be modified. Before optimizing a design to reach mean objective values for output characteristics, the Taguchi method was selected as one of the most influential experimental procedures for decreasing variance in design parameters. It made use of orthogonal arrays to evaluate all design issues with the fewest possible experiments. After selecting the L₉ orthogonal array the factors impacting the operation and the levels at which they should be modified were organized using them. With a minimum trial, the Taguchi technique collected the required data to establish which aspects affect product quality the most, saving time and resources(Macioszczyk et al. 2015).

Using Taguchi's method, the acquired values of the response parameters' were converted to signal-to-noise (S/N) ratios at various levels of process parameters. The (S/N) ratios described the variation in response characteristics across several experimental levels of process parameters. The optimal situation for testing was at the process parameter level for which the response parameter had the highest S/N ratio and lowest variable features. Analysis of variance (ANOVA) was used to uncover particular factors that substantially impact the response parameter using the data generated from the Taguchi design of experimentation.

Table 2.6 Taguchi L_9 Orthogonal arrays of (La^{3+} , Ce^{4+}) doped Phosphate glass samples

Sample code for La^{3+}	Sample code for Ce^{4+}	Compositions (mol.%)	Melting Temperature($^{\circ}C$)	Duration Time (min)
T1	E1	3	1300	90
T2	E2	3	1250	60
T3	E3	3	1200	30
T4	E4	2	1300	60
T5	E5	2	1250	30
T6	E6	2	1200	90
T7	E7	1	1300	30
T8	E8	1	1250	90
T9	E9	1	1200	60

The total degrees of freedom (DOF) of process parameters were used to choose orthogonal arrays for grouping the parameters. In the current scenario, the total degrees of freedom associated with three process parameters with three levels were 6 (i.e., 3×2). For this investigation, a L_9 orthogonal array with degrees of freedom equal to 8 was chosen. The statistical software Minitab 19 was utilized to select orthogonal arrays and the ANOVA. The experimental design of the current investigation is shown in Table 2.6. Experiments were run randomly to exclude the influence of uncontrollable factors, and each experiment was repeated three times and the average value of three trials was considered.

2.6 Techniques for Glass characterization

Glass characterization has a long history and is widely regarded as essential for the design, manufacture, and application of glass in technical applications. A complete discipline of glass characterization has grown from the earliest days of creating high-quality glass for scientific apparatus and optical applications to

understanding how to detect and manage fundamental qualities of glasses such as optical transmission and thermal expansion(Kohli et al. 2022).

For structural investigations, X-ray diffraction (XRD), Fourier transform infrared (FTIR) spectroscopy, Field emission Scanning electron microscopy (FESEM), and transmission electron microscopy (TEM) were used to characterize prepared glass samples. Energy Dispersive X-ray Spectroscopy (EDS) in conjunction with SEM was used to determine the elemental makeup of the samples. UV-Visible spectroscopy, refractive Index (RI) measurements, and photoluminescence spectroscopy were used to investigate optical properties. Density measurements were used to study physical parameters.

2.6.1 X-ray diffraction study

X-ray powder diffraction (XRD) is a quick analytical technique that can offer information on unit cell dimensions and is mainly used for the phase identification of crystalline materials (Cullity 1956). By comparing collected data with patterns from the Joint Committee on Powder Diffraction Standards (JCPDS) and the Inorganic Crystal Structure Database (ICSD). It is based on Bragg's law, according to equation 2.1.

$$n\lambda = 2d \sin \theta \quad (2.1)$$

where n is the order of reflection (considered 1 in this work), d is the inter-planer distance and θ is the angle formed by the wave vector of the incident beam with the lattice planes.

Powder XRD was employed in this investigation to confirm the amorphous nature of the quenched glasses and identify the phases present in the heat-treated glasses. A Raigaku Miniflex 600 X-ray diffractometer with Cu-K $_{\alpha}$ radiation was used for the XRD experiments. The X-ray tube was operated at a voltage of 40 kV and a current of 30 mA at a scanning rate of 2° per minute. The samples were scanned with Cu-K $_{\alpha}$ radiation of 1.542Å through 2θ ranging from 10° to 80°.



Figure 2.7 Raigaku Miniflex 600 X-ray diffractometer

2.6.2 Density and Molar volume

To get insight into the structure of prepared glasses, the density of glasses, which was related to molar volume and atomic packing density, was examined. Low reactive liquid xylene, was used as immersion liquid for glass density studies since many glasses easily react with water on contact (Shelby 2000). Glass samples were weighed with a 0.1 mg precision on a very sensitive weighing balance. The samples' density (ρ) was determined at room temperature using Archimedes' principles (Chowdhury, Mandal, and Ghosh 2019) using a Contech analytical balance and density kit which are shown in Figure 2.8. The immersion media was O-Xylene (C_8H_{10} , 99% -Alfa Aesar). As xylene ($\rho_l = 0.866 \text{ g/cm}^3$) was found to be less reactive to the phosphate glass sample. Equation 2.2 was used to compute the density of the bulk samples (Edathazhe and Shashikala 2018b; Narayanan and Shashikala 2015b).

$$\text{Density } (\rho) = \frac{(W_a)}{(W_a) - (W_l)} * (\rho_l) \quad (2.2)$$

where w_a , ρ_l , and w_l are the weight of the specimen in air, density of xylene, and weight of the specimen in xylene respectively.

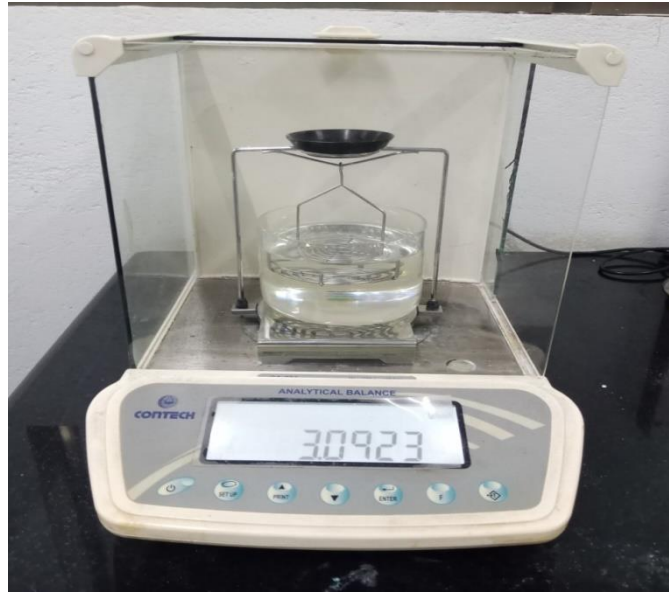


Figure 2.8 Contech analytical Microbalance with density kit

For each composition, the densities of at least three samples were tested, and the average value was recorded. Equation 2.3 was used to calculate the molar volume (V_m) from the measured density data and the error in density measurement was calculated using the standard deviation of the mean (SDOM).

$$V_m = \sum_i \frac{X_i * M_i}{\rho_m} \quad (2.3)$$

Where X_i and M_i are each component's molar fraction and molar weight, respectively (Narayanan and Shashikala 2015b).

Physical characteristics like ion concentration (N), Polaron radius (r_p), internuclear distance (r_i) and field strength (F) for the produced glasses were estimated using equations (2.4-2.7) (Dutebo and Shashikala 2020).

Ion Concentration (N) (ions/cm³) is given by

$$N = \frac{\text{Mol\% of RE} * N_A * \rho_s}{\text{Glass average molecular mass}} \quad (2.4)$$

Where N_A is Avogadro's number, ρ_s is the density of the sample, and N is ion Concentration

Polaron radius (r_p) in (Å) is given as

$$r_p = \frac{1}{2} * \sqrt[3]{\frac{\pi}{6N}} \quad (2.5)$$

Internuclear distance (r_i) in (Å)

$$r_i = \sqrt[3]{\frac{1}{N}} \quad (2.6)$$

Field Strength (F) in (cm^{-2})

$$F = \frac{Z}{r_p^2} \quad (2.7)$$

Where Z is the atomic number of Rare earth oxide (Alqarni et al. 2020; Dutebo and Shashikala 2020)

2.6.3 Fourier transform infra-red (FTIR) spectroscopy

FTIR spectroscopy (Fourier Transformed Infrared Spectroscopy) is a technique for obtaining an infrared spectrum of absorption or emission of a solid, liquid, or gas. The FTIR spectrometer simultaneously collects high resolution data over a wide spectral range. A Fourier transformation is necessary to convert the raw data to the real spectrum. Fourier Transformed Infrared Spectroscopy is the name given to this method. The vibrational spectroscopic technique of FTIR is one of the techniques used to analyze the structure of glasses. Specific vibrational modes in glasses are related to the arrangement of their structural bonds, which is dependent on their composition. The vibrational energies of compounds that are IR active are measured using FTIR spectroscopy. There must be a change in the molecule's dipole moment during the vibration for a transition to be IR dynamic. The molecular structure is shown by the absolute intensity and frequency of lines corresponding to IR active transitions. The FTIR spectra of oxide glasses can be improved by mixing the glass powder with a fixed ratio of potassium bromide (KBr) to form a pellet.

In the present work, structural bands in the glass network were identified and confirmed by recording transmission spectra using a Bruker ALPHA-200952

Spectrometer. The materials were investigated utilizing the KBr pellet method in the wave number range of 400-4000 cm^{-1} with resolution of 0.2 cm^{-1} .

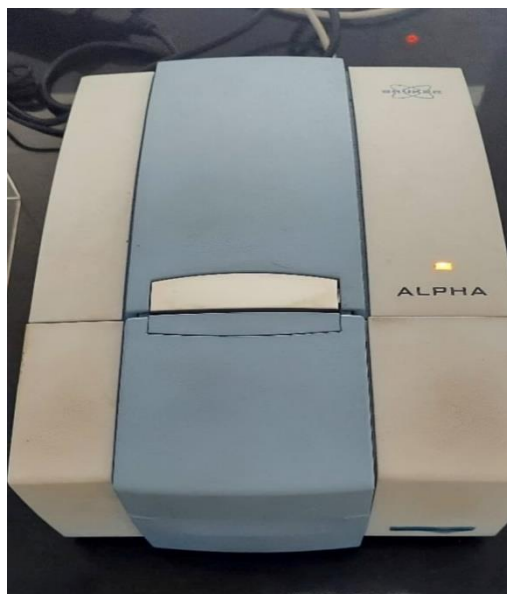


Figure 2.9 FTIR Spectrometer (Bruker ALPHA-200952 Spectrometer)

2.6.4 Field Effect Scanning electron microscope (FESEM)

Unlike optical microscopy, scanning electron microscopy offers images of a sample with higher magnification, higher resolution, and an immense depth of focus. SEM gives structural and chemical information on a specific surface region of a specimen that can endure the vacuum chamber pressure and electron beam bombardment (Cullity 1956). An energy-dispersive X-ray spectrometer (EDS) connected to a scanning electron microscope (SEM) is a tool for determining the elemental composition of materials under investigation. SEM combined with EDS would be an excellent way to get qualitative data on glass surface characteristics and elemental composition. An electromagnetic gun may produce a significantly more intense electron beam, effectively providing a better image with higher resolution. A Field-Effect Scanning Electron Microscope is one such microscope (FESEM).

In the present work, the surface morphology and elemental composition of glass samples were investigated using a FESEM [7610FPLUS, Jeol, Japan] and scanning Electron Microscope (SEM) coupled with an Energy Dispersive X-ray Spectrometer

(EDS). All-glass samples were polished and then gold-sputtered before SEM analysis to avoid the charging effect on non-conducting surfaces under electron beam analysis.



Figure 2.10 FESEM [7610FPLUS, Jeol, Japan] microscope, CRF-NITK

2.6.5 High Resolution Transmission Electron Microscope (HRTEM)

The transmission electron microscope (TEM) is a versatile microscopic tool for studying the morphology and structure of nanomaterials and nanocomposites. TEM examination is frequently performed on relatively thin samples that allow electrons to pass through them. SAED patterns, which vary depending on the structure of the samples, often exhibit a sequence of rings for randomly oriented microcrystals and sharp points, for example, with a single crystalline domain.

The size, shape, and distribution of nanoparticles implanted in the glass matrix after heat treatment were interpreted using TEM images with very high magnification and resolution (better than 10 \AA). At the same time, the structure of nanocrystallites was determined using the SAED pattern using a JEOL JEM 2100 transmission electron microscope. HRTEM operated with a 200 keV acceleration voltage was used in the study. The finely powdered sample is ultrasonically dispersed in acetone medium for 15 minutes before being dropped on a carbon-coated copper grid using a micropipette. The particle size and structural analyses were done using TEM micrograph and ImageJ software.

2.6.6 Index of Refraction (n) measurements

Due to their remarkable transparency to light in the visible and near IR regions, glasses belonging to the oxide systems have been used as essential materials for different optical components (Yamane and Asahara 2000). Their chemical composition largely determines glasses' most critical optical properties, such as refractive index, dispersion, transmission, and absorption.

One essential property that defines the optical characteristics of glasses is the refractive index. The polarizability of the ions coordinated with anion, the field strength of the ions, quantity of non-bridging oxygen atoms, and other factors influence the refractive index of glasses. The refractive index of glass samples increases as the electron density or polarizability of ions in the glass matrix increases (Shelby 2020). An Abbe refractometer is a bench-top instrument for measuring the index of refraction with high precision. The critical angle concept governs the operation of an Abbe refractometer. The sample is sandwiched between two prisms that measure and illuminate it. Light entering the sample through the illuminating prism, is refracted at a critical angle at the bottom surface of the measuring prism. Then the position of the border between bright and light areas is measured using a telescope. The sample's refractive index can be estimated using the angle and refractive index of the measurement prism.

The Abbe Refractometer (MAR-33), illustrated in Figure 2.10, was used to determine the refractive index (n) of all the samples of fine polished materials at room temperature with a 0.001 precision in this study. As previously mentioned, the average was taken from refractive indices of three different fine polished glass samples of the same composition. The contact layer between the glass and the refractometer prism was mono-Bromo naphthalene.

The Lorentz Lorenz equation (Dimitrov and Komatsu 2010), mentioned as equation 2.8, was utilized to analyze the metallization propensity of the samples.

$$\frac{R_m}{V_m} = \frac{n^2 - 1}{n^2 + 2} \quad (2.8)$$

R_m denotes molar refraction, V_m represents molar volume, and n is the refractive index of glasses.

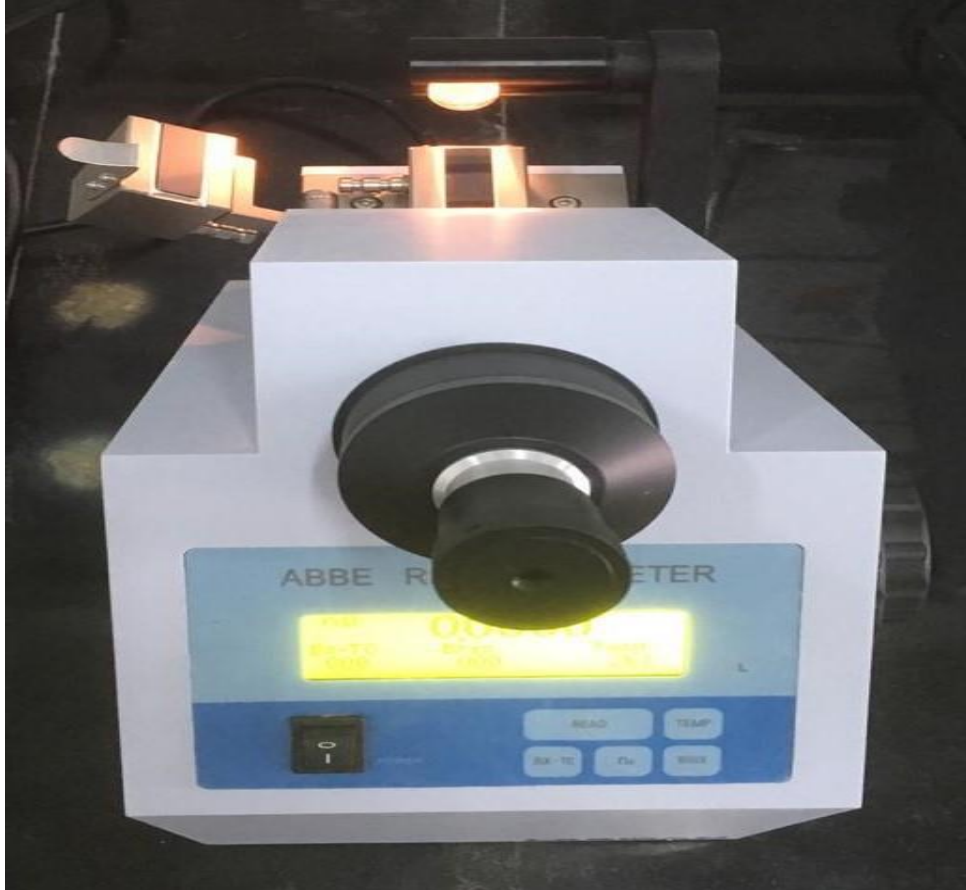


Figure 2.11 Abbe refractometer

If one starts with a material with a very high refractive index in a gaseous condition and condenses it until it solidifies and density increases to the point where $\frac{R_m}{V_m}$ approaches unity, the right-hand side of equation 2.8 becomes $n^2 - 1 = n^2 + 2$, according to Herzfeld's theory of metallization (Dimitrov and Komatsu 2010). Only when the value of n reaches infinity this is possible. This means that in the solidified state, the valence electrons that were quasi-elastically attached to their atoms in the gaseous state are now free to travel, transforming the solidified material into a metallic conductor. Based on this theory, a prediction of the material's metallic or insulating behaviour can be made. The metallization criterion is the difference shown in equation 2.9.

$$M_c = 1 - \left(\frac{n^2-1}{n^2+2} \right) \quad (2.9)$$

According to the Herzfeld theory of metallization (Herzfeld 1927), materials with a metallization requirement close to 1 are typical insulators. Materials having a lower metallization criterion value, which is closer to zero, show metallic properties. So, using measured refractive index of the glass, its metallization criterion value has been determined in the present work.

2.6.7 UV-ViS-NIR/UV-Vis spectrometer

UV-Visible absorption spectroscopy is used to calculate the intensity of attenuation of light after it passes through a substance over various wavelengths. The amount of light absorbed by a sample is calculated by dividing the intensity of incident radiation (I_0) by the intensity of transmitted radiation (I). The amount of light absorbed by a sample is measured in terms of absorbance or transmittance. The absorption spectrum of samples is determined by plotting the absorbance against the wavelength or frequency of incoming radiation.

UV-Visible spectroscopy measures light intensity attenuation over a wavelength range after it passes through or reflects off a sample. UV-Visible absorption spectra are formed when an electron in a molecule transits from a lower energy level to a higher energy level after absorbing ultra-violet radiation of frequency. Because of the lack of long-range order, the conduction and valence bands in amorphous materials such as glasses have band tails rather than sharp cut-offs, so there is no sharp absorption edge for glasses.

To examine the electronic band structure of glasses, optical transitions, direct or indirect, occurring at the fundamental optical absorption edges are investigated. The absorption constant at the optical absorption edge is used to study optically induced electronic transitions. When a light wave interacts with a valence electron in a direct transition, the electron's wave vector remains unaltered and is lifted across the energy gap to the conduction band. However, in an indirect transition, the electron's wave vector interacts with lattice vibrations, causing a shift in the wave vector.

The optical absorption spectra of amorphous and crystalline materials can reveal information about their band structures (Tauc and Menth 1972). Tauc proposed in 1966 that the absorption coefficient $\alpha(\nu)$ can be connected to the optical band gap energy (E_{opt}) using a power law at the high energy area of the absorption edge. Davis and Mott gave this power-law a more generic expression in 1970, which is expressed as

$$\alpha(\nu) = B \frac{(h\nu - E_{opt})^\gamma}{h\nu} \quad (2.10)$$

where α is absorption coefficients, $h\nu$ is photon energy, E_{opt} is band gap energy, B is a constant, and γ is an index that takes the values 1/3, 1/2, 2, and 3 depending on whether the transition is direct forbidden, direct allowed, indirect allowed, or indirect forbidden, respectively (Rao and Shashikala 2014a). For amorphous materials like glasses, the index value $\gamma = 2$, which corresponds to indirect permitted transitions, is commonly chosen since measured absorption data fits the equation 2.10. Taking the square root of both sides of equation 2.10 may be rewritten as:

$$(\alpha h\nu)^{\frac{1}{2}} = B^{\frac{1}{2}}(h\nu - E_{opt}) \quad (2.11)$$

Equation 2.11 is the equation of a straight line with the optical band gap energy as its x-intercept. As a result, extrapolating the straight-line section of the graph to the x-axis at $y = 0$ yields the sample's band gap energy, E_{opt} (Bhattacharya and Shashikala 2018).

Due to the disorder in the material, many localized electron states are extending into the band gap, which appears as an exponential tail known as the Urbach Tail, which is described by the Urbach empirical rule as stated in equation 2.12, the linear variation in UV absorption, which follows an exponential behavior obeying Urbach's empirical relation (Anigrahawati et al. 2015a)

$$\alpha(\nu) = \alpha_0 \exp\left(\frac{h\nu}{E_u}\right) \quad (2.12)$$

Where α_0 is a constant and E_u is the Urbach energy

By applying the natural logarithm to both sides of equation 2.12, we get

$$\ln \alpha(\nu) = \left(\frac{1}{E_u}\right) h\nu + \ln \alpha_0 \quad (2.13)$$

It is in the form of a straight line with a gradient. The Urbach Energy E_u is the reciprocal of the slope of the linear section of the graph of $(\ln \alpha)$ versus photon energy $(h\nu)$.

In this work, the absorption data was recorded at room temperature from 200 to 800nm using UV-Vis-NIR spectrometer which is shown in Figure 2.12. (Central research Facility, NITK) [Lambda 950, Perkin Elmer, Singapore].



Figure 2.12 UV-Vis-NIR spectrometer (from Central research Facility, NITK) [Lambda 950, Perkin Elmer, Singapore].

2.6.8 Photoluminescence (PL) study

When a molecule absorbs a photon in the visible spectrum, one of its electrons is excited to a higher electron energy state. As the electron returns to a lower energy state, a photon is emitted from the molecule. This process is known as photoluminescence (Righini and Ferrari 2005).

The intensity of released photons as a function of either the excitation wavelength or the emission wavelength can be recorded to produce sample's

photoluminescence (PL) spectra. The emission spectrum is obtained by recording the intensity of emitted radiation as a function of wavelength after exciting the samples at a fixed wavelength and varying the excitation wavelength. Excitation spectra are typically acquired to determine the appropriate excitation wavelength for recording emission spectra for quantitative or qualitative analysis.

Rare-earth ion-doped glasses are a significant class of materials that can be productively explored utilizing PL methods(Righini and Ferrari 2005). Their influence is primarily due to the advancement of optical communications and the current demand for expanding optical fiber systems' bandwidth capacity.

In this work, the emission spectra of rare-earth-doped calcium Phosphate glass containing silver nanoparticles were recorded using Fluoromax-4 spectrofluorometer (Figure 2.13) and analyzed.



Figure 2.13 Fluoromax-4 Photoluminescence spectrometer (PL)

2.7 Error Analysis

No matter how thoroughly a measurement is done, there will always be some uncertainty(Taylor 1997). Since measurements are a necessary component of scientific investigations, it is critical to evaluate these uncertainties and reduce them as much as possible. In order to make the mistakes as modest as possible, error

analysis is thus used to investigate and evaluate these inescapable experimental uncertainties.

The standard deviation of the mean (SDOM) of all the measurements was used to determine the inaccuracy in the observed values in the current experimental measurements.

2.7.1 Standard Deviation of the Mean (SDOM) Calculation

The best estimate for the amount x is determined by taking the average or mean \bar{x} of "N" measurements of that quantity done using the same instrument and process, such as " x_1, x_2, \dots, x_N ."

Here, the calculation for \bar{x} is

$$\bar{x} = \frac{x_1 + x_2 + x_3 + \dots + x_N}{N} = \frac{\sum_i x_i}{N} \quad (2.14)$$

By calculating the standard deviation of the mean or the standard error of the N measurements, one may determine the degree of uncertainty in a variable, \bar{x} , as shown by the equation (2.15)

$$\sigma_{\bar{x}} = \frac{\sigma_x}{\sqrt{N}} \quad (2.15)$$

where $\sigma_{\bar{x}}$ represents the mean's standard deviation and σ_x represents the average measurement's uncertainty. Equation (2.16) provides the standard deviation σ_x value

$$\sigma_x = \sqrt{\frac{1}{N-1} \sum_i d_i^2} = \sqrt{\frac{1}{N-1} \sum_i (x_i - \bar{x})^2} \quad (2.16)$$

where, the divergence of the i^{th} measurement x_i from the mean value \bar{x} is given by $x_i - \bar{x} = d_i$. The measurement will be accurate if these discrepancies are extremely modest. Averaging the variances may not provide accurate measurement uncertainty since some deviations may be positive and some may be negative. In order to achieve a quantity with the same unit as the measurements, deviations are first squared to generate a set of positive numbers, and then the square root of the average of the set of positive numbers is obtained. The standard deviation, abbreviated as σ_x , or root

mean square (RMS) deviation of the measurements is found to be beneficial in describing the accuracy of the measurements.

To acquire uncertainty in the value of x , standard deviation of the mean ($\sigma_{\bar{x}}$) is recommended over standard deviation (σ_x). Due to the existence of factor \sqrt{N} in the denominator, σ_x will provide more accurate uncertainty in the final result as the number of measurements grows. But when the number of measurements increases, σ_x will not vary significantly. The final result (X) of N measurements is written as

$$X = \bar{x} \pm \delta_x = \bar{x} \pm \frac{\sigma_x}{\sqrt{N}} \quad (2.17)$$

CHAPTER 3

INFLUENCE OF (Er^{3+} , La^{3+} , Ce^{4+}) ADDITIONS ON PHYSICAL AND OPTICAL PROPERTIES OF $50\text{CaO}-50\text{P}_2\text{O}_5$ GLASSES

Overview

In this chapter, the effect of increasing the rare earth (La_2O_3 , CeO_2 , Er_2O_3) ions content on the structural, physical, and optical characteristics of melt-quenched calcium phosphate glasses in the series $50\text{P}_2\text{O}_5-(50-x)\text{CaO}-x\text{REI}$ ($x = 0$ to 5 mol%) were examined. Density measurements, X-ray diffraction (XRD), Fourier transformed infrared (FTIR) spectroscopy, Ultraviolet-Visible spectroscopy (UV-Vis), and Abbe Refractometer were utilized to examine the effect of the addition of rare-earth ions on physical, optical, and structural features. The X-ray diffraction method confirmed the synthesized glass samples to be amorphous. To calculate the optical band gap energy E_{opt} , UV-visible absorption spectra have been obtained. When rare earth oxides (Er_2O_3 , La_2O_3 , and CeO_2) were added to the host glass with different concentrations, the band gap energy slightly decreased. According to FTIR data, the glass network was primarily made up of metaphosphate (Q^2) units arranged in chains and rings, with smaller number of ultra-phosphate and pyrophosphate units. The density of prepared glasses was measured using the Archimedes method, and related parameters were calculated. These values are compared with the un-doped metaphosphate glass. Various physical characteristics have been studied, including Ion Concentration (N), Inter-nuclear distance (r_i), Polaron radius (r_p), Field Strength (F), and Metallicity Factor (M_c). Based on measured density, the concentrations of added rare-earth ions were calculated. With the increase in ion concentration, the inter-nuclear distance decreased, increasing field strength. With the inclusion of RE ions, optical band gap energy was slightly reduced. Due to its extremely high solubility of laser-active rare earth (RE) ions, phosphate glass has recently shown to be a promising alternative to the more conventional silica glass as a host material for solid-state laser oscillators and amplifiers.

3.1 Introduction

The present chapter deals with the synthesis and property studies of La_2O_3 , CeO_2 , and Er_2O_3 added calcium phosphate glasses. This study helps in understanding the effect of different rare earth oxide additions on structure, density, refractive index, and band gap energy of the synthesized glasses.

3.2 Results and discussion

A series of rare-earth (La^{3+} , Ce^{+4} , Er^{3+}) ions added phosphate glasses were prepared with the compositions listed in Table 2.2. The subsequent investigation was performed on the influence of adding REI on CPRE glasses with changes in the structural, physical, and optical properties of rare-earth ion doped calcium phosphate glasses of the series $50\text{P}_2\text{O}_5 - (50 - x) \text{CaO} - x\text{REI}$ ($x = 0, 1, 2, 3,$ and $5 \text{ mol.}\%$).

3.2.1 XRD Analysis

The X-ray diffraction analysis of the samples has been done to check their amorphous nature. The X-ray diffraction patterns of synthesized glass samples with Lanthanum, Cerium, and Erbium ions are shown in Figure 3.1(a), (b), and (c), respectively. The hump observed near $20\text{-}30^\circ$ is due to the short-range order of the glass network and is typical of all phosphate glasses (Shelby 2007; Venkateswara Rao and Shashikala 2014c). The prepared glasses were confirmed to be amorphous in nature.

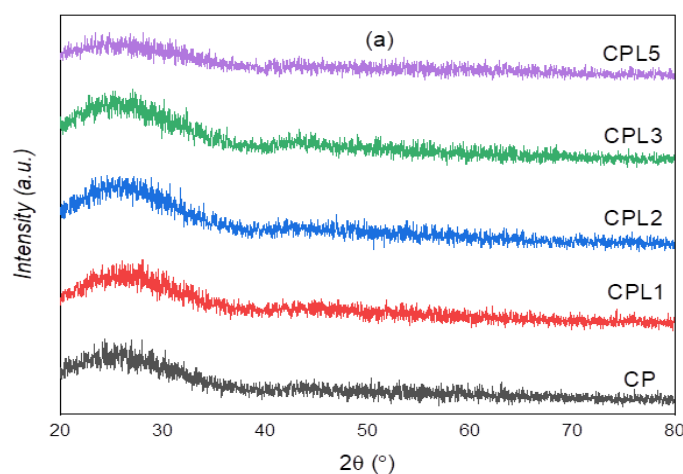


Figure 3.1(a) XRD pattern of the prepared samples of $50\text{P}_2\text{O}_5 - (50 - x) \text{CaO} - x\text{La}_2\text{O}_3$ ($x = 0, 1, 2, 3,$ and $5 \text{ mol.}\%$)

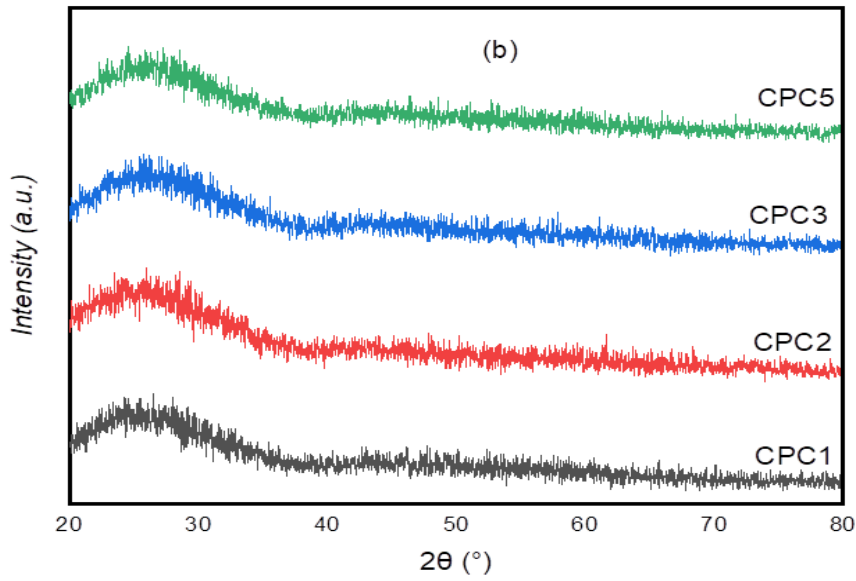


Figure 3.1(b) XRD pattern of the prepared samples of $50P_2O_5 - (50 - x) CaO - xCeO_2$ ($x = 1, 2, 3,$ and 5 mol. %)

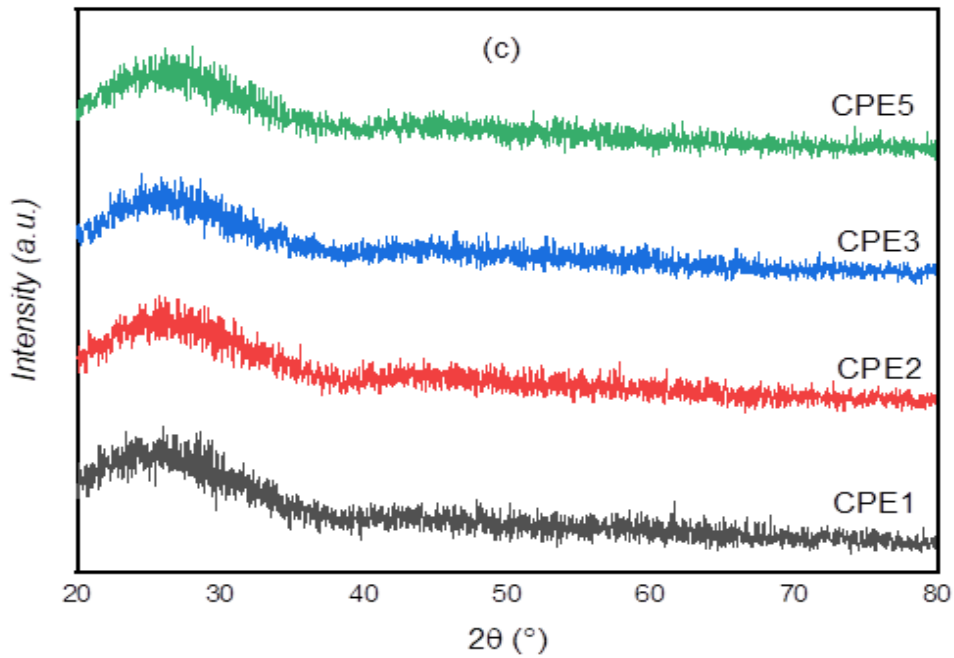


Figure 3.1(c) XRD pattern of the prepared samples of $50P_2O_5 - (50 - x) CaO - xEr_2O_3$ ($x = 1, 2, 3,$ and 5 mol. %)

3.2.2 Density and Molar volume

The annealed glasses' densities were measured using the Archimedes method with a 0.001 g precision (Anigrahawati et al. 2015b; Effendy et al. 2017; Shelby 2007) as presented in chapter 2 of this thesis, by weighing them while submerged in O-Xylene and in air at room temperature. The molar volume of the samples has been calculated using equation 2.3 given in chapter 2 of this thesis and it depends on the molar mass of the samples and density measured. Table 3.1(a), (b), and (c) show the measured values for density (ρ) and molar volume (V_m) for all the examined glass samples, and Figure 3.2 illustrates the variation of the glasses' density with rare-earth oxide content. It can be observed that the samples' densities increased when the rare earth ion concentrations in the glass matrix increased.

It can be seen from table 3.1(a) that the measured density of the calcium phosphate glass increased from 2.5991 g/cm³ to 2.8420 g/cm³ an increase of 8.54% on addition of 5 mol. % of La₂O₃. From figure 3.2(a) it can be observed that the increase in density is more up to 3 mol. % and not much between 3 mol. % and 5 mol. %. Similarly, the molar volume increased from 38.085 to 39.577 cm³ (3.76%), when the La₂O₃ content in the calcium phosphate glasses steadily increased from 0 to 5 mol. %.

Table 3.1(b) shows that the addition of 5 mol% CeO₂ increased the density of the calcium phosphate glass from 2.5991 g/cm³ to 2.7321 g/cm³, an increase of 4.86%. Figure 3.2(b) shows that the rise in density is more pronounced up to 3 mol% and barely noticeable between 3 mol% and 5 mol%. It can be seen from figure 3.2(b) molar volume decreasing up to 1 mol. % of CeO₂ and started to increase slightly from 38.085 cm³ to 38.575 cm³ after 2mol. % addition which is 1.27% increment.

It can be seen from table 3.1(c) that the measured density of the calcium phosphate glass increased from 2.5991 g/cm³ to 2.837g/cm³ an increase of 8.38% on addition of 5 mol. % of Er₂O₃. From figure 3.2(c) it can be observed that the increase in density is more up to 3 mol. % and not much between 3 mol. % and 5 mol. %. Similarly, the molar volume increased from 38.085 to 40.641 cm³ (6.28%), when the Er₂O₃ content in the calcium phosphate glasses steadily increased from 0 to 5 mol. %.

The heavier rare-earth (La^{3+} , Ce^{4+} , and Er^{+3}) ions with an atomic mass of 138.90, 140.126, and 167.26 g/mol, respectively, that were introduced to replace the lighter calcium ions (atomic mass = 40.078 g/mol.) may be the cause of the increase in density (Ahmed, Youssif, and Elzelaky 2019a). It is evident that the density is a valuable indication for examining the level of structural compactness and addition of rare earth ions causes the phosphate chains to depolymerize (A.V. et al. 2018b; Im et al. 2010; Liang et al. 2014) and the creation of NBOs, which expand the system's free spatial distances and increase the molar volume of the glass system (Mahraz et al. 2013). It can also be observed from figure 3.2 that the addition of rare earth oxides more than 3 mol. % does not increase density much. But in the case of Ce^{4+} added glasses, not much increase in density has been observed above 1 mol. % .

The presence of rare-earth ions helps to decrease the bond length or inter-atomic spacing between the atoms which may be attributed to the increase in the stretching force constant of the bonds inside the glass network. The development of non-bridging oxygen (NBO), which extends the network structure of Calcium-phosphate glass, may be accountable for the samples' increased molar volume. This might be caused by the inclusion of rare earth ions with larger radii than other glass matrix ingredients, which leads to the creation of non-bridging oxygens. Other researchers have also noted similar behaviour in Soda-Lime-Silicate and Boro tellurite glasses (Chimalawong et al. 2012; Damas et al. 2012).

Table 3.1(a) Density (ρ), Molar volume (V_m), Band gap Energy (E_{opt}) and Refractive Index (n) of $50\text{P}_2\text{O}_5 - (50 - x)\text{CaO} - x\text{La}_2\text{O}_3$ ($x = 0, 1, 2, 3, \text{ and } 5 \text{ mol. } \%$)

Sample code	Density (g/cm^3) (± 0.001)	Molar volume (cm^3)	Band gap Energy (eV)	Refractive Index(n) (± 0.001)
CP	2.5991	38.085	3.49	1.543
CPL1	2.7105	37.515	3.66	1.5311
CPL2	2.7652	37.749	3.29	1.5412
CPL3	2.8068	38.151	3.32	1.5491
CPL5	2.8420	39.577	3.17	1.6502

Table 3.1(b) Density (ρ), Molar volume (V_m), Band gap Energy (E_{opt}) and Refractive Index (n) of $50P_2O_5 - (50 - x) CaO - xCeO_2$ ($x = 0, 1, 2, 3, \text{ and } 5 \text{ mol. } \%$)

Sample code	Density (g/cm^3) (± 0.001)	Molar volume (cm^3)	Band gap Energy (eV)	Refractive Index(n) (± 0.001)
CP	2.5991	38.085	3.49	1.543
CPC1	2.6877	37.262	3.64	1.524
CPC2	2.7027	37.484	3.43	1.529
CPC3	2.7260	37.589	3.59	1.531
CPC5	2.7321	38.575	3.53	1.538

Table 3.1(c) Density (ρ), Molar volume (V_m), Band gap Energy (E_{opt}) and Refractive Index (n) of $50P_2O_5 - (50 - x) CaO - xEr_2O_3$ ($x = 0, 1, 2, 3, \text{ and } 5 \text{ mol. } \%$)

Sample code	Density (g/cm^3) ± 0.001)	Molar volume (cm^3)	Band gap Energy (eV)	Refractive Index(n) (± 0.001)
CP	2.5991	38.085	3.49	1.5430
CPE1	2.6694	38.305	3.03	1.5151
CPE2	2.7378	38.541	2.94	1.5191
CPE3	2.8003	38.846	2.87	1.5201
CPE5	2.837	40.641	2.76	1.5221

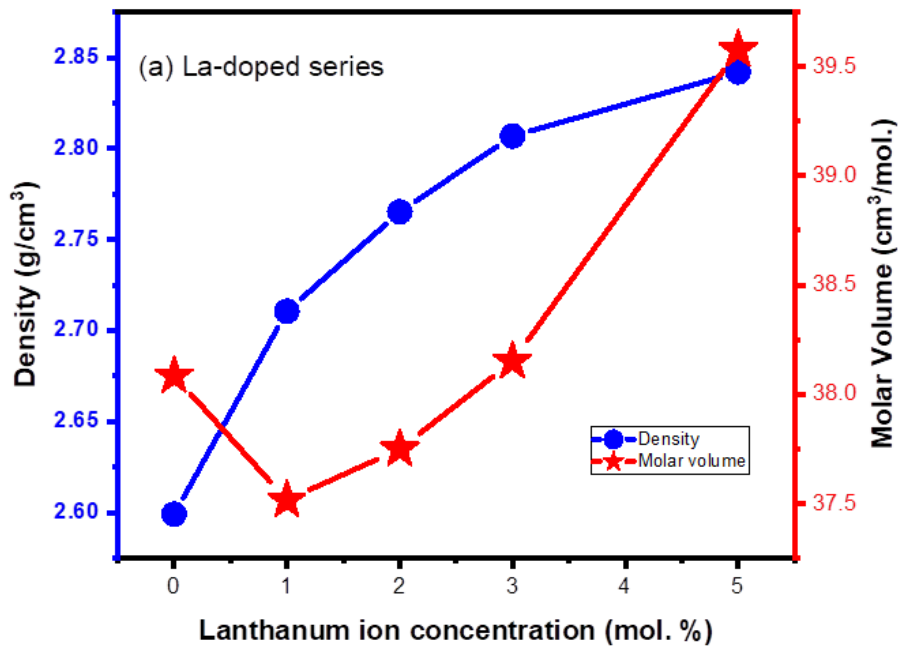


Figure 3.2(a) Variation of the density and molar volume of glasses in relation to the amount of La_2O_3

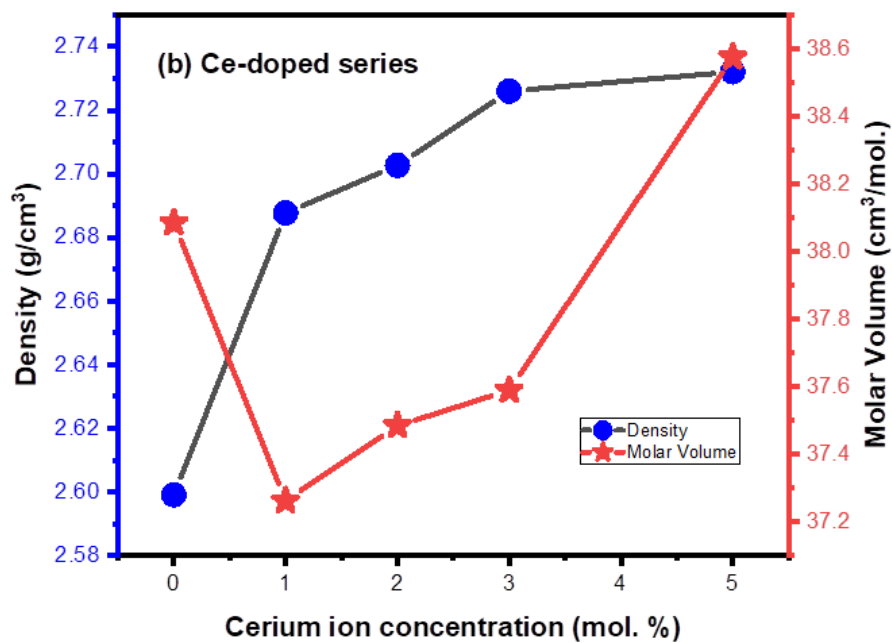


Figure 3.2(b) Variation of the density and molar volume of glasses in relation to the amount of CeO_2

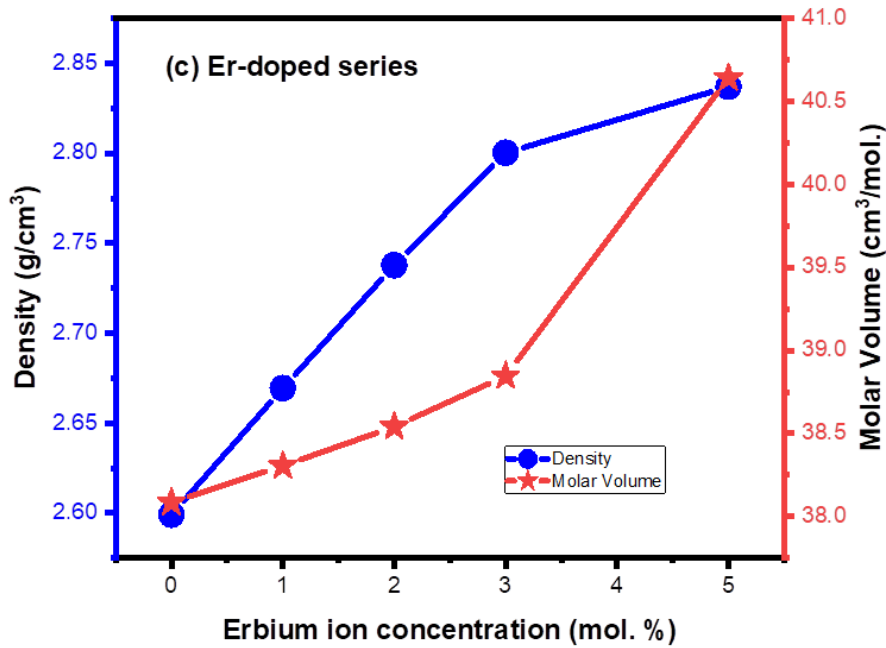


Figure 3.2(c) Variation of the density and molar volume of glasses in relation to the amount of Er_2O_3

3.2.3 Refractive Index and Metallization Criteria

In general, the index of refraction of a material is related to the optical density and the ability of speed of light in that material. Table 3.1(a), (b), and (c) provide a list of all the samples' refractive indices, as determined by the Abbe Refractometer. Generally, when glass density increases, the glass network becomes denser, the structure becomes more compact, and light propagates through the glass more slowly. As a result, the refractive index increases. As can be seen from Table 3.1, the index of refraction of Lanthanum oxide doped phosphate glasses has a higher value of 1.6502 compared to samples CP (1.543), CPE5 (1.5380), and CPC5 (1.5221). In general, the refractive index of a glass increases with its density. However, there does not exist an overall linear relationship between the refractive index and the density (Shelby 2007). The Lorentz Lorenz equation (Dimitrov and Komatsu 2010) presented as equation 2.9, described in chapter 2 of this thesis, was utilized to assess the samples' tendency for metallization, which can be used to estimate the material's metallic or insulating behavior based on this idea. Table 3.2 also includes a list of the values of M_c . Every sample has an M_c value greater than 0.63. The calculated theoretical values of the Metallicity factor (M_c) of Lanthanum doped glasses (0.6905 to 0.6351), Cerium doped

(0.6949 to 0.6872), and Erbium-doped (0.6984 to 0.6949) show that they are nearing unity rather than zero. This demonstrates that all samples tend more toward insulators, consistent with each sample's band gap being within the normal insulator range, as shown in Table 3.1.

3.2.4 Physical Parameters

For the prepared glasses, the concentration of RE ions(N), Polaron radius (r_p), inter-nuclear distance (r_i), and field strength (F) were calculated using the equations 2.4 - 2.7 as presented in chapter 2 of this thesis, and the values are tabulated in Table 3.2. From table 3.2 for the prepared samples, it can be seen that the value of ion concentration of rare earth ions is increased with increase ion concentrations. This may be due to the molecular mass of the rare earth oxides. It can be seen that the values of ion concentration (N) and field strength (F) increases as rare-earth ion content increases. In contrast, polaron radius (r_p) and inter-nuclear distance (r_i) act in a decreasing manner. The field strength (F) values are computed and shown in Table 3.2(Ahmed et al. 2019a). In general increase in ion concentration in a sample decreases the inter-nuclear distance leading to an increase in field strength. Similar variation is observed in the present work.

Table 3.2 Ion Concentration (N), Inter-nuclear distance (r_i), Polaron radius (r_p), Field Strength (F), and Metallicity Factor (M) of sample $50P_2O_5$ - CaO-REI (where REI= La, Ce, Er)

Sample code	Ion Concentration(N), $*10^{22}$ (ions/cm ³)	Inter nuclear distance(r_i), Å	Polaron radius (r_p), Å	Field Strength(F), $*10^{18}$ cm ⁻²	Metallicity Factor(M_c)
a) $50P_2O_5$ - (50 - X) CaO-XLa ₂ O ₃ (X = 0, 1, 2, 3, and 5 mol. %)					
CP	-	-	-	-	0.6847
CPL1	5.23	2.67	1.33	0.49	0.6905
CPL2	10.41	2.13	1.06	0.77	0.6856
CPL3	15.42	1.86	0.92	1.01	0.6818
CPL5	24.83	1.59	0.78	1.39	0.6351
b) $50P_2O_5$ - (50 - X) CaO-XCeO ₂ (X = 1, 2, 3, and 5 mol. %)					
CPC1	2.77	3.31	1.08	0.33	0.6994
CPC2	5.50	2.63	0.85	0.52	0.6955
CPC3	8.23	2.30	0.75	0.67	0.6915
CPC5	13.41	1.96	0.64	0.93	0.6872
c) $50P_2O_5$ - (50 - X) CaO-XEr ₂ O ₃ (X = 1, 2, 3, and 5 mol. %)					
CPE1	6.02	2.55	1.03	0.64	0.6984
CPE2	12.01	2.03	0.82	1.02	0.6964
CPE3	17.83	1.78	0.71	1.33	0.6959
CPE5	28.31	1.52	0.61	1.81	0.6949

3.2.5 FTIR studies

Fourier Transform Infrared (FTIR) Spectroscopy in the wave number range 400–4000 cm⁻¹ was carried out to investigate the modifications in the glass structure. Fourier Infrared transform spectrum of glasses is beneficial for qualitatively identifying glass-forming structural units. The Fourier transform infrared (FTIR) transmittance spectra of 50 mol. % P₂O₅ - (50-x) mol. %CaO-x mol. % REI (REI= La₂O₃, CeO₂, and Er₂O₃) glasses are shown in Figure 3.3(a)-(c). The bands of 1588 cm⁻¹, 1589 cm⁻¹, 1559 cm⁻¹ and 1591 cm⁻¹ are due to the P-OH or water (Ahmed, Youssif, and Elzelaky 2019b; A.V. et al. 2019b; Narayanan and Shashikala 2015c;

Shi et al. 2019; Venkateswara Rao and Shashikala 2014c). The other bands around 1332 cm^{-1} and 1406 cm^{-1} are assigned as P=O asymmetric stretching mode of phosphate tetrahedra and P=O stretching mode of the phosphate tetrahedra, respectively (Rai et al. 2011). The bands 1266 cm^{-1} to 1284 cm^{-1} are assigned to the asymmetric stretching vibrations of non-bridging oxygen of O-P-O in Q^2 species or PO_2 groups (Ahmed et al. 2019b; Li et al. 2019a; Rai et al. 2011; Venkateswara Rao and Shashikala 2014a). The bands near 1057 cm^{-1} to 1125 cm^{-1} show the presence of symmetric stretching vibrations of non-bridging oxygen of O-P-O linkage of $(PO_2)^-$ groups in Q^2 units (Li et al. 2019a). The other bands around 870 , 887 , 855 , and 911 cm^{-1} of the sample glasses of CP, CPL5, CPC5, and CPE5, are assigned as the asymmetric stretch of P-O-P, $V_s(P-O-P)$ linked with linear metaphosphate chain, while the bands at 749 cm^{-1} , 706 cm^{-1} and 760 cm^{-1} CP, CPL5 and CPE5 can be ascribed to symmetric stretching vibrations of P-O-P in the Q^2 tetrahedra $V_s(P-O-P)$ (Li et al. 2019a; Qian, Liang, et al. 2012a). The band recorded at 540 cm^{-1} for Lanthanum doped calcium phosphate glasses may be attributed to the bending mode of O-P-O linkage in the Q^1 structure (Li et al. 2019a; Qian, Liang, et al. 2012a) and 643 cm^{-1} (CPC5) and 649 cm^{-1} (CPE5) bands are due to bending mode of PO_4 in the Q^1 structure.

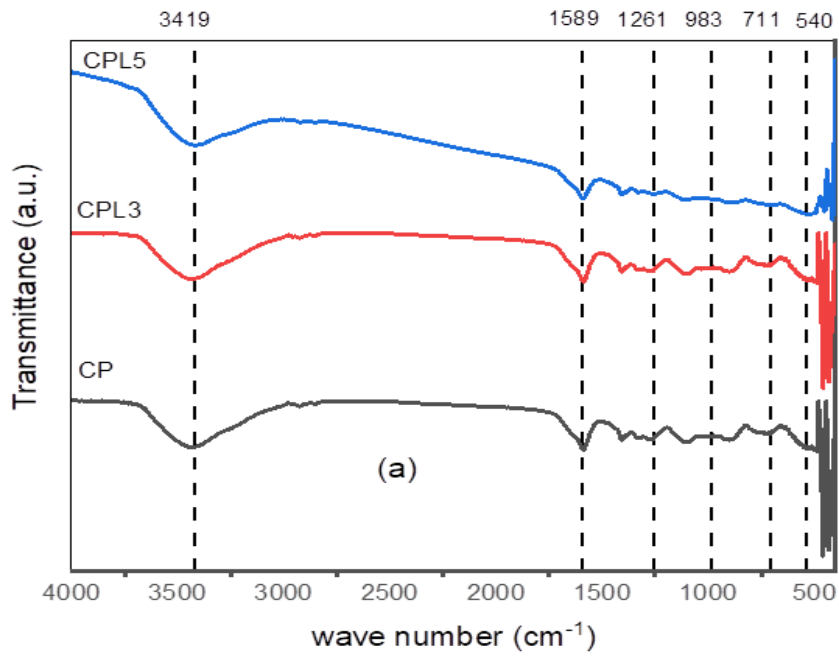


Figure 3.3(a) The FTIR spectra of $50\text{P}_2\text{O}_5-(50-x)\text{CaO}-x\text{La}_2\text{O}_3$ glasses

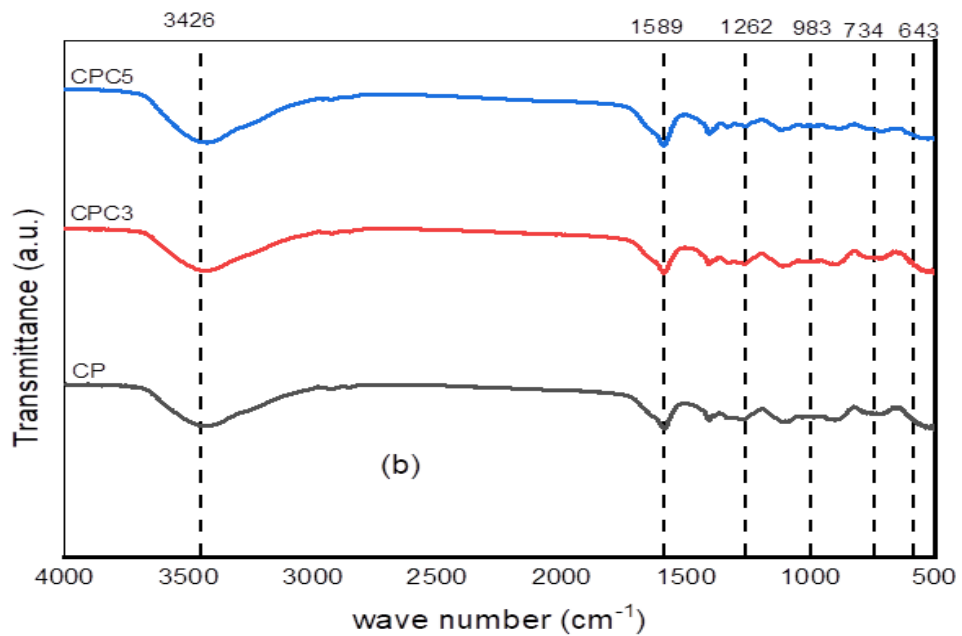


Figure 3.3(b) The FTIR spectra of $50\text{P}_2\text{O}_5-(50-x)\text{CaO}-x\text{CeO}_2$ glasses

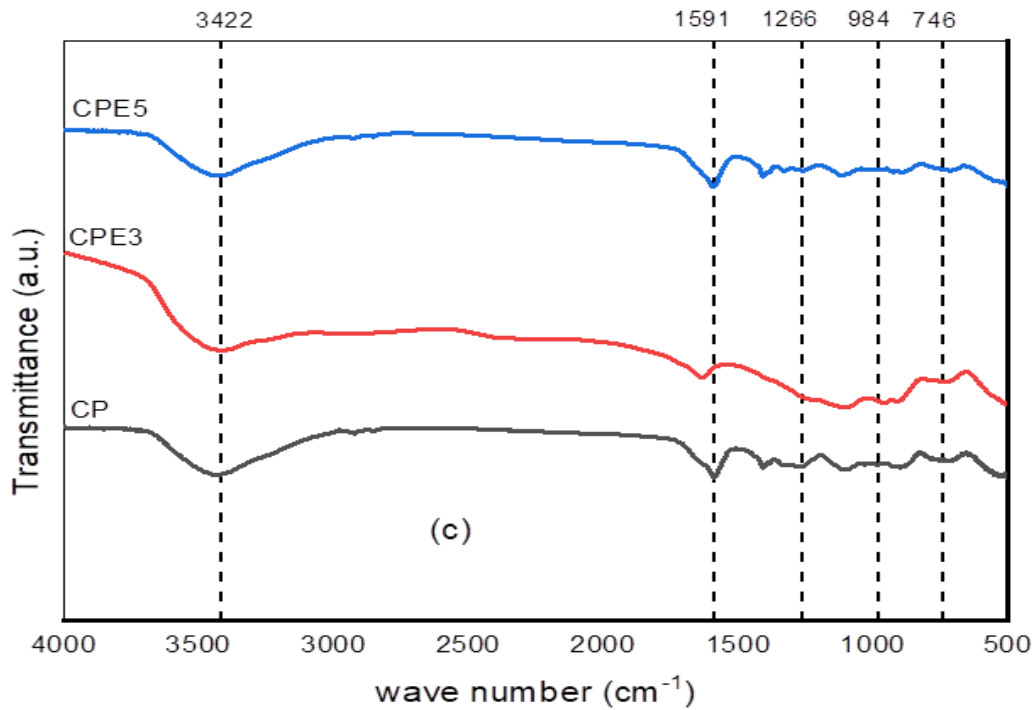


Figure 3.3(c) The FTIR spectra of 50 P₂O₅- (50-x) CaO-xEr₂O₃ glasses

The observed FTIR spectra peaks corresponding to the bonds and groups of the studied glasses show that adding Rare earth oxide does not change the basic calcium phosphate glass structure.

The observed FTIR spectra peaks corresponding to the bonds and groups of the studied glasses and their assignment are presented in Table 3.3.

Table 3.3 The FTIR spectra peaks of CP, La-doped, Ce-doped, and Er-doped glass samples with band assignments.

Wave numbers(cm ⁻¹)				Band assignment	References
CP	La-doped	Ce-doped	Er-doped		
-	540	-	-	Bending mode of O-P-O linkages in the Q ¹ structure	(Li et al. 2019a)
-	-	643	649	Bending mode of PO ₄ in the Q ¹ structure	
710-788	701-711	734	760	Symmetric stretching vibrations of P—O—P in the Q ² tetrahedra ν_s (P—O—P)	(Li et al. 2019a; Qian, Liang, et al. 2012a)
821-919	884-890	857	911	Asymmetric stretching vibrations of P—O—P linked with linear metaphosphate chain	(Li et al. 2019a; Qian, Liang, et al. 2012a)
984-1030	983-1022	966-1005	-	ν_s (PO ₃) symmetric	(Rai et al. 2011)
1091-1112	1088-1113	1057	1125	symmetric Stretching vibrations of non-bridging oxygen of O—P—O linkage of (PO ₂) ⁻ groups in Q ² Units	(Li et al. 2019a; Rai et al. 2011)
1266	1261	1262-1284	1263	asymmetric Stretching vibrations of non-bridging oxygen of O—P—O linkage of (PO ₂) groups in Q ² Units	(Li et al. 2019a; Rai et al. 2011)
1332	1328	1335	1333	P = O asymmetric Stretching mode of the Phosphate tetrahedra	(Rai et al. 2011)
1588	1589	1559	1591	P-OH bonds, Bending vibration of H-O-H group	(A.V. et al. 2018a; Qian, Liang, et al. 2012a; Shi et al. 2019)

3.2.6 UV-Vis spectroscopy study

At room temperature, the prepared glass samples' UV-Vis absorption spectra in the wavelength range of 200–800 nm were recorded using Ocean optics uv-vis spectrometer. Figures 3.4(a), 3.5(a), and 3.6(a) display the absorption spectra as a function of wavelength for 50P₂O₅ - (50 - x) CaO-x REI (REI = La₂O₃, CeO₂, and Er₂O₃) glass samples. Using the fundamental absorption edges of the absorption spectra, the optical transition and electronic band structure of crystalline and non-crystalline materials were investigated (Tauc and Menth 1972). Davis and Mott's theory (Anigrahawati et al. 2015b; A.V. et al. 2018b; Hraiech et al. 2013a) has been utilized to calculate the optical band gap energy of the samples.

The Tauc (Tauc and Menth 1972) plot of optical absorption spectra for the samples of (Lanthanum, Cerium, Erbium oxide) doped series of calcium phosphate glasses is shown in Figures 3.4(b), 3.5(b), and 3.6(b), respectively. The optical absorption, $\alpha(\nu)$ at higher energy ($\geq 10^4 \text{ cm}^{-1}$) above the exponential tail follows the power law given by Davis and Mott (Anigrahawati et al. 2015b)

$$\alpha(\nu) = \frac{B(h\nu - E_g)^n}{h\nu} \quad (3.1)$$

Where n is 2 or 1/2, either indirect or direct, E_g optical band gap energy, $\alpha(\nu)$ is absorption coefficient

The band gap energy values are shown in Table 3.1(a), (b), and (c). Table 3.1(a-c) show E_g values to decrease when RE ion concentrations increase. The indirect band gap energy of the series La oxide-doped varied from 3.66 to 3.17 eV, Ce oxide-doped varied from 3.64 to 3.43 eV, and Er oxide -doped varied 3.49 to 2.76 eV as shown in Tables 3.1. The increase in non-bridging oxygens in the glass network causes this decrease.

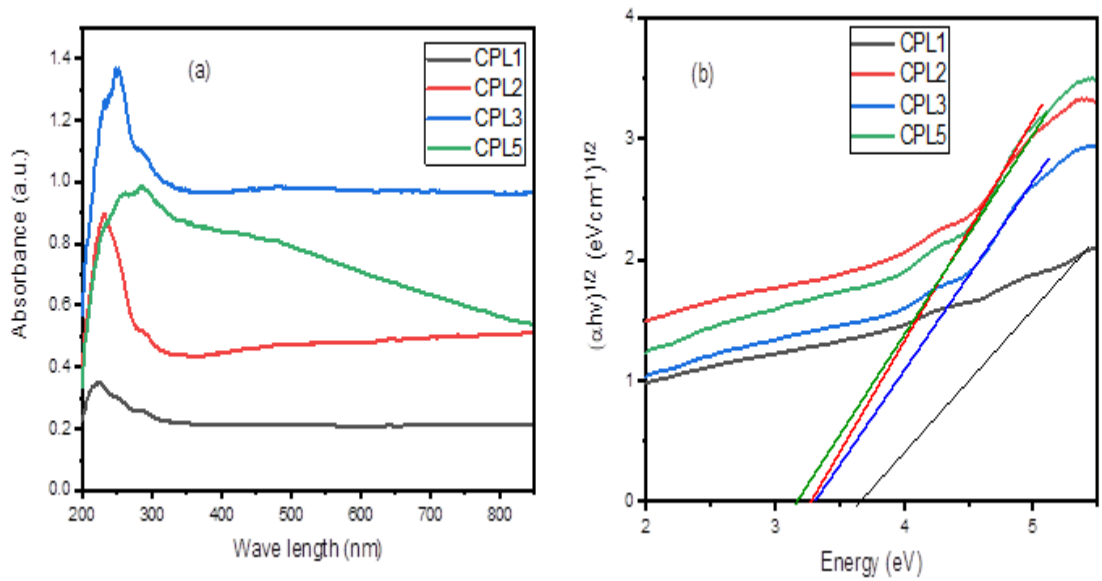


Figure 3.4 The UV-Vis spectra of $50\text{P}_2\text{O}_5-(50-x)\text{CaO}-x\text{La}_2\text{O}_3$ glasses (a) absorbance and (b) optical band gap energy obtained from Tauc plots.

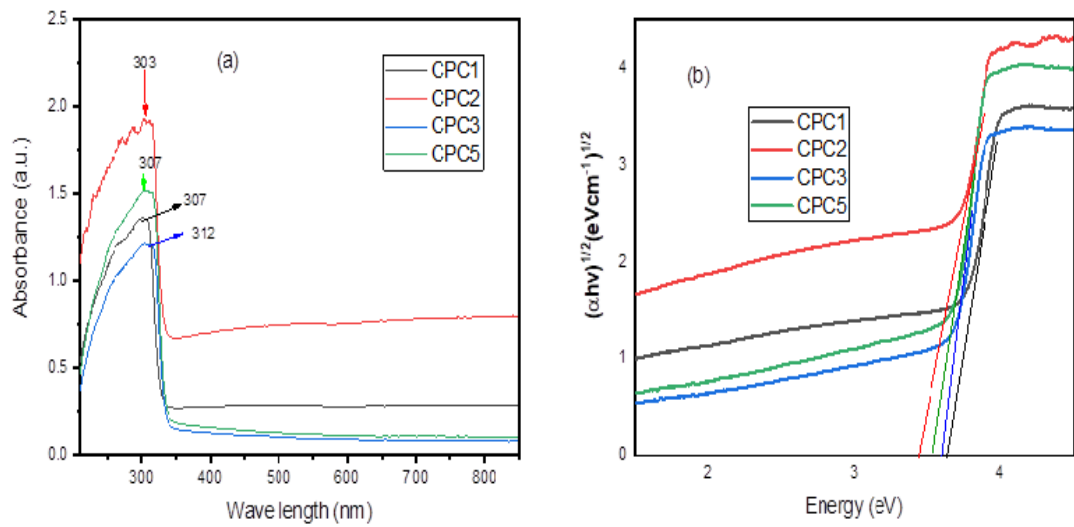


Figure 3.5 The UV-Vis spectra of $50\text{P}_2\text{O}_5-(50-x)\text{CaO}-x\text{CeO}_2$ glasses (a) absorbance and (b) optical band gap energy obtained from Tauc plots.

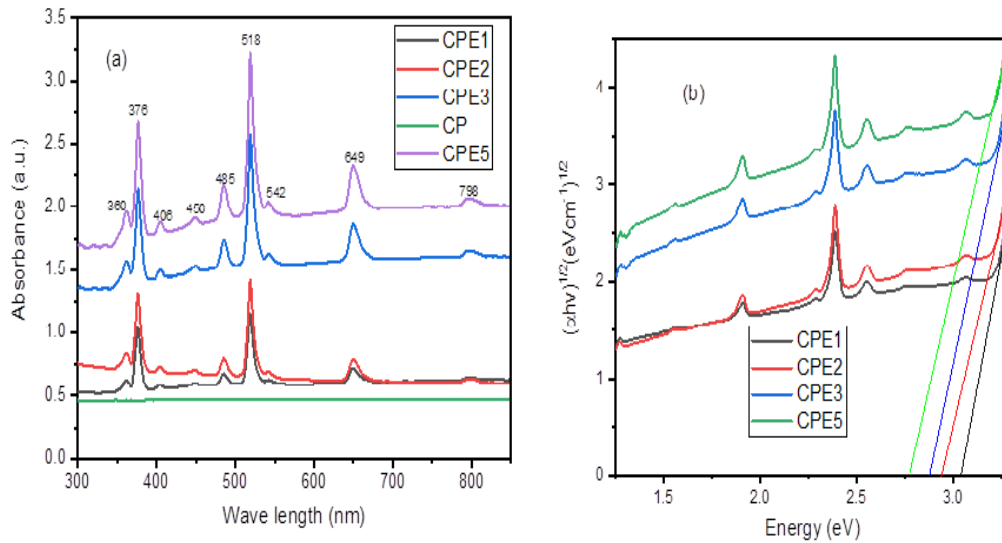


Figure 3.6 The UV-Vis spectra of $50P_2O_5-(50-x)CaO-xEr_2O_3$ glasses (a) absorbance (b) optical band gap energy obtained from Tauc plots

3.3 Conclusions

Rare earth (Er^{3+} , La^{3+} , Ce^{4+}) ions added to calcium phosphate glasses were synthesized by melt quenching. The influence of rare-earth oxide doping on the physical, optical, and structural properties of calcium phosphate glass was investigated. The FTIR study showed that adding up to five mol. % of rare earth (Lanthanum, Cerium, and Erbium) oxides added to the calcium phosphate glass did not affect the primary phosphate glass network. Results from XRD showed that the glasses remain amorphous after addition. The densities of samples increased by replacing the CaO with La_2O_3 , CeO_2 , Er_2O_3 , which could be due to rare earth ions higher molecular weight than the other oxides in the glass matrix and cation field strength. NBO production causes an increase in molar volume. The optical absorption edge shifted to longer wavelengths with increased REI content, and the optical band gap decreased. More non-bridging oxygens are produced as the REI content increases, enhancing the refractive indices. With the increase in ion concentration, the inter-nuclear distance decreased, increasing the field strength.

CHAPTER 4

STATISTICAL OPTIMIZATION OF MELT-QUENCHING PROCESS PARAMETERS OF RARE-EARTH IONS DOPED CALCIUM PHOSPHATE GLASSES USING TAGUCHI METHOD

Overview

In this chapter, usage of the Taguchi method of Design of Experiments is examined. For this purpose, the melt-quenching approach was used to synthesize rare earth (La^{3+} , Ce^{4+}) ion doped glasses $50\text{P}_2\text{O}_5 - (50-x) \text{CaO}-x\text{REI}$, where REI stands for the added rare earth ion and $x=1$ to 3mol.% as L_9 orthogonal array. The amorphous nature of the generated glasses was established using X-ray diffraction (XRD). The Taguchi method of Design of Experiments (DOE) applied to L_9 orthogonal array to optimise the process parameters of glass preparation utilising the melt quenching technique is explained in this chapter. It was investigated how the response parameter was affected by process variables such as composition, melting temperature, and melting duration. The controllable process parameters with the greatest influence on the response parameter (density) were identified using ANOVA on S/N ratios of physical or optical components. Using Minitab software, main effects plots and response tables were used to identify the ideal process parameter circumstances that would result in the most palatable and ideal values of the response parameter (density). Analysis of variance (ANOVA) revealed that REI content was the sole factor significantly affecting a number of performance indicators, with a 95% confidence level. The estimated value and the empirically determined value of the density of glass synthesised under optimal conditions were more closely related to the ideal set of predicted value.

4.1 Introduction

An effective method for choosing the ideal inputs and parameter settings for a high-quality output is experiment design. An important part of the experiment design is choosing the variables that have an impact on the product's attributes. As many parameters as possible should be used in the design to quickly identify non-significant parameters (Mohan et al. 2005).. Using simulation or the conventional trial-and-error

method, previous investigations in glass research have primarily concentrated on the impact of batch composition changes on the characteristics of glass samples. Using orthogonal arrays, the Taguchi technique determines the parameters that affect the process and the levels at which they should be modified. Before optimizing a design to reach mean objective values for output characteristics, the Taguchi method is one of the most influential experimental procedures for decreasing variance in design parameters. It uses orthogonal arrays to evaluate all design issues with the fewest possible experiments. As three process parameters and three levels are selected for optimizations, the L_9 is chosen in the current project. The factors impacting the operation and the levels at which they should be modified are organized using orthogonal arrays (Macioszczyk et al. 2015).

4.2 Results and discussion

Glasses were made in accordance with the experimental design described in Table 2.5 of chapter 2 of this thesis. The produced samples' amorphous nature, short-range structure were examined using X-ray diffraction and the Archimedes method is applied for density measurements with xylene ($\rho = 0.866 \frac{g}{cm^3}$) as the immersion liquid.

4.2.1 X-ray Diffraction study

Figure 4.1(a) and 4.1(b), show X-ray diffraction pattern of synthesized glass samples obtained using a Rigaku Miniflex 600 x-ray diffractometer, at a scanning rate of 2° per minute. The samples were scanned with $Cu-K_\alpha$ radiation of 1.542 \AA through 2θ ranging from 20° to 80° . The broad hump seen in Figure 4.1 in the region 20° - 30° is caused by the glass network's short-range order, which is common in all phosphate glasses (Dutebo and Shashikala 2020; Narayanan and Shashikala 2015a; Shelby 2007) indicating the synthesized samples to be amorphous in nature.

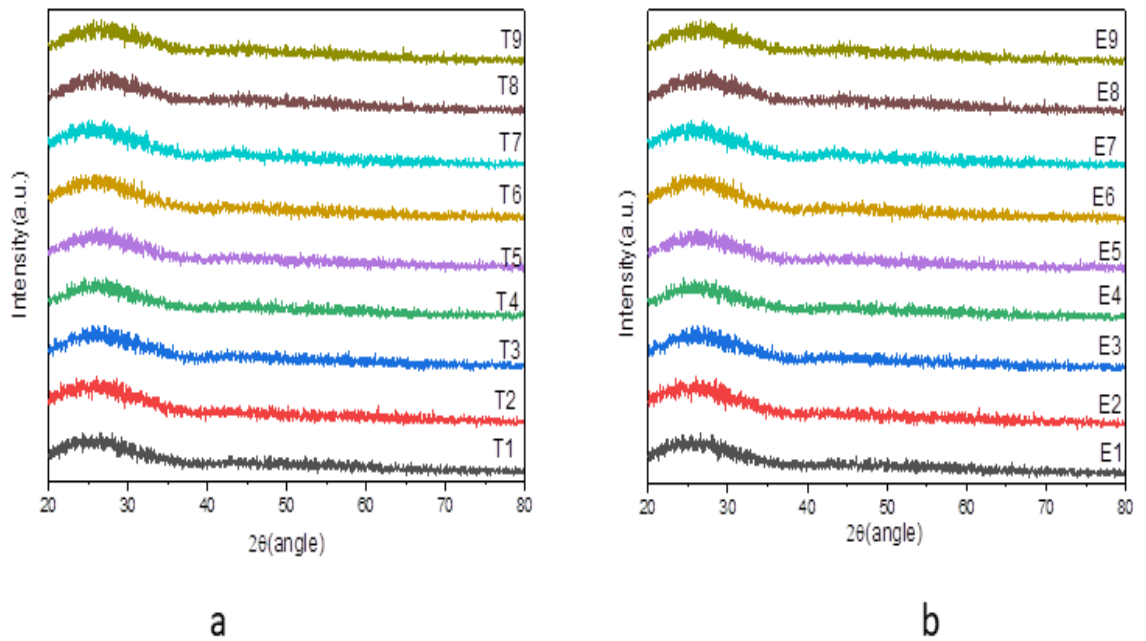


Figure 4.1 Patterns of X-ray diffraction in (a) La^{3+} doped and (b) Ce^{4+} doped samples prepared for optimization

4.2.2 Application of Design of experiment (DOE) Taguchi Method to glasses synthesized as L_9 orthogonal array

By using design of experiments (DOE) to optimise the parameters that affect a material's properties, one can produce a material with improved properties (Montgomery 2017; Narayanan et al. 2015). The statistical design of experiments is a vital tool for understanding the relationships between the various controllable parameters and for locating the crucial factor that affects a material's properties.

The process parameters used in this experiment, as well as their levels, are listed in Table 4.1.

Table 4.1: Melt-quenching Process parameters used in the experiment

Process Parameters	Symbol	High	medium	Low
Compositions (mol.%)	A	3	2	1
Melting temperature(T) , °C	B	1300	1250	1200
Melting time (Time), min	C	90	60	30

Using orthogonal arrays, the Taguchi technique determines the parameters that affect the process and the levels at which they should be modified. For optimizing a design to reach mean objective values for output characteristics, the Taguchi method is one of the most effective experimental procedures for decreasing variance in design parameters. It uses orthogonal arrays to evaluate all design issues with the fewest possible experiments. As three process parameters and three levels of them are selected for optimizations L_9 orthogonal array is chosen in the current project.

Taguchi's method is used to convert the acquired values of the signal-to-noise (S/N) ratios of the response parameter at various levels of process parameters. The (S/N) ratios describe the variation in response characteristic across several experimental levels of process parameter circumstances. The optimal situation for testing is at the process parameter level when the response parameter has the highest S/N ratio and lowest variable features.

S/N ratios are classified as smaller- is- better, larger- is- better, or nominal is the best, depending on the desired performance features. Larger is better for glass density in this study is chosen, which is ideally suited for many technical applications. The density of the synthesized glasses has been chosen as a response parameter in the present work as it is one of the basic physical properties that have to be qualified for the glass application.

4.2.3 Melt-quenching process parameter statistical optimization

For each factor level combination, mean value of density which is an average of three trials of the same composition and the (S/N) signal-to-noise ratios are determined. In the present work, a larger is a better condition for density is considered due to the fact that the most glass technologies demand dense and stronger glasses for various applications.

The following is the formula for the larger-is-better S/N ratio for the response parameter (Mohan et al. 2005):

$$\frac{S}{N} = -10 \log \left\{ \frac{1}{n} \sum_{i=1}^n \frac{1}{y_i^2} \right\} \quad (4.1)$$

Where y_i is the average density of i^{th} experiment and n is the total number of experiments

The mean density values of (Lanthanum, Cerium) ion-doped Phosphate glasses, as well as their S/N ratios, are shown in Table 4.2.

After calculating S/N ratios with the larger is better formula, response tables, and the major effect of each level of process parameters (compositions, melting/soaking temperature, and durations of melting) on density were created. Table 4.3 and Table 4.4 are the response tables for S/N ratio for larger is better and the mean of response parameter, density. The main effect plot for the S/N ratio of density is depicted in figure 4.2.

Table 4.2 S/N ratio and mean values of a measured density of (La^{3+} , Ce^{4+}) doped Phosphate glass

Exp.	La^{3+} doped		Exp.	Ce^{4+} doped	
	Mean Value	S/N ratios		Mean value	S/N ratios
T1	2.7370	8.74550	E1	2.7230	8.70095
T2	2.8130	8.98339	E2	2.7270	8.71370
T3	2.7290	8.72007	E3	2.7150	8.67540
T4	2.7015	8.63210	E4	2.6430	8.44194
T5	2.7230	8.70095	E5	2.6810	8.56594
T6	2.7630	8.82762	E6	2.6570	8.48783
T7	2.6590	8.49437	E7	2.6100	8.33281
T8	2.7210	8.69457	E8	2.6920	8.60150
T9	2.7130	8.66900	E9	2.6910	8.59827

Table4.3 (a) Response table for Signal- to- Noise(S/N) ratio for larger is better characteristics of Lanthanum oxide doped sample

Level	La^{3+} compositions (mol%)	Temperature (C)	Time (min.)
	A	B	C
1	8.619	8.739	8.638
2	8.720	8.793	8.761
3	8.816	8.624	8.756
Delta	0.197	0.169	0.123
Rank	1	2	3

Table 4.3 (b) Response table for Signal- to- Noise(S/N) ratio for larger is better characteristics of Cerium oxide doped sample

Level	Ce ⁴⁺ Compositions (mol. %)	Temperature(°C)	Time (min)
	A	B	C
1	8.511	8.587	8.525
2	8.499	8.627	8.585
3	8.697	8.492	8.597
Delta	0.198	0.135	0.072
Rank	1	2	3

Table 4.4 (a) Response table for means of density of Lanthanum oxide doped

Level	La ³⁺ compositions (mol. %)	Temperature (°C)	Time (min.)
	A	B	C
1	2.698	2.735	2.704
2	2.729	2.752	2.742
3	2.760	2.699	2.740
Delta	0.062	0.053	0.039
Rank	1	2	3

Table 4.4 (b) Response tables for means of density of Cerium oxide doped

Level	Ce ⁴⁺ compositions (mol. %)	Temperature (°C)	Time (min)
1	A	B	C
2	2.664	2.688	2.669
3	2.660	2.700	2.687
4	2.722	2.659	2.691
Delta	0.061	0.041	0.022
Rank	1	2	3

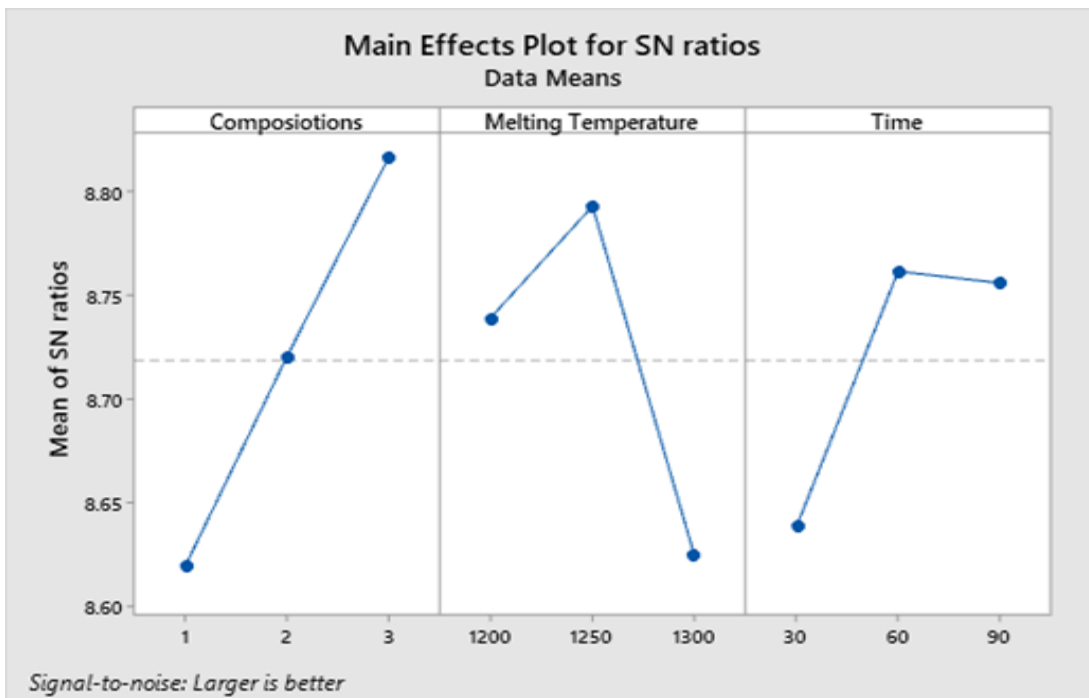


Figure 4.2(a) Main effects plots for Signal-Noise ratio of the density of Lanthanum oxide doped glass

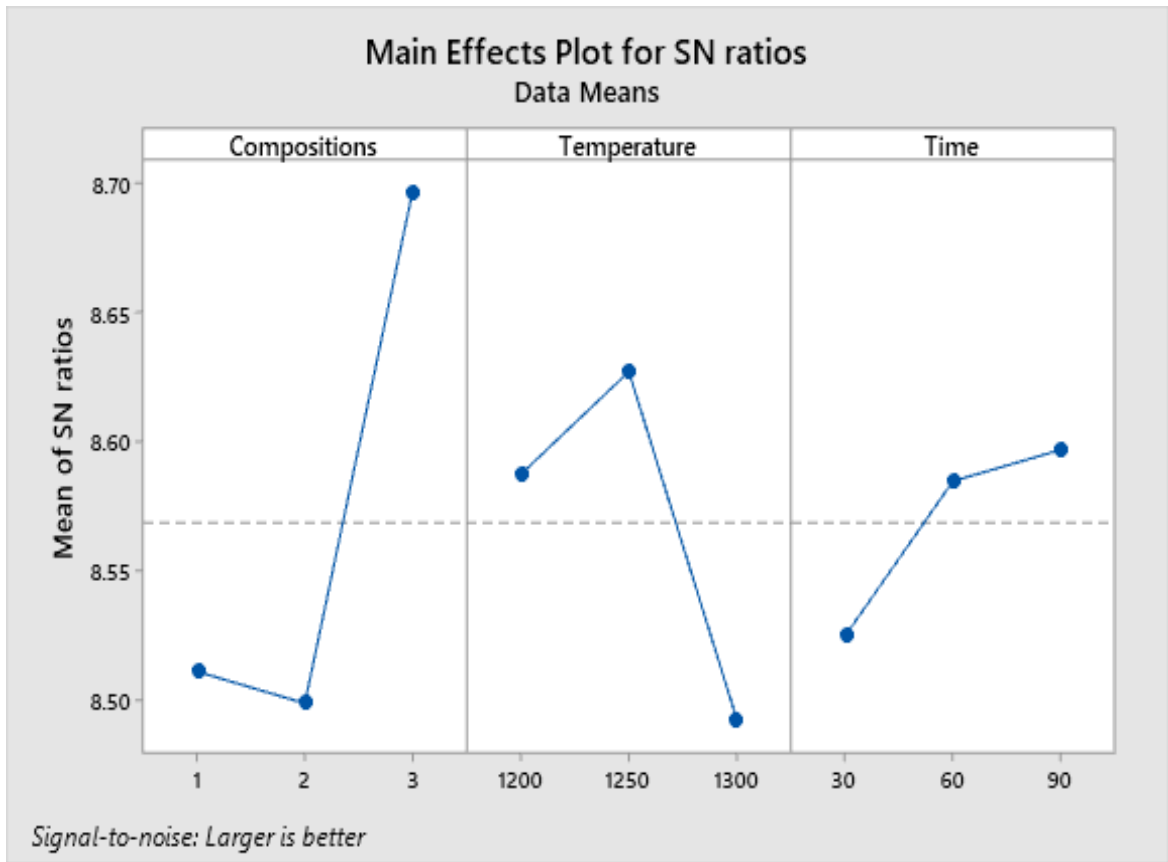


Figure 4.2(b) Main effects plots for Signal-Noise ratio of the density of Cerium oxide doped glasses

The Delta value shown in table 4.3 is obtained by finding out the difference between the maximum and minimum values of mean S/N ratios of a particular response parameter at a particular level. Since the larger the better condition is chosen, the maximum delta value is awarded rank 1 and so on. Table 4.3a, Table 4.3b, and Figure 4.2 reveal that the rare earth ion composition has the greatest effect on the density signal-noise-ratios (rank1), while the duration of the soaking time has the least effect (rank3). Similar delta values obtained and rank awarded for average densities are shown in table 4.4. The major effect plot in figure 4.2 demonstrates, that compositions (A, rank 1, level 3), melting temperature (B, rank2, level2), and durations(C, rank3, level2) have a maximum value of S/N ratios satisfying larger-the better conditions.

So, A₃B₂C₂ combination is the ideal setting for experimenting to produce a larger density for Lanthanum oxide doped Calcium phosphate glasses, on the other hand, A₃B₂C₃ combinations correspond to cerium doped glass samples.

The Signal-Noise ratio of the density is subjected to Analysis of Variance (ANOVA) using the software Minitab19 to identify particular elements that have a substantial impact on the response parameter. The composition of both Lanthanum (La³⁺) and Cerium (Ce³⁺) ions has a substantial impact on the density of the glass, as indicated in ANOVA results in Table 4.6 with a 95% confidence level. The major parameters collected by ANOVA are utilized to forecast the ideal density value.

Table 4.5 Analysis of Variance (ANOVA) for Transformed Response a) Lanthanum oxide doped glasses and b) Cerium oxide doped glasses

a) La³⁺-doped glasses

Source	DF	Seq SS	Contribution	Adj SS	Adj MS	F-Value	P-Value
La ³⁺	2	0.005687	40.99%	0.00568	0.00284	6.63	0.131
Composiotion (mol%)				7	4		
Melting Temperature(c)	2	0.004440	32.00%	0.00444	0.00222	5.17	0.162
Time(Min.)	2	0.002890	20.83%	0.00289	0.00144	3.37	0.229
				0	5		
Error	2	0.000858	6.19%	0.00085	0.00042		
				8	9		
Total	8	0.013875	100.00%				

b) Ce⁴⁺-doped glasses

Source	DF	Seq SS	Contribution	Adj SS	Adj MS	F-Value	P-Value
Ce⁴⁺ Composiotions (mol. %)	2	0.017122	88.48%	0.017122	0.008561	41.85	0.023
Melting Temperature(°C)	2	0.001104	5.70%	0.001104	0.000552	2.70	0.270
Time(Min.)	2	0.000717	3.71%	0.000717	0.000359	1.75	0.363
Error	2	0.000409	2.11%	0.000409	0.000205		
Total	8	0.019352	100.00%				

From Table 4.5a (La³⁺ doped), it can be observed that the contributions of compositions, melting temperature, and duration of melting are 40.99%, 32.00%, and 20.83%, respectively, similarly, from Table 4.5b, it can be seen that the compositions(88.48%), melting temperature(5.70%), and duration of melting(3.71%) in Cerium doped calcium phosphate glasses according to ANOVA for transformed responses. From this reading, it can be concluded that the density of Lanthanum ion-doped glasses is impacted significantly by compositions and melting temperature parameters. But for cerium doped samples the most significant affecting parameter is Composition.

Following equation can be used to estimate optimal response parameter values.

$$Y_{opt} = Y_m + \sum_{i=1}^n (Y_i - Y_m) \quad (4.2)$$

Where Y_{opt} , Y_m and Y_i are the response parameters' optimum values, overall mean value and mean values at optimal levels, where n is the number of process parameters that have a substantial impact on the response.

Table 4.6 optimized process parameters and the corresponding density values

Response Parameters	Density	
	La ³⁺ -doped	Ce ⁴⁺ -doped
Optimal parameters confirmation	A ₃ B ₂ C ₂	A ₃ B ₂ C ₃
Significant parameters (95% confident level)	A,B	A
Predicted optimum value	2.722	2.673
Experimental value at an optimum level	2.737	2.672

Table 4.6 illustrates the experimental value of response achieved by repeating the confirmatory experiment at the optimum level of process parameters, as well as the ideal density value predicted using equation(4.2). The experimental density values found by doing the confirmatory experiments at the optimum level for Lanthanum oxide doped (A₃B₂C₂) and Cerium oxide doped (A₃B₂C₃) glasses show good agreement with the predicted values.

4.3 Conclusions

The melt-quenching process was used to make rare earth (La³⁺, Ce⁴⁺) ions doped 50P₂O₅ - (50-x) CaO-xREI glasses (where RE indicates rare-earth ions and x=1 to 3mole %). The amorphous behavior of the produced glasses was confirmed using X-ray Diffraction analysis. The Taguchi approach of Design of Experiments (DOE) with orthogonal array (L₉) was used to optimize the process parameters of glass preparation utilizing the melt quenching technique. The influence of process variables composition, melting temperature, and melting time on the response parameter (density) was investigated. The rare-earth ions (Lanthanum, Cerium) composition has a vital effect on the density S/N ratio and has a higher percentage of contribution in comparison with melting temperature and durations of melting. It has been discovered that as the rare-earth ion content rises, density rises as well. Using the primary effect plot of the S/N ratio, the ideal condition for density is found to increase the quality of the response parameter.

CHAPTER 5

EFFECT OF RARE EARTH ION DOPING ON THE PHYSICAL, STRUCTURAL AND OPTICAL PROPERTIES OF SILVER OXIDE-CONTAINING CALCIUM PHOSPHATE GLASSES

Overview

This chapter presents the structural, physical, and optical properties of $50\text{P}_2\text{O}_5$ - $(50-x)\text{CaO}$ - $x\text{Er}_2\text{O}_3$ - $4\text{Ag}_2\text{O}$ - 4SnO (mol.%) glasses. The composition and nomenclature of these glasses are shown in Table 2.4. A series of calcium phosphate glasses with erbium oxide containing equal amounts of silver oxide and Tin oxide were synthesized using the melt-quenching process. X-ray diffraction (XRD), SEM with EDAX, Fourier transform infra-red (FTIR), UV-Vis-NIR, and density measurements were used to evaluate the produced glass samples at room temperature. The XRD spectra obtained in this study showed that the glass samples were amorphous. Molar volume and atomic packing density were derived from observed density to analyze structural changes in the glass matrix. The density measurements showed that the density increased linearly with the concentration of erbium oxide, from 2.817 to 3.078 g/cm^3 indicating that the glass strength increased. Similarly, the molar volume of the sample increased from 37.951 to 42.217 cm^3/mol . Due to the presence of erbium ions, UV-Vis spectroscopy revealed nine f-f electronic transitions for the examined system. With the partial replacement of CaO with Er_2O_3 in the glass batch, optical parameters of synthesised samples, such as optical band gap energy, decreased while Urbach energy and refractive index increased. The calculated changes in measured optical characteristics were supported by calculations of theoretical optical basicity and metallization criteria of glasses. Furthermore, the values of optical band gap energy (E_g) demonstrated that when the erbium ion content grows, the E_g values fall, owing to the increase in network's non-bridging oxygen atoms. Fourier-transformed infrared spectroscopy was used to investigate the glasses' local structure. The results revealed that the glass network primarily comprised metaphosphate units, with smaller amounts of ultraphosphate and pyrophosphate units.

5.1 Introduction

Among the various rare earth oxides doped calcium phosphate glasses, Erbium oxide doped calcium phosphate glass system was selected to add silver oxide and an equal amount of tin oxide as a reducing agent.

5.2 Results and discussion

Erbium oxide-doped CPAS glasses with the compositions listed in Table 2.2 were prepared. Absorption spectra and FTIR spectra were analysed. The following sections explain the experimental results of these glasses.

5.2.1 X-ray diffraction study

Figure 5.1 shows the XRD patterns for Erbium ion-doped $50\text{P}_2\text{O}_5 - (50-x) \text{CaO} - x\text{Er}_2\text{O}_3 - 4\text{Ag}_2\text{O} - 4\text{SnO}$ phosphate-based glass samples. The samples were analyzed using a Rigaku Miniflex 600 X-ray diffractometer, and at a scan rate of 2degree per minute, the samples were scanned with Cu-K_α radiation of 1.542\AA through 2θ ranging from 10 to 80 degrees. The hump seen between 20° - 30° is caused by the glass network's short-range order, which is common in all phosphate glasses(Dutebo and Shashikala 2020; Hraiech et al. 2013b; Shelby 2007). The glasses that had been made were amorphous

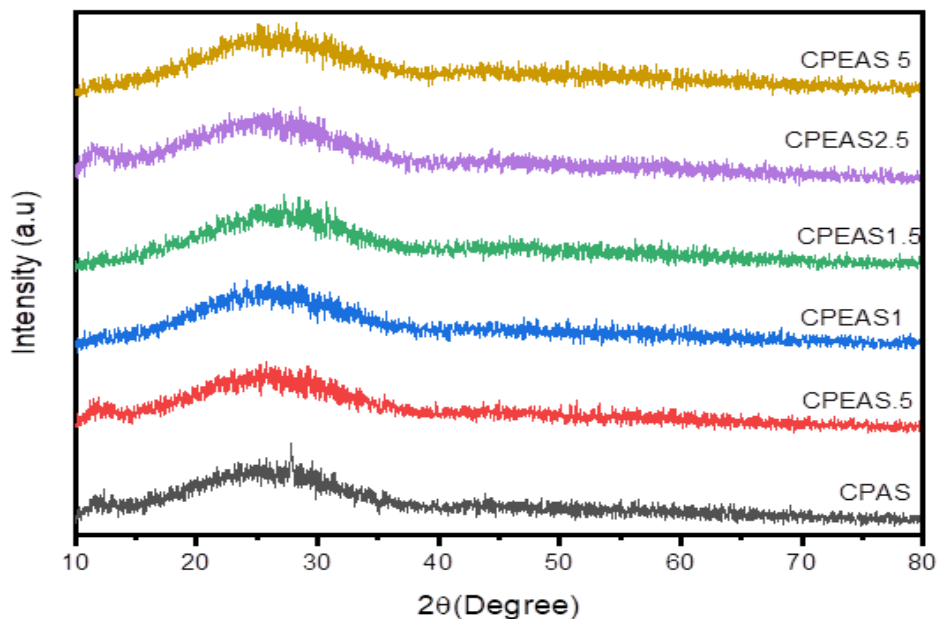


Figure 5.1 Patterns of X-ray diffraction in samples $50\text{P}_2\text{O}_5 - (50-x) \text{CaO} - x\text{Er}_2\text{O}_3 - 4\text{Ag}_2\text{O} - 4\text{SnO}$ where $x=0, 0.5, 1, 1.5, 2.5$ and $5\text{mol}\%$

5.2.2 Density and molar volume

Density is a crucial factor in the physical characteristics that affect how compact the structure is and how the geometrical arrangements of the glass matrix change (Shelby 2007; Varshneya and Mauro 2019a; Zaman et al. 2022).

Density (ρ) was measured using the Archimedes method given in equation 2.2 in chapter 2 of this thesis with the precision of (0.001). From Table 5.1 and Figure 5.2, the density (ρ) and molar volume (V_m) of synthesized glasses were found to increase as a function of Er_2O_3 concentrations. According to the density measurements, the density increased with the concentration of Er_2O_3 , from 2.817 (CPAS) to 3.078 g/cm^3 (CPEAS5), and the molar volume rose from 37.951 to 42.217 cm^3/mol . The molecular weight of Er_2O_3 (382.516 g/mol) is higher than that of P_2O_5 , Ag_2O , SnO , and CaO , which have molecular masses of 141.9, 231.73, 134.71, and 56.08 g/mol ., respectively. This explains the increased density of the glasses. Due to the increase of rare-earth ions, the glass matrix becomes denser (Amjad, M. R. Sahar, et al. 2012; Soltani, Hraiech, Horchani-Naifer, Massera, et al. 2016). The rates of change in molecular weight and density have an impact on the change in molar volume. The development of non-bridging oxygen (NBO), which extends the network structure of Calcium-phosphate glass, may be accountable for the samples' increased molar volume. This increase might be caused by the inclusion of rare-earth ions with larger radii than other glass matrix ingredients, which leads to the creation of non-bridging oxygens. However, the relative rise in molecular weight outweighs the relative increase in density. The increase in Er_2O_3 , which causes the rise in the number of non-bridging oxygens is associated with an increase in the molar volume of the glass systems (NBOs) (Effendy et al. 2017; Faznny, Halimah, and Azlan 2016). Many parameters, such as changes in the bond length of the substituted cations, directly impact the molar volume values. As a result, the data acquired revealed the increase in molar volume. Similar properties have also been seen in other glass systems (Amjad, M. R. Sahar, et al. 2012; Bhattacharya and Shashikala 2018; Chimalawong et al. 2012; Damas et al. 2012).

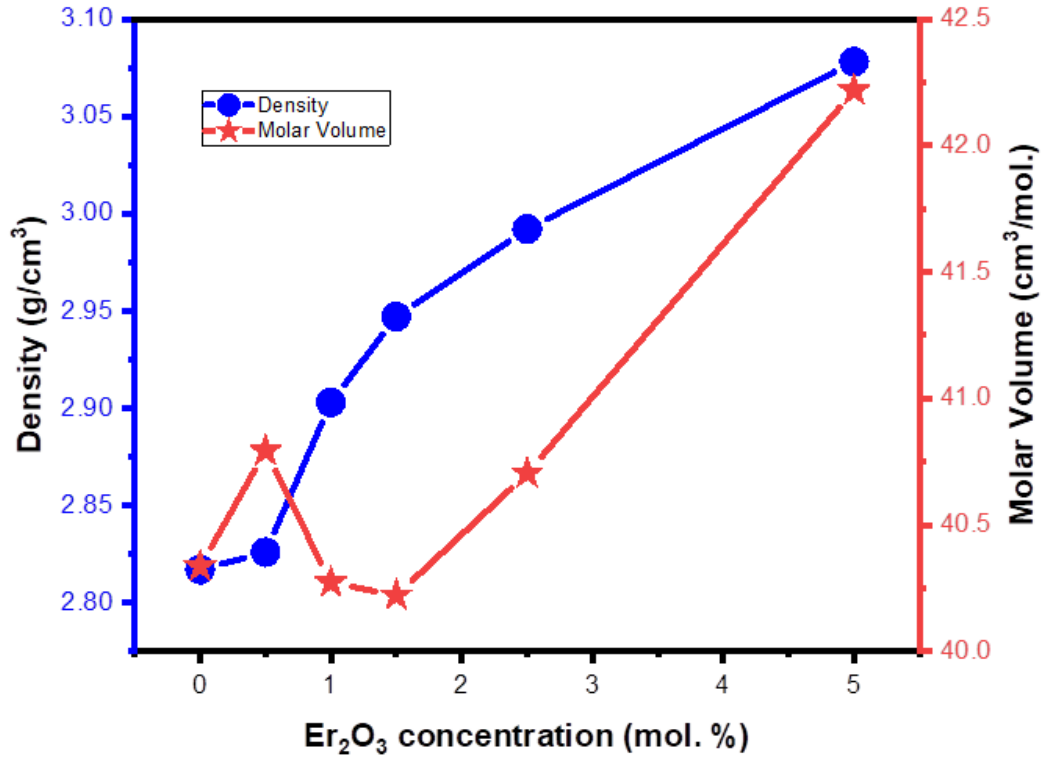


Figure 5.2 Density and Molar volume of the $50P_2O_5-(50-x)CaO-xEr_2O_3-4Ag_2O-4SnO$ $x=0, 0.5, 1, 1.5, 2.5$ and 5 (mol.%)

5.2.2.2 Physical Parameters

For the prepared glasses, physical parameters like Erbium ion Concentration (N_{Er}), Polaron radius (r_p), inter-nuclear distance (r_i), and field strength (F) were calculated using equations 5.1-5.4 (Alqarni et al. 2020; Dutebo and Shashikala 2020), and the values are tabulated in Table 5.1.

Erbium ion Concentration (N_{Er}) in (ions/cm³)

$$N_{Er} = \frac{\text{Mol.\% of Er ion} * N_A * \rho_s}{M_w} \quad (5.1)$$

Where N_A is Avogadro's number, ρ_s is the density of the sample, and N_{Er} is Erbium ion Concentration

Polaron radius, $r_p(\text{\AA})$ is given as

$$r_p = \frac{1}{2} * \sqrt[3]{\frac{\pi}{6N_{Er}}} \quad (5.2)$$

Inter-nuclear distance (r_i) in (Å)

$$r_i = \sqrt[3]{\frac{1}{N_{Er}}} \quad (5.3)$$

Field Strength (F) in (cm^{-2})

$$F = \frac{Z}{r_p^2} \quad (5.4)$$

Where Z is the atomic number of Rare earth elements, and r_p is Polaron radius

Table 5.1 Molecular mass, Density (ρ), Molar Volume, Ion Concentration(N_{Er}), Polaron radius (r_p), Inter ionic distance (r_i), Field Strength(F), Index of refraction, and Metallicity Factor (M_c) of the investigated glasses

Physical properties	Sample Code					
	CPAS	CPEAS .5	CPEAS1	CPEAS1. 5	CPEA S2.5	CPEAS 5
Molecular mass (g/mole)	113.64 64	115.27 70	116.9104	118.5390	121.80 90	129.968 0
Density ρ (g/cm^3)	2.817	2.826	2.903	2.947	2.992	3.078
Molar Volume ($\text{cm}^3/\text{mol.}$)	40.336	40.792	40.272	40.222	40.704	42.217
Ion Concentration(N), 10^{22} * (ions/cm^3)	-	2.823	5.718	8.588	14.144	27.276
Polaron radius r_p (Å)	-	1.3185	1.0460	0.9134	0.7734	0.6214
Inter ionic distance r_i (Å)	-	3.2842	2.595	2.2665	1.9192	1.5419
Field Strength(F), 10^{17} (cm^{-2})	-	1.7249	2.7419	3.5958	5.0154	7.769
Refractive index (n)	1.547	1.512	1.535	1.548	1.564	1.572
Metallicity Factor(M_c)	0.6838	0.6999	0.6886	0.6824	0.6747	0.6747

The above relations(Algradee et al. 2017; Alqarni et al. 2020; Dutebo and Shashikala 2020) were used to get the polaron radius (r_p), mean inter-ionic distance (r_i), Erbium ion concentration (N_{Er}), and field strength (F).

From Table 5.1 for the prepared samples, it can be seen that the value of Erbium ion concentration (N_{Er}) increases with erbium content. This may be due to the molecular mass of the rare earth oxides. From the table, it can be inferred that a general increase in ion concentration in a sample indicates a decrease in the inter-ionic distance leading to the rise in field strength. Figure 5.3 shows Inter-ionic distance (r_i) and Field strength interms of Erbium ion content. The observed decline in r_i with rising Er_2O_3 is connected to the rising Er-concentration value. This causes the Er-O distance to decrease, and as a result, the strength of the Er-O bond increases, creating stronger field strength near Er^{3+} ions(Algradee et al. 2017).

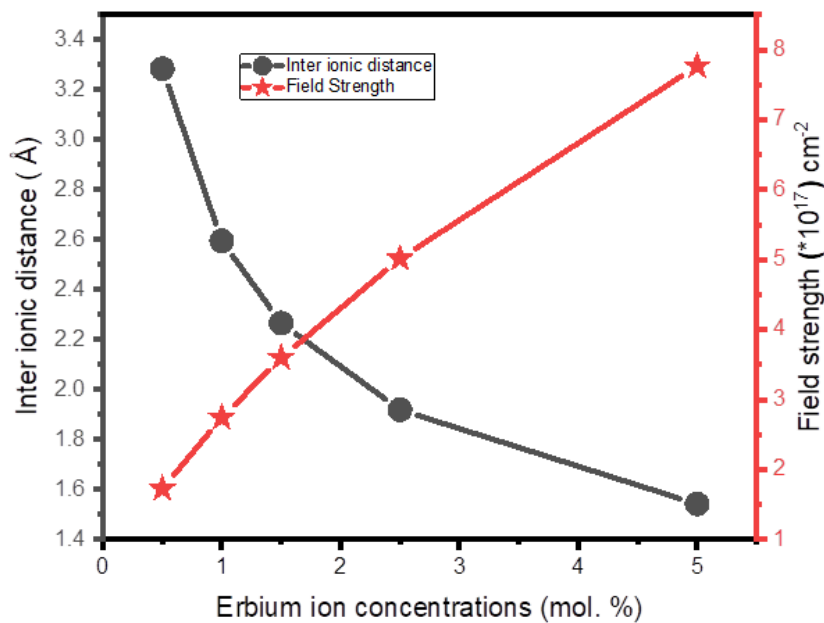


Figure 5.3 Inter-ionic distance and field strength variations in glasses as a function of Er_2O_3 concentration

With an increase in Er^{3+} ion concentration, it can be seen that the average molecular weight rises while the interatomic distance falls; this suggests that the atoms in the titled glass network are packed more closely.

5.2.3 Refractive index and Metallization criterion

The molar refractivity of a material is a critical quality derived from optical (refractive index) and structural (density and average molecular weight) variables that describe its polarizability. The electron density, glass composition, density, molar and ionic refractivity, and polarizability of the anions in the glass influence the refractive index. Oxygen ions provide a significant contribution to the refractive index. Non-bridging oxygen ions, in particular, are more polarisable than bridging oxygen ions, resulting in a greater refractive index. When network modifiers like CaO are added to phosphate glasses, the P–O–P linkages are broken, resulting in non-bridging oxygen ions and electric dipoles which makes the refractive index to increase (Venkateswara Rao and Shashikala 2014b).

The Lorentz-Lorenz formula connects two fundamental parameters that affect refractive index (n), density, and mean polarizability (Kakiuchida, Saito, and Ikushima 2004). The refractive index (n) of glasses is a critical optical feature for photonic devices, such as fiber optics doped amplifiers. The electron density and glasses' electronic polarizability (α) are related to this feature (Gomes et al. 2017; Reddy et al. 2001). An increase in measured refractive index as a function of Er_2O_3 content is tabulated in the table 5.1. The range was 1.514 to 1.572, with the rise in 'n' being proportional to the increase in density. Also, using the well-known Clausius-Mosotti relation (Reddy et al. 2001), the electronic polarizability (α) of glasses was computed (Gomes et al. 2017). Clausius-Mosotti relation is given below.

$$\alpha = \left(\frac{3}{4\pi N_A} \right) \left(\frac{n^2-1}{n^2+2} \right) V_m \quad (5.5)$$

where N_A denotes the Avogadro number, n the refractive index, and V_m the volume of a molar of glasses.

The difference in electronic polarizability between the doped erbium ion and the host component causes the n variation induced by the dopant at a visible wavelength. Furthermore, the dopant may cause a structural change, such as a reorganization of the P_2O_5 tetrahedral network, and this structural change may affect 'n' (Kakiuchida et al. 2004).

5.2.4 Metallization criterion

According to Bhattacharya & Shashikala, (2018b), the metallization criteria of material indicate the substance's non-metallic nature based on its bandgap energy. According to the Herzfeld theory of metallization(Herzfeld 1927), materials with a metallization requirement close to 1 are typical insulators.

$$M_c = 1 - \left(\frac{n^2-1}{n^2+2} \right) \quad (5.6)$$

Materials having a lower metallization criterion value, which is close to zero, show metallic properties. The values of calculated metallization factor of the prepared glasses are 0.6838, 0.6999, 0.6886, 0.6824, 0.6747, and 0.6747 for different compositions of Er₂O₃ as seen in Table 5.1. The results indicate that all the synthesized glasses tend to be insulators.

5.2.5 FTIR Analysis

It is well known that the fundamental building blocks of phosphate glasses are PO₄ tetrahedra(Brow 2000; Qian, Yang, et al. 2012; Shelby 2007). The Qⁿ notation expresses tetrahedral units, where n is the number of bridging oxygens (BOs) that connect nearby P-tetrahedra. Q³ P-tetrahedra forms a three-dimensional cross-linked network with three BOs and one double-bound oxygen in the vitreous P₂O₅ structure. The structural elements Q³ and Q² P-tetrahedra are both present in ultraphosphate glasses. The modifying cation polyhedra and the Q² P-tetrahedra share two terminal oxygens in the metaphosphate glasses. Long chains are formed by the Q² tetrahedra linking (or rings). Making phosphate glasses based on pyrophosphate (Q¹) and orthophosphate (Q⁰) is also feasible.

Phosphate glasses are generally hygroscopic(Brow 2000; Hoppe 1996; Shelby 2007). It was reported by earlier workers that the addition of CaO, Er₂O₃, Ag₂O, and SnO to P₂O₅ produced connected PO₄ structural units. The phosphate network was compacted by covalent bonding of oxygens in the newly generated structural units, and water resistance, chemical durability, and mechanical qualities were all improved by compaction(Saddeek et al. 2018).

The Fourier transform infrared (FTIR) transmittance spectra of glasses CP, CPAS, CPEAS1, CPEAS2.5, and CPEAS5 are presented in Figure 5.4. The FTIR spectra of glasses were measured in the 400–4000 cm^{-1} wavenumber range. The band around 1634 cm^{-1} is caused by the P-OH vibration (Saddeek et al. 2018). The asymmetric stretching of P=O and the vibration of $[\text{PO}_2]$ are responsible for the peak at 1257–1300 cm^{-1} (Saddeek et al. 2018) (Liu et al. 2016b). The symmetrical stretching vibration of $[\text{PO}_4]$ is ascribed to the small band at 1050 cm^{-1} . The bending vibration of P-O-P causes the band to be around 710–782 cm^{-1} .

As the concentration of Er_2O_3 grows, the band at 770 cm^{-1} , which represents the vibration of P-O-P, gradually decreases. This behavior shows that P-O-Er eventually replaces P-O-P in the glass structure, potentially lowering the peak's intensity. The band near 1300 cm^{-1} , caused by the vibration of P=O and $[\text{PO}_2]$, rapidly decreases as the concentration of Er_2O_3 increases. It means that the P=O in the structure will split and produce a new P-O-Er, which improves structure compactness and thereby increase the density of the glass.

As the concentration of Er_2O_3 increases, the O/P ratio steadily increases from 3.00 to 3.28, indicating a change in glass structure from Q^2 chains to Q^1 species. P-O-P is substituted with P-O-Er, resulting in a more compact structure (Liu et al. 2016b). The bands associated with PO_2 group vibrations, the bands related to symmetric stretching vibrations of PO_4^{3-} in Q^2 units, and the bands associated with H-O appear compositionally independent (Saddeek et al. 2018). In addition, three influential bands have been observed to expand. As Er_2O_3 increases, their position shifts to a higher wavenumber, and their intensity increases. These bands are related to asymmetric vibrations of P-O-P, symmetric stretching vibrations of P-O-P, and vibrations of P-O overlapped with structural unit vibrations.

The addition of Er_2O_3 polymerized the local structure around atoms by shortening the phosphate chain's bond length and increasing the O/P ratio (Saddeek et al. 2018). The high value of the bond strength of Er-O correlated with that of P-O can also be attributed to polymerization. As a result, the OH content and, as a result, the optical losses are reduced, indicating that the investigated network modified by Er_2O_3

is appropriate for optical applications and can provide a chemical environment that is quite suitable for Er^{3+} .

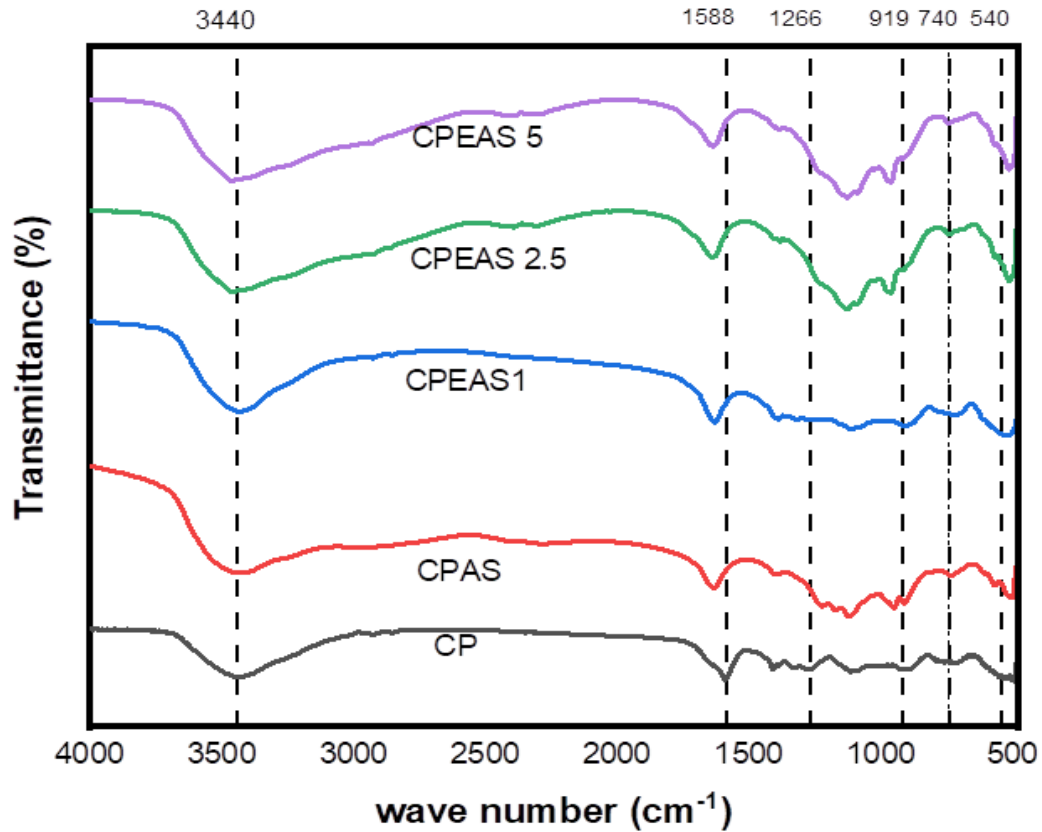


Figure 5.4 FTIR (Fourier Transform Infrared) spectra of the investigated glass system $50\text{P}_2\text{O}_5-(50-x)\text{CaO}-x\text{Er}_2\text{O}_3-4\text{Ag}_2\text{O}-4\text{SnO}$ with ($x = 0$ to 5 mol%)

The metaphosphate chains are depolymerized and the quantity of non-bridging oxygen atoms is increased as a result of the RE ions, which are implanted in the phosphate network and acting as vitreous network modifiers (Elisa et al. 2021). The RE-O-P bonds provide non-bridging oxygen, increasing their chemical resistance (Li et al. 2014).

Table 5.2 lists the vibrational modes assigned to the FTIR analysis, which is consistent with the literature. The presence of Er^{3+} ions influences the surrounding of the P-O bond. According to the FTIR spectra and band assignments, it occupies a position by a partial rupture of the phosphate network.

Table 5.2 The FTIR spectra bands of CP, CPAS, CPEAS1, CPEAS2.5, and CPEAS5 glass samples with band assignments.

Sample code					Band Assignment	References
CP	CPAS	CPEAS1	CPEAS2.5	CPEAS5		
-	504-540	515	523	513	Bending mode of O-P-O groups in the Q ¹ structure	(Alqarni et al. 2020; Li et al. 2019b; Liu et al. 2016b)
710-788	733	717	730	744	Symmetric stretching vibrations of P-O-P in the Q ² tetrahedral v _s (P-O-P)	(Dutebo and Shashikala 2020; Saddeek et al. 2018; Venkateswara Rao and Shashikala 2014b)
880-919	912	912	922	915	Asymmetric stretching vibrations of P-O-P linked with linear metaphosphate chain	(Li et al. 2019b; Narayanan and Shashikala 2015a; Qian, Liang, et al. 2012b)
1266	1261	1262-1284	1263	1268	asymmetric Stretching vibrations of non-bridging oxygen of O-P-O linkage of (PO ₂) groups in Q ² Units	(Elisa et al. 2021). (Dutebo and Shashikala 2020)
1332	1328	1335	1333	1337	P = O asymmetric Stretching mode of the Phosphate tetrahedra	(Li et al. 2019b; Shi et al. 2019; Venkateswara Rao and Shashikala 2014b)
1384-1408	1385	1386	1407	1384	P = O Stretching mode of the Phosphate tetrahedra	(Li et al. 2019b; Shi et al. 2019; Venkateswara Rao and Shashikala 2014b)
1588	1634	1631	1629	1637	Deformation mode of OH groups, water groups, H-O-H	(Chowdhury et al. 2019; Li et al. 2019b; Qian, Liang, et al. 2012b)

5.2.6 UV-Vis spectroscopy

Understanding the electronic band structures of glasses can be accomplished by studying optical absorption in the UV region. The fundamental absorption edge is the wavelength corresponding to the abrupt increase in absorption coefficient. Glasses

will be opaque to electromagnetic radiation over this UV "cut-off" value. When the photon energy exceeds the optical band gap between the valence and conduction bands at wavelengths less than 200 nm, the majority of oxide glasses become opaque. Measuring this band gap in glasses can reveal structural changes and the type of chemical bonds present in the matrix(Mallur et al. 2015).

Table 5.3 Absorption Transitions (From the Ground State, $^4I_{15/2}$) to another excited states of CPEAS5 glass

S.No.	Transitions $^4I_{15/2} \rightarrow$	absorption peaks (nm)			
		Present work CPEAS5	References		
			(Amjad, M.R. Sahar, et al. 2012)	(Soltani, Hraiech, Horchani-Naifer, Massera, et al. 2016)	(Mariselvam, Kumar, and Rao 2019)
1.	$^4H_{9/2}$	362			360
2.	$^4G_{11/2}$	376	375	375	373
3.	$^2G_{9/2}$	406	405	405	406
4.	$^4F_{5/2}$	450	451		450
5.	$^4F_{7/2}$	486	488	488	487
6.	$^2H_{11/2}$	519	520	520	521
7.	$^4S_{3/2}$	542	543		540
8.	$^4F_{9/2}$	650	650	650	651
9.	$^4I_{9/2}$	797	808	808	802

Figure 5.5 shows the absorption spectra of Er^{3+} doped Phosphate glasses containing silver and tin oxide. Considering 5mol% of Erbium ion doped glass sample with 4mol% of silver and tin oxides coded as CPEAS5 in Figure 5.4, the spectra exhibits approximately nine transitions in the range of 300 to 800 nm. These transitions from the ground state to the indicated excited states are observed and ascribed to the Er^{3+} characteristic bands 362nm($^4H_{9/2}$), 376nm($^4G_{11/2}$), 406nm($^2G_{9/2}$), 450nm($^4F_{5/2}$), 486nm($^4F_{7/2}$), 519nm($^2H_{11/2}$), 541nm($^4S_{3/2}$), 650nm($^4F_{9/2}$), and 797nm($^4I_{9/2}$) (Ahmadi et al. 2018; Mariselvam et al. 2019; Reddy et al. 2011; Soltani, Hraiech, Horchani-Naifer, Massera, et al. 2016). The samples doped with different

amounts of erbium ions have almost similar spectra with the intensities of the absorption peaks increasing with composition of Erbium oxide in CPEAS5.

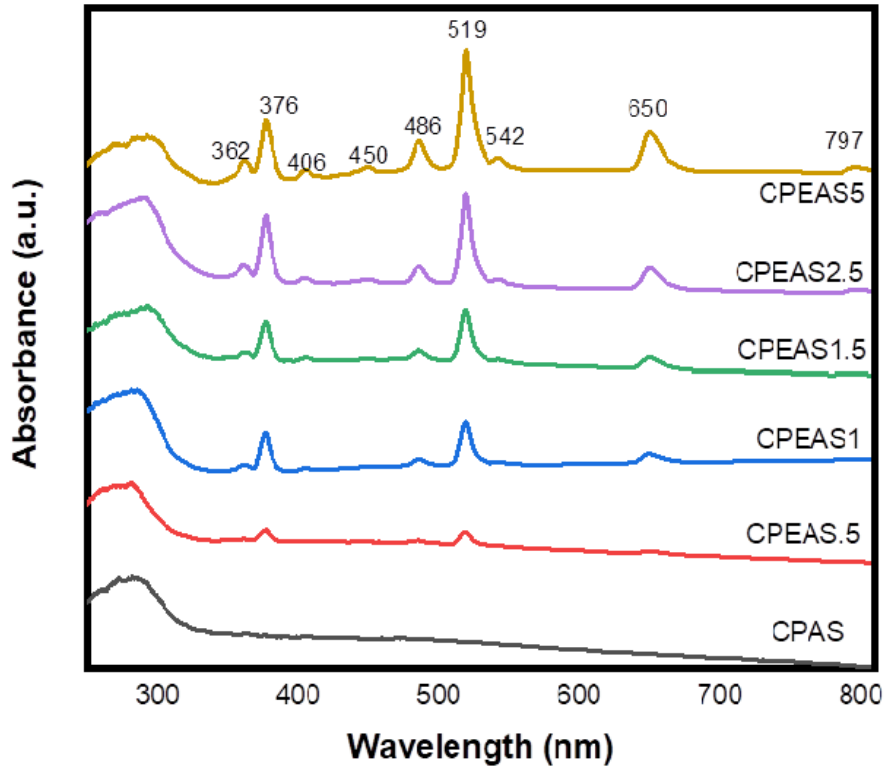


Figure 5.5 UV-Vis Absorbance of Erbium oxide doped CPAS system

5.2.6.1 Optical band gap and Urbach energy

The bandgap energy is defined as the difference in energy between the valence and conduction bands. Optical absorption coefficients have been used to assess this attribute in both crystalline and amorphous materials (Gomes et al. 2017; Shelby 2007). Using the following equations (Tauc and Menth 1972).

$$\alpha h\nu = A(h\nu - E_g)^n \quad (5.7)$$

$n = 1/2$ for direct allowed transition and $n = 2$ for indirect allowed transition, where α is the optical absorption coefficient, $h\nu$ refer to photon energy, and n is an index number connected to distinctive band gap transition.

Table 5.4 Indirect Band gap Energy and Urbach energy of synthesized glasses

Sample Code	Indirect Band gap Energy (eV)	Urbach Energy (eV)
CPAS	3.61	0.37
CPEAS.5	3.41	0.34
CPEAS1	3.29	0.33
CPEAS1.5	3.19	0.32
CPEAS2.5	3.56	0.36
CPEAS5	3.05	0.29

Band gap energy and Urbach energy are calculated using equations mentioned in chapter 2. The calculated values of indirect band gap energy of the samples as tabulated in Table 5.3 which is decreasing from 3.61eV (CPAS) to 3.05eV (CPEAS5) with Erbium oxide addition, showing that the lattice characteristics have changed and that is due to non-bridging oxygen(NBO) formation. The increase in non-bridging oxygens in the glass network is what causes this decline(Hraiech et al. 2018).

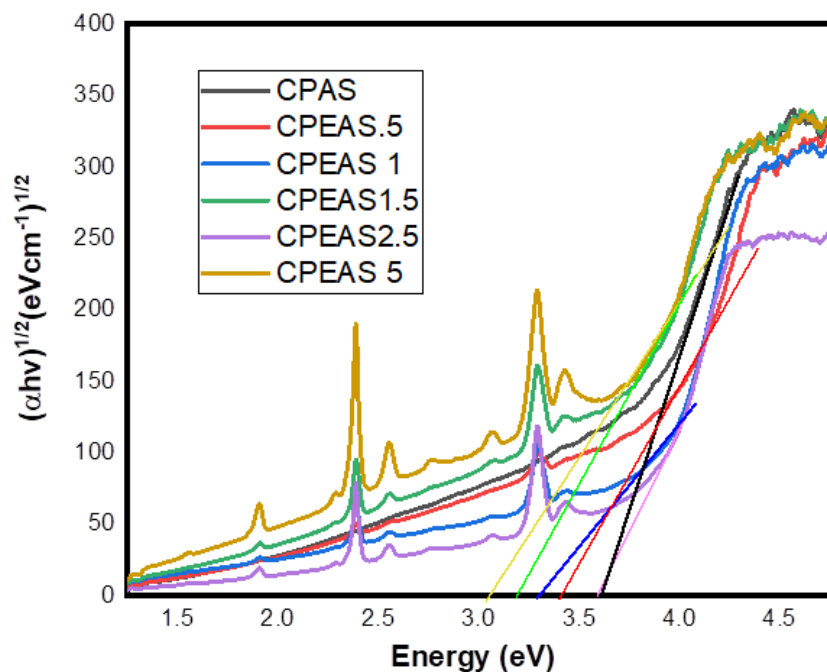


Figure 5.6 Tauc plot of direct bandgap energy of CPAS, CPEAS.5, CPEAS1, CPEAS1.5, CPEAS2.5, and CPEAS5.

The Urbach energy is calculated using absorption spectra, a technique for analyzing optical transitions and electronic band structures (Arifin et al., 2015). The exponential character of the absorption coefficient towards the absorption edge is indicated by the linear variation in UV absorption, which follows an exponential behavior obeying Urbach's empirical relation (Anigrahawati et al. 2015a)

$$\alpha(\vartheta) = \alpha_0 \exp\left(\frac{h\vartheta}{E_u}\right) \quad (5.8)$$

where α_0 is constant and E_u is the width of the localized states in the forbidden energy gap

Table 5.4 lists the Urbach energy values of the prepared samples. The difference in particle sizes and shapes is responsible for the variation in Urbach energy when Er_2O_3 oxide concentration increases.

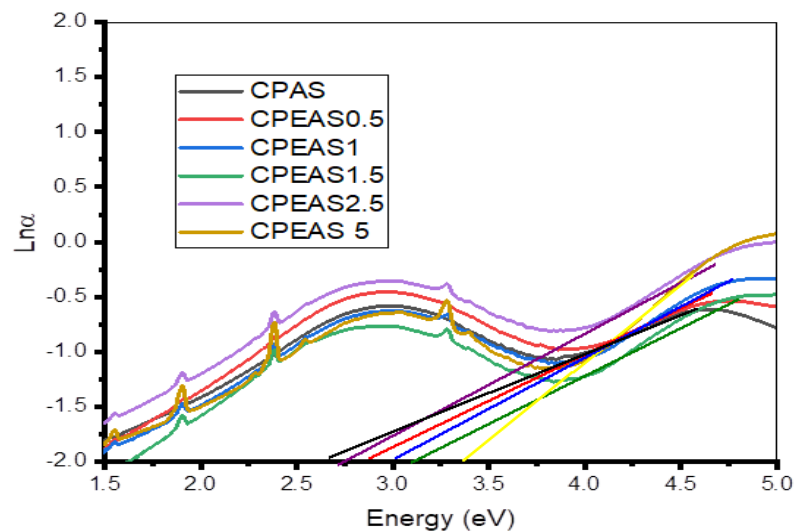


Figure 5.7 The urbach energy diagram of investigated glass system $50\text{P}_2\text{O}_5-(50-x)\text{CaO}-x\text{Er}_2\text{O}_3-4\text{Ag}_2\text{O}-4\text{SnO}$ with ($x = 0$ to 5 mol%)

5.2.7 EDAX analysis

The EDAX analysis gathered detailed information about the predicted elemental (chemical) reagents in the glass sample. The representative EDAX spectrum of the CPEAS1 glass sample is shown in Figure 5.8. The presence of Calcium (Ca), silver (Ag), oxygen (O), tin (Sn), phosphorous (P), and Erbium (Er) elements in the glass are confirmed in the EDAX analysis.

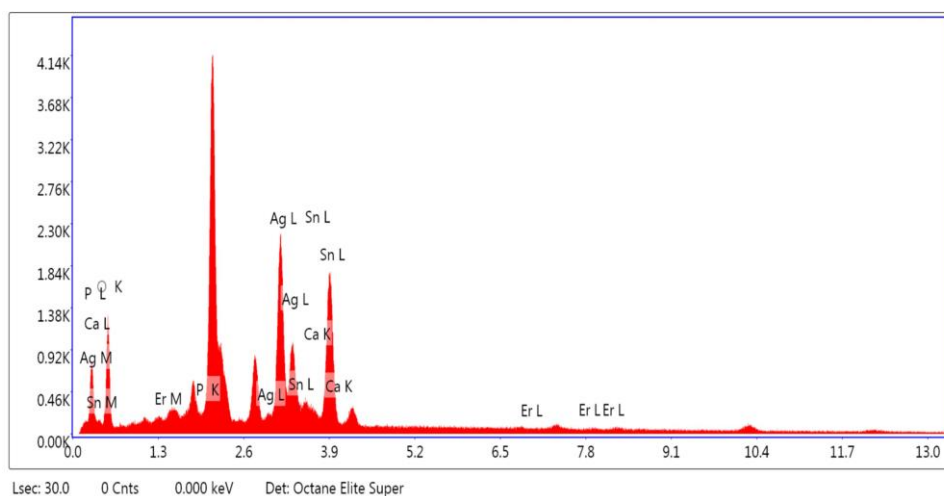


Figure 5.8 The EDAX spectrum of CPEAS1 glass.

5.3 Conclusion

Rare earth (Er^{3+}) ions doped CPAS were successfully synthesized by melt quenching. The results of the FTIR study showed that Erbium ions doped to the CPAS glass did not affect the basic structure of the phosphate glass network. The densities of samples increased by replacing the CaO with Er_2O_3 , which could be due to the larger molecular mass and cation field strength. With an increase in ion concentration, the internuclear distance decreased, leading to an increase in field strength. The values of the Metalicity factor (M_c) showed that they were nearing unity rather than zero, implying the samples were more insulating. The optical band gap energy decreased as the Er_2O_3 content in the glass matrix increases, showing that the lattice characteristics have changed and that non-bridging $-\text{oxygens}$ have formed. The prepared glass may be potentially used as a solid state laser host.

CHAPTER 6

THE EFFECT OF HEAT TREATMENT ON THE STRUCTURAL AND OPTICAL CHARACTERIZATION OF SILVER NANOPARTICLES EMBEDDED IN RARE EARTH (ERBIUM, EUROPIUM) ION DOPED CALCIUM PHOSPHATE GLASSES

Overview

The current chapter mentions the preliminary investigations on the impact of various heat treatment durations on the structural and optical characteristics of glasses with embedded silver nanoparticles with the compositions $50\text{P}_2\text{O}_5 - 49 \text{CaO}-1\text{REI}$ (mol%) (Where REI=Er, Eu). Glasses co-doped with silver oxide and tin oxide were made using the standard melt-quenching method with a modified synthesis path. To convert silver ions (Ag^+) into silver nanoparticles (NPs) (Ag^0), subsequent heat treatment was used, with various time intervals (0, 3, 10, 25, 50 hrs.) at a temperature of 550°C . X-ray diffraction(XRD), EDX analysis, Fourier transform infrared (FTIR spectroscopy), HRTEM, UV-Vis absorption spectroscopy, photoluminescence (PL) spectroscopy, and density measurements were used to evaluate annealing time-dependent structural, physical and optical features of manufactured glass samples. The primary metaphosphate glass structure had not been affected by the production or development of silver nanoparticles, according to Fourier-infrared (FTIR) spectroscopy. In order to investigate the optical characteristics of silver in the various oxidation and aggregation states found in the obtained samples, optical absorption and photoluminescence (PL) spectroscopy were used. The existence of highly crystalline, well disseminated, non-agglomerated silver nanoparticles in the heat treated samples was confirmed by TEM images and a selected area electron diffraction (SAED) pattern. The increase in density indicates the creation of a densely packed structure inside the matrix by the precipitated silver nanoparticles.

6.1 Introduction

Glasses with the compositions $50\text{P}_2\text{O}_5-49\text{CaO}-1\text{REI}-4\text{Ag}_2\text{O}-4\text{SnO}$ (mol%) (Where REI= Er^{3+} and Eu^{3+}) were selected to study the effect of heat treatment

duration on reduction of silver ions to silver metal nanoparticles. Presence of nanoparticles influences the optical properties of calcium phosphate glasses.

6.2 Results and discussion

Phosphate glasses are a unique kind of optical glasses made of metal-based metaphosphate. The glass melting process is accelerated, and several unique glass qualities are enhanced when rare earth ions are used as dopants in the glass matrix. Melt quenching was used to develop a phosphate glass system doped with rare earth ions. The current study's objective is to ascertain the impact of various heat treatment times at a fixed annealing temperature on reduction of silver ions into silver nanoparticles in a P_2O_5 -CaO-REI glass matrix. These glasses' optical, structural, and optical characteristics were investigated using FTIR, UV-Visible spectroscopy, and their microstructure using transmission and scanning electron microscopy.

Table 6.1 the sample code and composition of Erbium oxide and Europium oxide doped glasses

Sample code	Compositions (mol%)	Duration of heat treatment (hrs.)
a) Erbium oxide doped system		
CPEAS1-0	50P ₂ O ₅ -49CaO-1Er ₂ O ₃ -4Ag ₂ O-4SnO	0
CPEAS1-3	50P ₂ O ₅ -49CaO-1Er ₂ O ₃ -4Ag ₂ O-4SnO	3
CPEAS1-10	50P ₂ O ₅ -59CaO-1Er ₂ O ₃ -4Ag ₂ O-4SnO	10
CPEAS1-25	50P ₂ O ₅ -49CaO-1Er ₂ O ₃ -4Ag ₂ O-4SnO	25
CPEAS1-50	50P ₂ O ₅ -49CaO-1Er ₂ O ₃ -4Ag ₂ O-4SnO	50
b) Europium oxide doped system		
CPASEu1-0	50P ₂ O ₅ -49CaO-1Eu ₂ O ₃ -4Ag ₂ O-4SnO	0
CPASEu1-3	50P ₂ O ₅ -49CaO-1Eu ₂ O ₃ -4Ag ₂ O-4SnO	3
CPASEu1-10	50P ₂ O ₅ -49CaO-1Eu ₂ O ₃ -4Ag ₂ O-4SnO	10
CPASEu1-25	50P ₂ O ₅ -49CaO-1Eu ₂ O ₃ -4Ag ₂ O-4SnO	25
CPASEu1-50	50P ₂ O ₅ -49CaO-1Eu ₂ O ₃ -4Ag ₂ O-4SnO	50

6.2.1 X-ray diffraction study

The XRD pattern for the quenched glass samples CPAS, CPEAS1, and CPASEu1 exhibits a broad hump typical of the amorphous state, as shown in Figure 6.1.

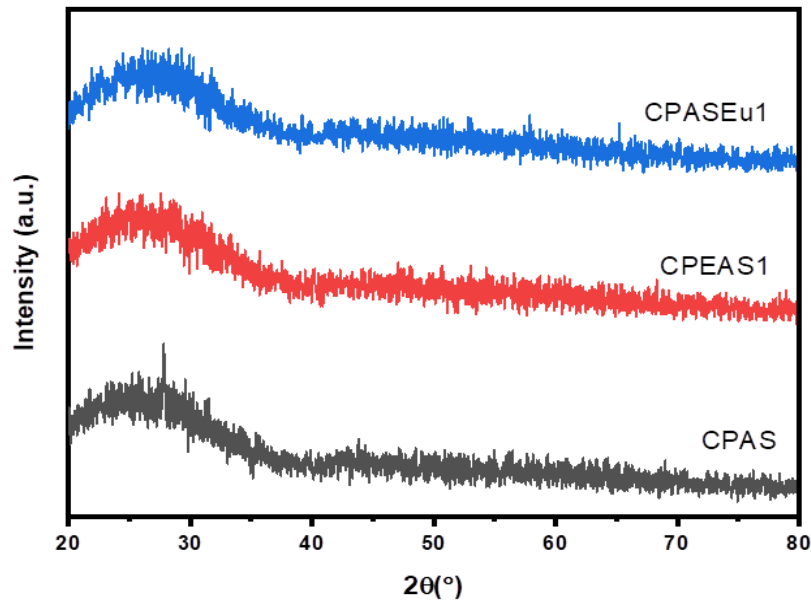


Figure 6.1 X-ray diffraction patterns of samples CPAS, CPEAS1, and CPASEu1 without heat treatment

6.2.2 Energy Dispersive X-ray analysis (EDAX) of heat treated samples

The compositions of a number of glasses were ascertained using energy dispersive X-ray analysis (EDAX). The EDAX analysis gathered detailed information about the elemental (chemical) reagents in the glass sample. The representative EDAX spectrum of the CPEAS1-3 glass sample is shown in Figure 6.2. The presence of Calcium (Ca), silver (Ag), oxygen (O), tin (Sn), phosphorous (P), and Erbium (Er) elements in the glass are confirmed in the EDAX analysis.

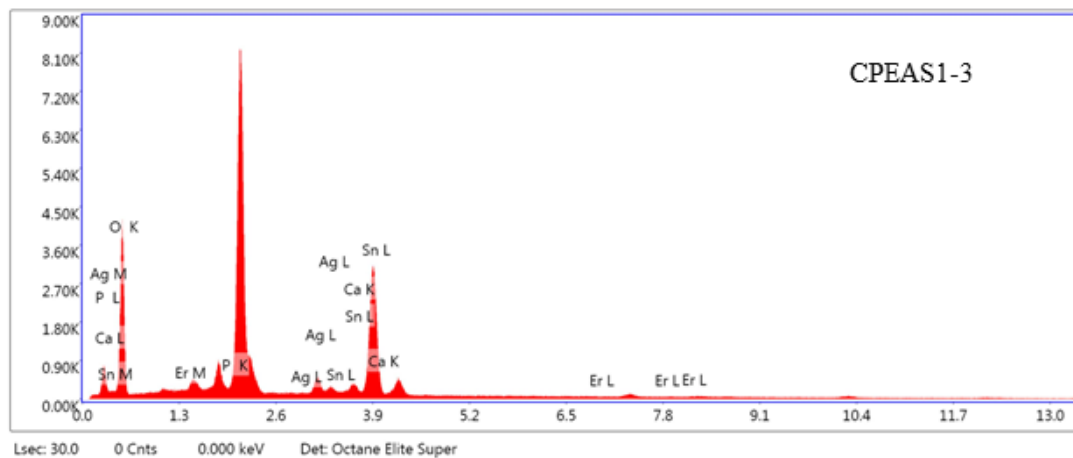


Figure 6.2 The EDAX spectrum of CPEAS1-3 glass

6.2.3 Physical Properties

Density (ρ)

The densities of the samples CPEAS1 and CPASEu1 series were calculated using the Archimedes technique using Xylene (C_6H_8) as the immersion liquid. At least three samples of each composition were utilised, and the average values were reported. Tables 6.2(a) and (b) list the densities of samples of heat treated rare earth (Er, Eu) ion doped calcium phosphate glass with Silver nanoparticles (Ag NPs) that were measured and computed using equation (2.4). With Increase in heat treatment duration from 0hrs to 50 hrs the density of glasses increased from 2.8783 to 2.8957 g/cm^3 for CPEAS1glasses and from 2.8680 to 2.9129 g/cm^3 CPASEu1glasses. According to Som and Karmakar (Karmakar et al. 2010) and Rao and Shashikala(Rao and Shashikala 2014), the larger and more evenly distributed precipitated silver nanoparticles that create a densely packed structure inside the glass matrix are the reason for the rise in density of glasses with increased heat treatment time.

Table 6.2(a) Density (ρ) and Refractive Index (n) of $50P_2O_5 - 49 CaO-1Er_2O_3-4Ag_2O-4SnO$ (heat treated at 0, 3, 10, 25, and 50hr)

Sample code	Density (g/cm^3) (± 0.005)	Refractive Index(n) (± 0.001)
CPE1	2.6694	1.515
CPEAS1-0	2.8783	1.529
CPEAS1-3	2.8805	1.532
CPEAS1-10	2.8889	1.541
CPEAS1-25	2.8919	1.543
CPEAS1-50	2.8957	1.546

Table 6.2(b) Density (ρ) and Refractive Index (n) of $50P_2O_5 - 49 CaO-1Eu_2O_3-4Ag_2O-4SnO$ (heat treated at 0, 3, 10, 25, and 50hr)

Sample code	Density (g/cm ³) (-/+ 0.005)	Refractive Index(n)
CPEu1	2.6780	1.510
CPASEu1-0	2.8680	1.512
CPASEu1-3	2.8747	1.514
CPASEu1-10	2.8822	1.515
CPASEu1-25	2.9121	1.523
CPASEu1-50	2.9129	1.526

6.2.4 The impact of various heat treatment times on structural investigations

In this section, FTIR spectroscopy was used to examine changes brought about in the local structure of glasses by precipitated nanoparticles in their matrix. In addition to that glass samples that had been post-annealed at 550 °C for 0–50 h were examined using TEM and XRD to look at the mean particle size and distribution of embedded silver nanoparticles.

6.2.4.1 FTIR Analysis

The Fourier transform infrared (FTIR) transmittance spectra of glasses CPE, CPEAS1-0, CPEAS1-10, CPEAS1-25, CPEu, CPASEu1-0, CPASEu1-10, and CPASEu1-25 are shown in Figure 6.3(a) and (b). The FTIR spectra are measured in the region of wave number 400 - 4000 cm⁻¹. The respective band assignments are shown in Tables 6.3(a), and 6.3(b).

Similar vibrational bands related with the structure of metaphosphate glass may be seen in the FTIR spectra of samples that have been heat treated and those that have not been heat treated. This demonstrates that fundamental metaphosphate glass structure is not affected by the production or development of nanoparticles, as evidenced by the fact that the absorption peaks and line shape of FTIR spectra of heat-treated glasses are not significantly different from those of unheated glasses (Kabi and Ghosh 2012; Rao and Shashikala 2014b).

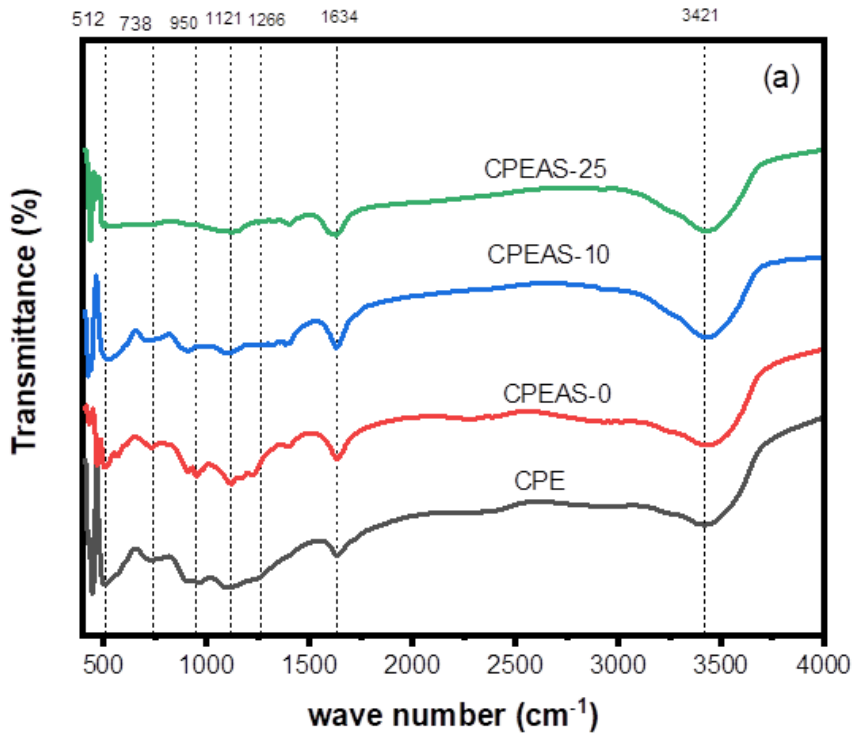


Figure 6.3(a) Fourier transforms infrared (FTIR) transmittance spectra of the CPEI, CPEAS1-0, CPEAS1-10, and CPEAS1-25 glasses

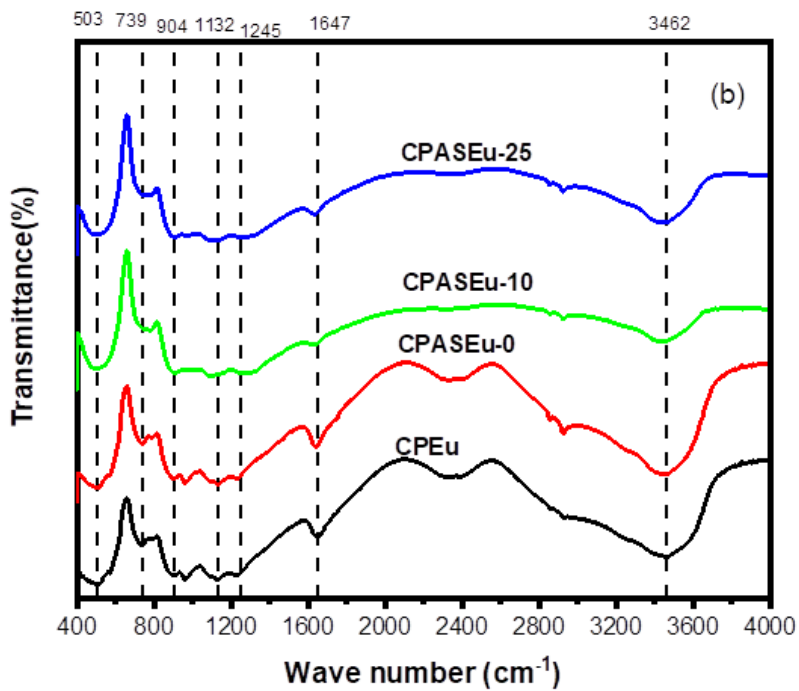


Figure 6.3(b) Fourier transforms infrared (FTIR) transmittance spectra of the CPEu1, CPASEu1-0, CPASEu1-10, and CPASEu1-25 glasses

Table 6.3 (a) The FTIR spectra peaks of CPE1, CPEAS1-0, CPEAS1-10, and CPEAS1-25 glass samples with band assignments.

Sample code				Band Assignment
CPE1	CPEAS1-0	CPEAS1-10	CPEAS1-25	
512	521	522	517	Bending ₁ mode of O-P-O groups in the Q ₁ structure
738	730	730	739	Symmetric stretching vibrations of P-O-P in the Q ₂ tetrahedral ν_s (P-O-P)
950	920	931	949	Asymmetric stretching vibrations of P-O-P linked with linear metaphosphate chain
1121	1106	1110	1115	Asymmetric stretch of P-O ⁻ groups
1266	1332	1328	1245	asymmetric Stretching vibrations of non-bridging oxygen of O-P-O linkage of (PO ₂) groups in Q ₂ Units
1634	1638	1630	1638	Deformation mode of OH groups, water groups , H-O-H

Table 6.3 (b) The FTIR bands of CPE1u, CPASEu1-0, CPASEu1-10, and CPASEu1-25 glass samples with band assignments.

Sample code				Band Assignment
CPEu1	CPASEu1-0	CPASEu1-10	CPASEu1-25	
503	500	504	503	Bending ₁ mode of O-P-O groups in the Q ₁ structure
739	730	765	745	Symmetric stretching vibrations of P-O-P in the Q ₂ tetrahedral ν_s (P-O-P)
890	904	904	897	Asymmetric stretching vibrations of P-O-P linked with linear metaphosphate chain
1132	1123	1115	1117	Asymmetric stretch of P-O ⁻ groups
1245	1237	1272	1272	asymmetric Stretching vibrations of non-bridging oxygen of O-P-O linkage of (PO ₂) groups in Q ₂ Units
1647	1642	1638	1647	Deformation mode of OH groups, water groups , H-O-H

6.2.4.2 HRTEM Analysis

The nucleation and growth hypothesis may provide a good explanation for how silver nanoparticles develop in the phosphate glass matrix. Tin oxide is added as a thermal stabiliser and reducing agent to the glass matrix in the fabrication of the silver nanoparticle embedded glass using the traditional melt quenching procedure in order to prevent the undesirable homogenous nucleation and crystal development of the nanoparticles from the silver oxide (Uchida et al. 1994; Venkateswara Rao and Shashikala 2015). Both the reducing agent and the silver are present in the glass matrix as dissolved ions at high temperatures during melting. When the melt is rapidly cooled and the reduction mechanism that leads to the creation of nanoparticles occurs during annealing, the glass system becomes supersaturated with regard to silver. The Ag^+ ions are converted to Ag^0 atoms during further post heat treatment at temperature of 550°C by the reducing agent Sn^{2+} .

The CPEAS-50 sample's transmission electron micrograph shown in Figure 6.4(a) reveals non-agglomerated, evenly distributed, spherical silver nanoparticles with a narrow distribution. In Figure 6.4 (b), the SAED pattern of the CPEAS-50 sample shows a variety of circular rings with spots, each of which corresponds to a different crystal plane such as to the (111), (200), (220), and (311) planes of the silver face centred cubic structure. Figure 6.2(c) displays a histogram of CPEAS-50 sample with an average particle size of roughly 12 nm. It is confirmed that the precipitated nanoparticles are crystalline by the well-organized and uniform lattice planes visible in HRTEM micrographs. Figure 6.4(d) displays one of these planes with d-spacing of 0.242 nm which is equal to the d_{111} spacing of the face-centered cubic (fcc) structure of silver nanoparticles (Mehtab, Zaidi, and Siddiqi 2018; Robinson et al. 2022).

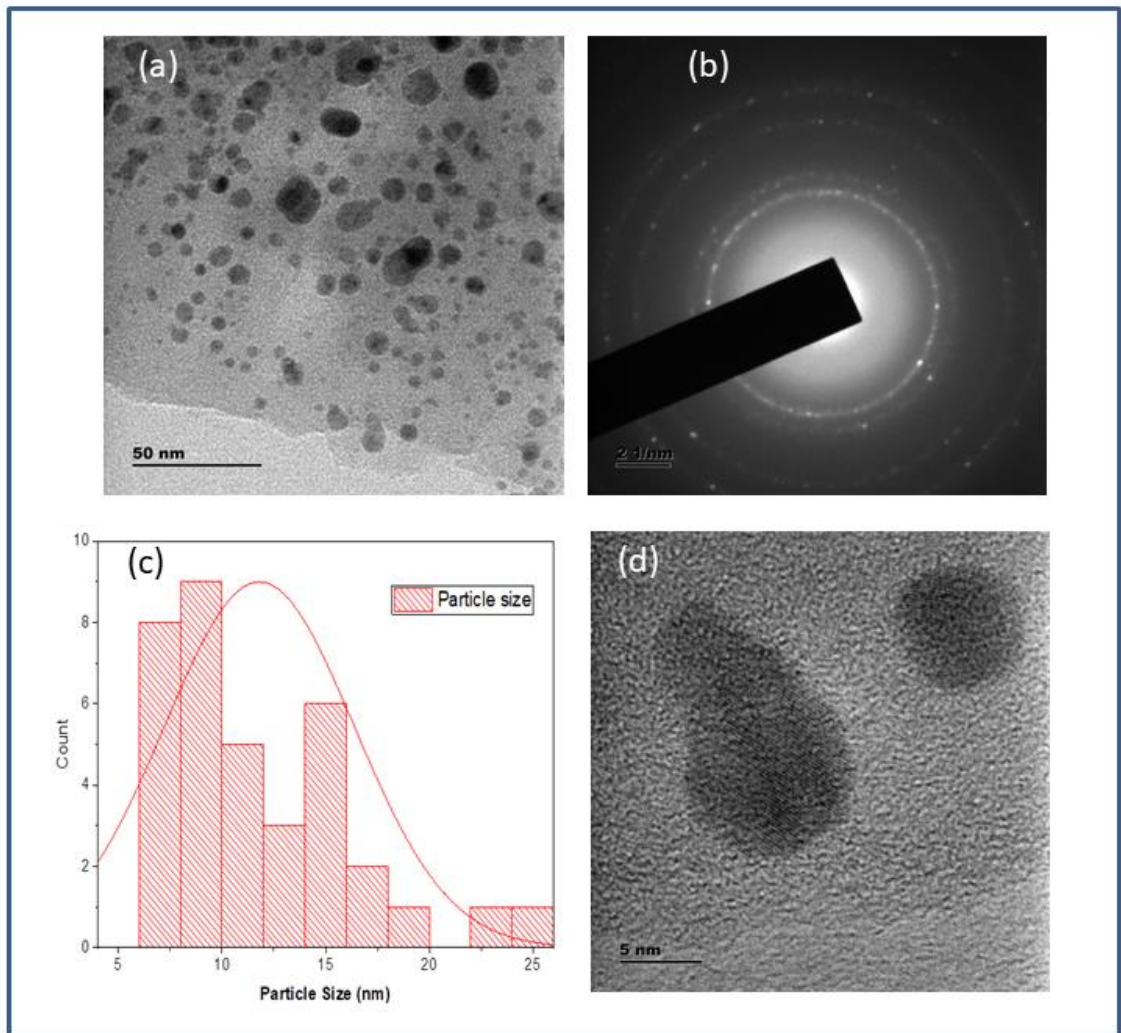


Figure 6.4 The CPEAS-50 (a) TEM micrograph (b) Different silver nanoparticle planes are shown in the SAED pattern (c) average particle distribution histogram (d) high crystallinity of the silver nanoparticles as shown by a magnified image.

6.2.4.3 Particle Size of CPEAS1 as a function of duration of heat treatment

Figure 6.5 Shows HRTEM images of glass samples CPEAS1-3, CPEAS1-10, and CPEAS1-50 and histogram of nanoparticle distribution of them. Average particle Size of CPEAS1 glass series heat treated at 3hr, 10hrs and 50hrs with the resolution of 20 nm estimated using imagej software and the values are 4.585nm, 5.428nm, and 9.762nm respectively. The particle size increased with the increase of heat treatment duration.

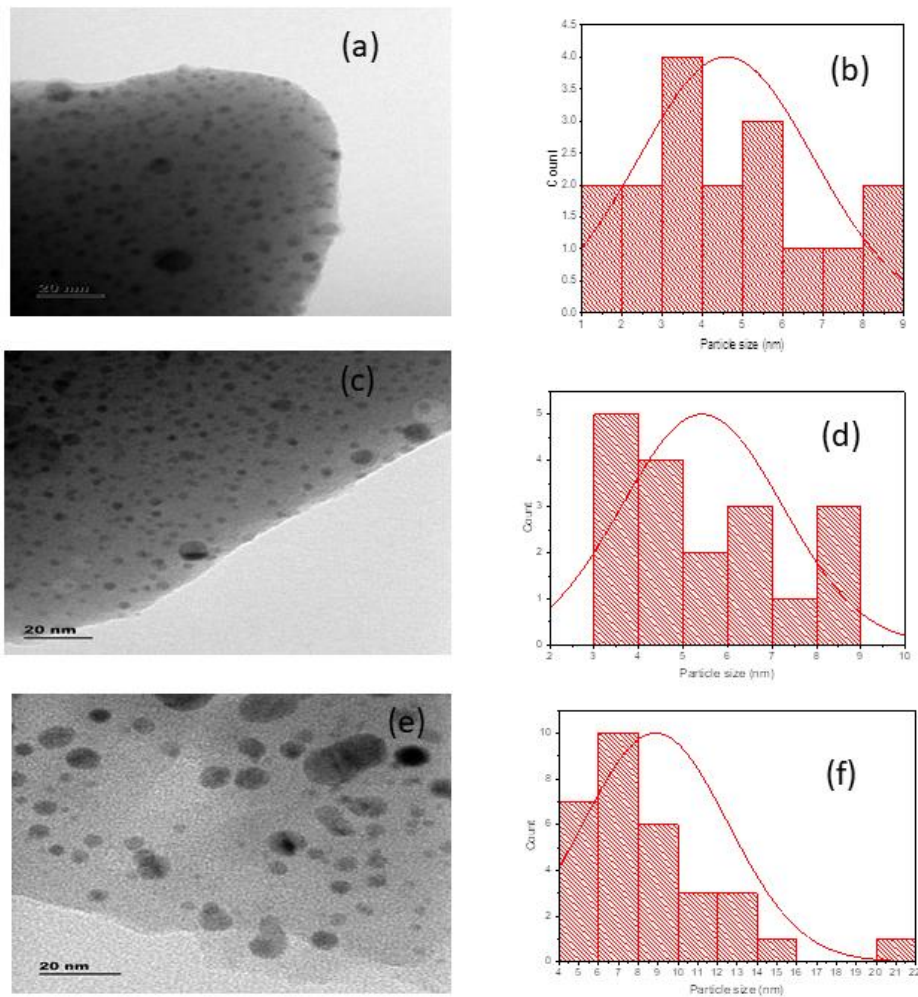


Figure 6.5 (a) HRTEM images of of CPEAS1-3 (b) Histogram of nano particle distribution of CPEAS1-3 (c) TEM image of CPEAS1-10, (d) Particle size distribution of nanoparticles in CPEAS1-10, (e) HRTEM image of CPEAS1-50, (f) shows the size distribution of nanoparticles, of CPEAS1-50 glass samples.

6.2.5 Photoluminescence (PL) studies CPEAS-Series

The photoluminescence record is taken for the CPEAS1 glass series with different excitation wavelength (λ_{ex} =280nm, 350nm, 370nm, 488nm). There are no emission peaks detected for different excitation wavelength used. Only the excitation wavelength of 280nm is recorded a prominent emission peaks.

Figure 6.6 depicts the photoluminescence spectra (PL) of heat treated CPEAS1 glass series under excitation wave length 280 nm.

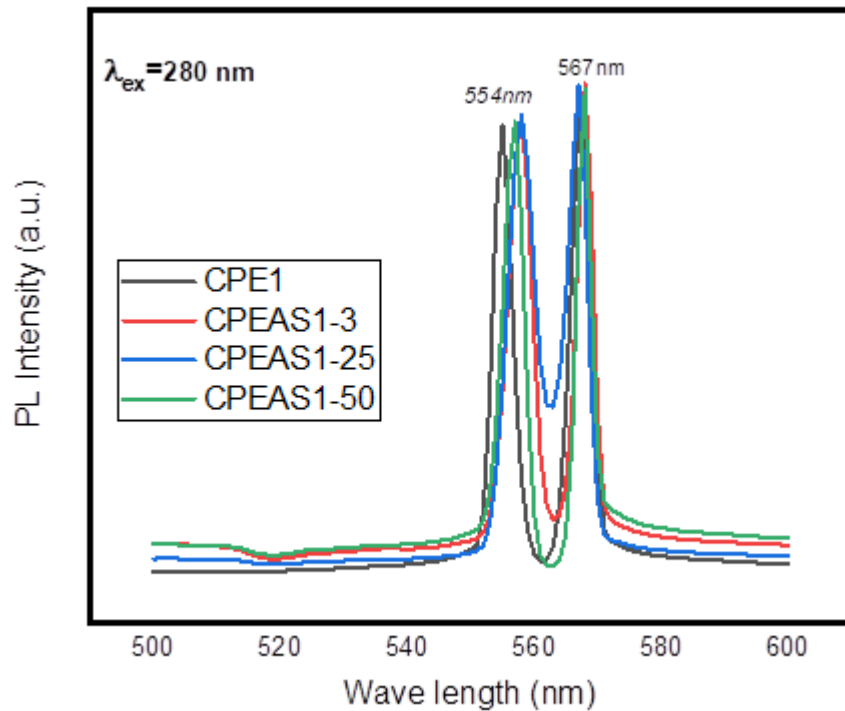


Figure 6.6 Photoluminescence (PL) spectra of the CPE1, CPEAS1-3, CPEAS1-25, and CPEAS1-50 glasses

It is demonstrated that the peak intensities around 545 and 565 nm have shown to be similar for CPE1, CPEAS1-3, CPEAS1-25, CPEAS-50 glass samples. The heat treatment duration did not affect the peak intensity. The literature reviews slightly supported the present results(Zaman et al. 2022)

CPASEu-Series

Strong luminescence in the red spectral region of the trivalent europium ion (Eu^{3+}) is widely recognized. Figure 6.7 shows the photoluminescence (PL) of $50\text{P}_2\text{O}_5 - 49\text{CaO}-1\text{Eu}_2\text{O}_3-4\text{Ag}_2\text{O}-4\text{SnO}$ (heat-treated at 0, 3, 10, 25, and 50hr) glasses in the wavelength range between 400 and 750 nm at an excitation wavelength of 397 nm recorded at room temperature. Five transitions were visible in each spectrum: 576 nm ($^5\text{D}_1 \rightarrow ^7\text{F}_2$), 590 nm ($^5\text{D}_0 \rightarrow ^7\text{F}_1$), 612 nm ($^5\text{D}_0 \rightarrow ^7\text{F}_2$), 652 nm ($^5\text{D}_0 \rightarrow ^7\text{F}_3$), and 699 nm ($^5\text{D}_0 \rightarrow ^7\text{F}_4$). As shown in Figure 6.8, the relatively integrated intensity of the emission band centered at 612 nm, which is more intense than the other transitions, has increased at 50 hours of heat treatment. At the same time, the peak with the maximum intensity was noticed at 612 nm (red) and was linked to the electric dipole transition

Eu³⁺ (Danmallam et al. 2019). These peaks can be explained to be existing due to the phonon energy splitting of europium ions (Danmallam et al. 2019).

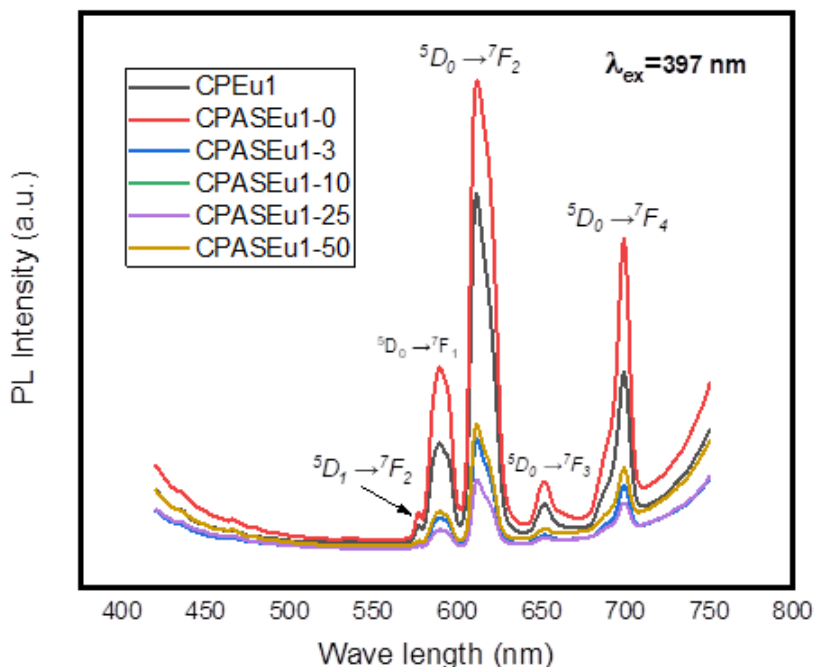


Figure 6.7 Photoluminescence (PL) spectra of the CPEu, CPASEu1-0, CPASEu1-3, CPASEu1-10, CPASEu1-25, and CPASEu1-50 glasses

The observed enhancement and quenching are caused by a rise in NP concentration brought on by heat treatment, which reduces the average distance between Ag-Ag NPs and, in turn, causes the local field to grow until it reaches saturation. The local field effect produced by the SPR of metallic NPs can be a factor in the change of fluorescence, and it can also be linked to fluorescence enhancement. Second, there is energy transfer between various active centers, particularly when annealing time increases (Saad et al. 2017). Applications for glasses doped with Eu³⁺ ions include light emitting diodes (LED), displays, and visible orange/red lasers (Chanthima et al. 2018).

6.3 Conclusion

Following an alternative synthesis path, silver nanoparticle embedded CPEAS and CPASEu glasses were developed utilising the common melt-quenching technique and subsequent heat treatment procedure. The amorphous nature of the generated as-quenched glass samples were confirmed using the X-ray diffraction method. The

production and development of silver nanoparticles had little impact on the glass matrix's metaphosphate chain structure, according to FTIR spectroscopy. The particle size measurements of rare earth-doped glasses containing silver oxide and tin oxide that underwent varying heat treatment times revealed that the production and development of nanoparticles were highly dependent on the length of the heat treatment. The existence of well-dispersed, non-agglomerated and crystalline silver nanoparticles in the heat-treated samples was confirmed by transmission electron microscopy (TEM) pictures and a selected area electron diffraction (SAED) pattern.

CHAPTER 7

SUMMARY AND CONCLUSIONS

The key findings and conclusions from the current research are outlined in this chapter. Additionally, the current chapter includes information on the scope of the future work.

7.1 Summary and conclusions

It can be summarised from the findings and discussions in Chapters 3, 4, 5, and 6 as follows.

Chapter 3 discusses addition of rare earth has a major impact on the physical, structural, and optical characteristics of binary metaphosphate glasses. Through the process of melt quenching method, rare earth (Er^{3+} , La^{3+} , and Ce^{4+}) ions were introduced to calcium phosphate glasses. Through the process of melt quenching, rare earth (Er^{3+} , La^{3+} , and Ce^{4+}) ions were introduced to calcium phosphate glasses. The effects of rare-earth doping on the structural, optical, and physical characteristics of calcium phosphate glass were examined. The FTIR analysis revealed that adding up to five mol. % of rare earth oxides (Lanthanum, Cerium, and Erbium) to the calcium phosphate glass had no effect on the network of primary phosphate crystals. The glasses continue to be amorphous after addition, according to XRD results. Because RE oxide has a larger molecular weight than the other oxides in the glass matrix and has a stronger cation field, the densities of the samples rose when CaO was replaced with La_2O_3 , CeO_2 , and Er_2O_3 . With more RE oxide content, the optical absorption edge moves to longer wavelengths and the optical band gap reduces. As the RE concentration increases, more non-bridging oxygens are created, improving the refractive indices. With the increase in ion concentration, the inter-nuclear distance decreased, increasing field strength.

Chapter 4 explains the effect of the rare earth (La^{3+} , Ce^{4+}) ions addition to $50\text{P}_2\text{O}_5 - (50-x) \text{CaO}-x\text{REI}$ glasses using the melt-quenching method, where $x=1$ to 3mole percent and RE stands for rare-earth ions. Utilizing X-ray Diffraction studies, the amorphous behaviour of the generated glasses was confirmed. The process

parameters of glass preparation using the melt quenching technique were optimised using the Taguchi approach of Design of Experiments (DOE) with orthogonal array (L_9). Investigations were done into how the process variables composition, melting temperature, and melting time affected the response parameter (density). The density S/N ratio is significantly impacted by the composition of rare-earth ions (Lanthanum, Cerium). It has been found that density increases along with the rare-earth ion content. DOE assisted in demonstrating that the only parameter that has a substantial impact on the various performance aspects is REI content, whereas melting temperature and melting time had no bearing.

Chapter 5 explains the successful synthesise of Rare earth (Er^{3+}) ions doped CPAS glass by melt quenching method. The results of the FTIR study showed that Erbium ions doped to the CPAS glass did not affect the basic structure of the phosphate glass network. The densities of samples increased by replacing the CaO with Er_2O_3 , which could be due to the larger molecular mass and cation field strength. With an increase in ion concentration, the internuclear distance decreased, leading to an increase in field strength. The values of the Metalicity factor (M_c) show that they are nearing unity rather than zero, implying the samples are more insulating. The optical band gap energy decreases as the Er_2O_3 content in the glass matrix increases, showing that the lattice characteristics have changed and that non-bridging –oxygens have formed. The prepared glass may be potentially used as a solid state laser host.

Chapter 6 discuss that the synthesis of glass by using Melt quenching with embedded silver nanoparticles (NPs) and rare earth (Er^{3+} , Eu^{3+}) ions that are doped calcium-phosphate. To convert silver ions (Ag^+) into silver nanoparticles (NPs) (Ago), heat treatment is used, with various time intervals above the glass transition temperature. To evaluate annealing time dependent structural and optical features, XRD, HRTEM, UV-Vis absorption spectroscopy, and photoluminescence (PL) spectroscopy are used. Subsequent heat treatment at various temperatures and time intervals resulted in the embedding of silver nanoparticles of various sizes. The optical characteristics of silver in various oxidation and aggregation states found in

the produced samples were examined using optical absorption and photoluminescence (PL) spectroscopy.

7.2 Future work's scope

The need to develop noble materials has driven materials engineers and scientists to seek out new materials with low cost, high efficiency, long durability, and recyclability. These applications range from decorative items, optoelectronic devices, and military facilities to medical interferences such as drug-deliverers, artificial bones, and sturdy dental ceramics. Due to the great variety in their structure and elemental makeup, glass and glass-ceramic technology is regarded as one of the most significant branches of materials research. This is because these composites can offer a variety of optical, chemical, thermal, electrical, and magnetic properties. The glasses are commonly utilised as optical materials because they typically exhibit non-linear optical absorption and extensive transparency in the ultraviolet (UV) to near-infrared (NIR) region, which might be combined with their other promising features to produce innovative materials. When the glasses are doped with rare earth (RE) ions, they can emit light in a variety of spectral ranges, including ultraviolet, visible, near-infrared, and far-infrared wavelengths. The host glass, RE ion concentration, co-doping species, heat treatments, and other engineering techniques can all be used to control the intensity, peak wavelength, excited state lifetime, and quantum efficiency of those emissions.

One of the novel approaches to improve the optical characteristics of rare earth doped oxide glasses is the use of metallic nanoparticles. The difficult problem of controlling the size and structure of metallic nanoparticles is one that significantly and ambiguously depending on the heat treatment's temperature, duration, and concentration. A possible approach to enhancing the optical characteristics of various oxide glasses for a variety of applications, including amplifiers, solid state lasers, sensors, etc., is the introduction of metallic nanoparticles. Further study is required to fully comprehend the function of metallic nanoparticles on rare earth ion doped glasses and manage their size distribution and structure, though.

- ✓ To examine the special qualities of synthesised glasses that contains integrated silver nanoparticles and other rare earth ions, such as their non-linear optical and dielectric properties.
- ✓ To develop glasses with various nanoparticle precursor concentrations and equivalent amounts of suitable reducing agents (tin oxide or antimony oxide), as well as to research the impact of various heat treatment temperatures and times on the size and distribution of silver nanoparticles. These efforts will aid in the development of glasses with improved properties.
- ✓ To develop rare earth ions and metal nanoparticles (copper and gold) embedded in glass matrix utilising a novel synthesis technique for laser applications.
- ✓ Apply Taguchi-based grey analysis to all systems of melt-quenched glasses in order to optimise various performance aspects.
- ✓ Effect of different heat treatment Temperature on structural, physical , optical, luminescence and surface Plasmon resonance properties for different applications
Metal nanoparticles /RE co-doped phosphate glasses
- ✓ Extending different rare earth ions as a dopant in Phosphate glasses for LED, energy storage, solar cell , telecommunication
- ✓ Mechanical and Thermal properties of RE and Metal nanoparticles doped oxide glasses
- ✓ Adding directly metal nanoparticles to the glasses doped REE and comparing that by heat treated/reduction method.

LISTS OF PUBLICATIONS, INTERNATIONAL CONFERENCES, AND WORKSHOP ATTENDED

i) List of Journal Publications:

1. **Dutebo, M. T.**, & Shashikala, H. D. (2020). Influence of (Er^{3+} , La^{3+} , Ce^{4+}) additions on physical and optical properties of $50\text{CaO}-50\text{P}_2\text{O}_5$ glasses. *Physica B: Condensed Matter*, 597, 412358.
2. Avinash Ishwer Ingle, H.D. Shashikala, Manoj Kumar Narayanan, **Dutebo, M.T.** , Shubham Gupta (2022). Optimization and analysis of process parameters of melt quenching technique for multiple performances of rare earth doped barium borate glass synthesis using Taguchi's design and grey relational approach. *Results in Engineering* Volume 17, 100784
3. Statistical optimization of melt-quenching process parameters of rare-earth ions doped calcium phosphate glasses using Taguchi method: *Materials today Proceeding*. (status: under review)

ii) Lists of International conferences

1. International conferences on "Variational Study Of Densities Of Phosphate Glasses using empirical relation from its composition" for the National Seminar on Ferroelectrics and Dielectrics (NSFD-2021)
2. International conference during January 15-17, 2020 titled "Current Trends in Functional Materials (CTFM-2020)" organized by Department of Physics, National Institute of Technology Karnataka, Surathkal, Mangalore – 575025, India
3. International Conference on Advanced on advanced Materials and Mechanical characterization (ICAMMC 2021) Dec 02-04, 2021
4. International Conference on Advances in Chemical and Materials Sciences ACMS-2022, April 14/2022-16/2022

iii) Workshop attended

1. Springer Nature Webinar_ Publishing Ethics: the role of publishers, journals, researchers and institutions _25th June'2020
2. MRL FACILITIES FREE WEBINAR SERIES: Optical Characterization Julio Soares - MRL – 07022020 Jul 2, 2020

BIBLIOGRAPHY

- Ahmadi, F., R. Hussin, and S. K. Ghoshal. 2018. 'On the Optical Properties of Er³⁺ Ions Activated Magnesium Zinc Sulfophosphate Glass: Role of Silver Nanoparticles Sensitization'. *Journal of Luminescence* 204:95–103. doi: 10.1016/j.jlumin.2018.07.033.
- Ahmed, E. M., M. I. Youssif, and A. A. Elzelaky. 2019a. 'Structural, Thermal and Photoemission Properties of Erbium Doped Phosphate Glass'. *Ceramics International* 45(18):24014–21. doi: 10.1016/j.ceramint.2019.08.104.
- Ahmed, E. M., M. I. Youssif, and A. A. Elzelaky. 2019b. 'Structural, Thermal and Photoemission Properties of Erbium Doped Phosphate Glass'. *Ceramics International* 45(18):24014–21. doi: 10.1016/j.ceramint.2019.08.104.
- Algradee, M. A., M. Sultan, O. M. Samir, and A. Elwhab B. Alwany. 2017. 'Electronic Polarizability, Optical Basicity and Interaction Parameter for Nd₂O₃ Doped Lithium–Zinc–Phosphate Glasses'. *Applied Physics A* 123(8):1–12.
- Alqarni, Areej S., R. Hussin, S. N. Alamri, and S. K. Ghoshal. 2020. 'Customized Physical and Structural Features of Phosphate-Based Glass-Ceramics: Role of Ag Nanoparticles and Ho³⁺ Impurities'. *Journal of Taibah University for Science* 14(1):954–62. doi: 10.1080/16583655.2020.1791536.
- Amjad, Raja J., M.R. Sahar, S. K. Ghoshal, M. R. Dousti, S. Riaz, and B. A. Tahir. 2012. 'Enhanced Infrared to Visible Upconversion Emission in Er³⁺ Doped Phosphate Glass: Role of Silver Nanoparticles'. *Journal of Luminescence* 132(10):2714–18. doi: 10.1016/j.jlumin.2012.05.008.
- Amjad, Raja J., M. R. Sahar, S. K. Ghoshal, M. R. Dousti, S. Riaz, and B. A. Tahir. 2012. 'Optical Investigation of Sm³⁺ Doped Zinc-Lead-Phosphate Glass'. *Chinese Physics Letters* 29(8):087304. doi: 10.1088/0256-307X/29/8/087304.
- Anigrahawati, Puzi, M. R. Sahar, Md Supar Rohani, and Sib Krishna Ghoshal. 2015a. 'Optical Absorption of Erbium Doped Zinc Phosphate Glass Containing Fe₃O₄ Nanoparticles'. *Advanced Materials Research* 1107:420–25. doi: 10.4028/www.scientific.net/AMR.1107.420.
- Anigrahawati, Puzi, M. R. Sahar, Md Supar Rohani, and Sib Krishna Ghoshal. 2015b. 'Optical Absorption of Erbium Doped Zinc Phosphate Glass Containing Fe₃O₄ Nanoparticles'. *Advanced Materials Research* 1107:420–25. doi: 10.4028/www.scientific.net/AMR.1107.420.
- Arifin, R., N. A. Zulkifeli, M. R. Sahar, and S. K. Ghoshal. 2015. 'ZnO Nanoparticles Concentration Dependent Optical Properties of Erbium Doped Phosphate Glass'. *Advanced Materials Research* 1107:471–76. doi: 10.4028/www.scientific.net/AMR.1107.471.

- Atwood, David A. 2013. *The Rare Earth Elements: Fundamentals and Applications*. John Wiley & Sons.
- A.V., Deepa, Priya Murugasen, P. Muralimanohar, and S. Praveen Kumar. 2018a. 'Optical Studies of Lanthanum Oxide Doped Phosphate Glasses'. *Optik* 160:348–52. doi: 10.1016/j.ijleo.2018.01.108.
- A.V., Deepa, Priya Murugasen, P. Muralimanohar, and S. Praveen Kumar. 2018b. 'Optical Studies of Lanthanum Oxide Doped Phosphate Glasses'. *Optik* 160:348–52. doi: 10.1016/j.ijleo.2018.01.108.
- A.V., Deepa, Priya Murugasen, P. Muralimanohar, K. Sathyamoorthy, and P. Vinothkumar. 2019a. 'A Comparison on the Structural and Optical Properties of Different Rare Earth Doped Phosphate Glasses'. *Optik* 181:361–67. doi: 10.1016/j.ijleo.2018.12.045.
- A.V., Deepa, Priya Murugasen, P. Muralimanohar, K. Sathyamoorthy, and P. Vinothkumar. 2019b. 'A Comparison on the Structural and Optical Properties of Different Rare Earth Doped Phosphate Glasses'. *Optik* 181:361–67. doi: 10.1016/j.ijleo.2018.12.045.
- Bhattacharya, Soumalya, and H. D. Shashikala. 2018. 'Optical and Structural Properties of BCBS Glass System with and without Alumina'. *Physica B: Condensed Matter* 548:10–19. doi: 10.1016/j.physb.2018.08.013.
- Brauer, Delia S. 2012. 'Phosphate Glasses'. *Bio-Glasses: An Introduction* 45–64.
- Brauer, Delia S., and Doris Möncke. 2016. 'Introduction to the Structure of Silicate, Phosphate and Borate Glasses'. *Bioactive Glasses* 61–88.
- Brow, Richard K. 2000. 'Review: The Structure of Simple Phosphate Glasses'. *Journal of Non-Crystalline Solids* 263–264:1–28. doi: 10.1016/S0022-3093(99)00620-1.
- Chanthima, Natthakridta, Yaowaluk Tariwong, Hong Joo Kim, Jakrapong Kaewkhao, and Narong Sangwaranatee. 2018. 'Effect of Eu³⁺ Ions on the Physical, Optical and Luminescence Properties of Aluminium Phosphate Glasses'. Pp. 122–26 in *Key Engineering Materials*. Vol. 766. Trans Tech Publ.
- Chimalawong, P., K. Kirdsiri, J. Kaewkhao, and P. Limsuwan. 2012. 'Investigation on the Physical and Optical Properties of Dy³⁺ Doped Soda-Lime-Silicate Glasses'. *Procedia Engineering* 32:690–98. doi: 10.1016/j.proeng.2012.01.1328.
- Chowdhury, Swarup, Pabitra Mandal, and Subhankar Ghosh. 2019. 'Structural Properties of Er³⁺ Doped Lead Zinc Phosphate Glasses'. *Materials Science and Engineering: B* 240:116–20. doi: 10.1016/j.mseb.2019.01.014.

- Cramer, Alisha J., Jacqueline M. Cole, Vicky FitzGerald, Veijo Honkimaki, Mark A. Roberts, Tessa Brennan, Richard A. Martin, George A. Saunders, and Robert J. Newport. 2013. 'Effects of Rare-Earth Co-Doping on the Local Structure of Rare-Earth Phosphate Glasses Using High and Low Energy X-Ray Diffraction'. *Physical Chemistry Chemical Physics* 15(22):8529. doi: 10.1039/c3cp44298e.
- Cullity, Bernard Dennis. 1956. *Elements of X-Ray Diffraction*. Addison-Wesley Publishing.
- Damas, Pedro, Joao Coelho, Graham Hungerford, and N. Sooraj Hussain. 2012. 'Structural Studies of Lithium Boro Tellurite Glasses Doped with Praseodymium and Samarium Oxides'. *Materials Research Bulletin* 47(11):3489–94.
- Danmallam, Ibrahim Mohammed, S. K. Ghoshal, R. Ariffin, Siti Aishah Jupri, and Sunita Sharma. 2019. 'Europium Ions and Silver Nanoparticles Co-Doped Magnesium-Zinc-Sulfophosphate Glasses: Evaluation of Ligand Field and Judd-Ofelt Parameters'. *Journal of Luminescence* 216:116713.
- Dimitrov, V., and T. Komatsu. 2010. 'An Interpretation of Optical Properties of Oxides and Oxide Glasses in Terms of the Electronic Ion Polarizability and Average Single Bond Strength'. *J. Univ. Chem. Technol. Metall* 45(3):219–50.
- Dousti, M. Reza, and Raja J. Amjad. 2016. 'Plasmon Assisted Luminescence in Rare Earth Doped Glasses'. Pp. 339–86 in *Reviews in Plasmonics 2015*. Vol. 2015, edited by C. D. Geddes. Cham: Springer International Publishing.
- Du, Jincheng, Monia Montorsi, Silvia Barbi, and Xiaonan Lu. 2022. 'Rare Earth and Transition Metal Containing Glasses'. *Atomistic Simulations of Glasses: Fundamentals and Applications* 367–438.
- Dutebo, Mathewos Tulore, and H. D. Shashikala. 2020. 'Influence of (Er³⁺, La³⁺, Ce⁴⁺) Additions on Physical and Optical Properties of 50CaO–50P₂O₅ Glasses'. *Physica B: Condensed Matter* 597:412358. doi: 10.1016/j.physb.2020.412358.
- Edathazhe, Akhila B., and H. D. Shashikala. 2018a. 'Optical Properties of BaO Added Bioactive Na₂O–CaO–P₂O₅ Glasses'. P. 020072 in. Karnataka, India.
- Edathazhe, Akhila B., and H. D. Shashikala. 2018b. 'Optical Properties of BaO Added Bioactive Na₂O–CaO–P₂O₅ Glasses'. P. 020072 in. Karnataka, India.
- Effendy, Nuraidayani, Zaidan Abdul Wahab, SidekHj. Abdul Aziz, Khamirul Amin Matori, Mohd Hafiz Mohd Zaid, and Siti Syuhaida Abdul Rashid. 2017. 'Characterization and Optical Properties of Erbium Oxide Doped ZnO–SLS Glass for Potential Optical and Optoelectronic Materials'. *Materials Express* 7(1):59–65. doi: 10.1166/mex.2017.1328.

- Elisa, M., S. M. Iordache, A. M. Iordache, I. C. Vasiliu, C. E. A. Grigorescu, B. A. Sava, L. Boroica, A. V. Filip, M. C. Dinca, and C. Bartha. 2021. 'Peculiarities of the Structural and Optical Properties of Rare-Earth-Doped Phosphate Glasses for Temperature Sensing Applications'. *Journal of Non-Crystalline Solids* 556:120569.
- Faznny, M. F., M. K. Halimah, and M. N. Azlan. 2016. 'Effect of Lanthanum Oxide on Optical Properties of Zinc Borotellurite Glass System'. *Journal of Optoelectronics and Biomedical Materials* 8(2):49–59.
- Gomes, J. F., A. M. O. Lima, M. Sandrini, A. N. Medina, A. Steimacher, F. Pedrochi, and M. J. Barboza. 2017. 'Optical and Spectroscopic Study of Erbium Doped Calcium Borotellurite Glasses'. *Optical Materials* 66:211–19. doi: 10.1016/j.optmat.2017.02.010.
- Herzfeld, K. F. 1927. 'On Atomic Properties Which Make an Element a Metal'. *Physical Review* 29(5):701–5. doi: 10.1103/PhysRev.29.701.
- Hoppe, Uwe. 1996. 'A Structural Model for Phosphate Glasses'. *Journal of Non-Crystalline Solids* 195(1–2):138–47. doi: 10.1016/0022-3093(95)00524-2.
- Hraiech, S., M. Ferid, Y. Guyot, and G. Boulon. 2013a. 'Structural and Optical Studies of Yb³⁺, Er³⁺ and Er³⁺/Yb³⁺ Co-Doped Phosphate Glasses'. *Journal of Rare Earths* 31(7):685–93. doi: 10.1016/S1002-0721(12)60343-3.
- Hraiech, S., M. Ferid, Y. Guyot, and G. Boulon. 2013b. 'Structural and Optical Studies of Yb³⁺, Er³⁺ and Er³⁺/Yb³⁺ Co-Doped Phosphate Glasses'. *Journal of Rare Earths* 31(7):685–93. doi: 10.1016/S1002-0721(12)60343-3.
- Hraiech, S., N. Sdiri, K. Horchani-Naifer, and M. Férid. 2018. 'Thermal and Optical Properties of Er³⁺ Doped Phosphate Glasses'. *Journal of Non-Crystalline Solids* 482:73–77. doi: 10.1016/j.jnoncrysol.2017.12.018.
- Hu, Yue Bo, Jian Bei Qiu, Qing Jiao, Zhi Guo Song, Da Cheng Zhou, Zheng Wen Yang, and Yong Yang. 2013. 'Noble Metals Enhanced Frequency Conversion Luminescence of Ln³⁺ Ions Doped Glasses'. *Advanced Materials Research* 815:171–78. doi: 10.4028/www.scientific.net/AMR.815.171.
- Huang, Wenhua, and Jinglong Jiang. 2022. 'Synthesis, Characterization and Optical Studies of Mixed Alkali Phosphate Glasses Containing MnO₂'. *Chinese Journal of Physics* 77:81–91.
- Im, Sang Hyeok, Young Hoon Na, Nam Jin Kim, Dong Hwan Kim, Cha Won Hwang, and Bong Ki Ryu. 2010. 'Structure and Properties of Zinc Bismuth Phosphate Glass'. *Thin Solid Films* 518(24):e46–49.
- Jiao, Qing, Xi Wang, Jianbei Qiu, and Dacheng Zhou. 2015. 'Effect of Silver Ions and Clusters on the Luminescence Properties of Eu-Doped Borate Glasses'.

Materials Research Bulletin 72:264–68. doi:
10.1016/j.materresbull.2015.08.012.

Jiménez, José A. 2016. ‘Absorption Spectroscopy Analysis of Calcium-Phosphate Glasses Highly Doped with Monovalent Copper’. *ChemPhysChem* 17(11):1642–46. doi: 10.1002/cphc.201600026.

Jiménez, José A., Sergiy Lysenko, Huimin Liu, and Mariana Sendova. 2011. ‘Luminescence of Trivalent Samarium Ions in Silver and Tin Co-Doped Aluminophosphate Glass’. *Optical Materials* 33(8):1215–20. doi: 10.1016/j.optmat.2011.02.013.

Jiménez, José A., and Mariana Sendova. 2014. ‘Enhanced 1.53 μ m Emission of Er³⁺ Ions in Phosphate Glass via Energy Transfer from Cu⁺ Ions’. *Journal of Applied Physics* 116(3):033518. doi: 10.1063/1.4890716.

Kabi, S., and A. Ghosh. 2012. ‘Structural Investigation on Silver Phosphate Glasses Embedded with Nanoparticles’. *Journal of Alloys and Compounds* 520:238–43.

Kakiuchida, Hiroshi, Kazuya Saito, and Akira J. Ikushima. 2004. ‘Refractive Index, Density and Polarizability of Silica Glass with Various Fictive Temperatures’. *Japanese Journal of Applied Physics* 43(No. 6A):L743–45. doi: 10.1143/JJAP.43.L743.

Karmakar, Basudeb, Tirtha Som, Shiv Prakash Singh, and Mithun Nath. 2010. ‘Nanometal-Glass Hybrid Nanocomposites: Synthesis, Properties and Applications’. *Transactions of the Indian Ceramic Society* 69(3):171–86. doi: 10.1080/0371750X.2010.11090834.

Kohli, Jeffrey T., Mathieu Hubert, Randall E. Youngman, and David L. Morse. 2022. ‘A Corning Perspective on the Future of Technical Glass in Our Evolving World’. *International Journal of Applied Glass Science* 13(3):292–307. doi: 10.1111/ijag.16560.

Kreibig, Uwe, and Michael Vollmer. 2010. *Optical Properties of Metal Clusters*. Berlin: Springer.

Kuwik, Marta, Joanna Pisarska, and Wojciech A. Pisarski. 2020. ‘Influence of Oxide Glass Modifiers on the Structural and Spectroscopic Properties of Phosphate Glasses for Visible and Near-Infrared Photonic Applications’. *Materials* 13(21):4746. doi: 10.3390/ma13214746.

Li, Haijian, Xiaofeng Liang, Cuiling Wang, Huijun Yu, Zhen Li, and Shiyuan Yang. 2014. ‘Influence of Rare Earth Addition on the Thermal and Structural Stability of CaOFe₂O₃P₂O₅ Glasses’. *Journal of Molecular Structure* 1076:592–99.

- Li, Haijian, Jianhua Yi, Zhao Qin, Zhihua Sun, Yi Xu, Changjian Wang, Fengqi Zhao, Yucheng Hao, and Xiaofeng Liang. 2019a. 'Structures, Thermal Expansion, Chemical Stability and Crystallization Behavior of Phosphate-Based Glasses by Influence of Rare Earth'. *Journal of Non-Crystalline Solids* 522:119602. doi: 10.1016/j.jnoncrysol.2019.119602.
- Li, Haijian, Jianhua Yi, Zhao Qin, Zhihua Sun, Yi Xu, Changjian Wang, Fengqi Zhao, Yucheng Hao, and Xiaofeng Liang. 2019b. 'Structures, Thermal Expansion, Chemical Stability and Crystallization Behavior of Phosphate-Based Glasses by Influence of Rare Earth'. *Journal of Non-Crystalline Solids* 522:119602. doi: 10.1016/j.jnoncrysol.2019.119602.
- Liang, Xiaofeng, Haijian Li, Cuiling Wang, Huijun Yu, Zhen Li, and Shiyuan Yang. 2014. 'Physical and Structural Properties of Calcium Iron Phosphate Glass Doped with Rare Earth'. *Journal of Non-Crystalline Solids* 402:135–40. doi: 10.1016/j.jnoncrysol.2014.05.021.
- Liang, Xiaofeng, Guangfu Yin, Shiyuan Yang, Yuanming Lai, and Junxia Wang. 2011. 'Lanthanum Oxide Effects on the Structure of Calcium Phosphate Glasses'. *Spectroscopy Letters* 44(6):418–23. doi: 10.1080/00387010.2011.574183.
- Liu, Hongting, Yadong Lu, Ya Qu, Hao Lu, and Yunlong Yue. 2016a. 'Effect of the Content of Al₂O₃ on Structure and Properties of Calcium-Phosphate Glasses: Two Experimental Case Studies'. *Journal of Non-Crystalline Solids* 450:95–102. doi: 10.1016/j.jnoncrysol.2016.07.043.
- Liu, Hongting, Yadong Lu, Ya Qu, Hao Lu, and Yunlong Yue. 2016b. 'Effect of the Content of Al₂O₃ on Structure and Properties of Calcium-Phosphate Glasses: Two Experimental Case Studies'. *Journal of Non-Crystalline Solids* 450:95–102. doi: 10.1016/j.jnoncrysol.2016.07.043.
- Lysenko, S., J. Jimenez, G. Zhang, and H. Liu. 2006. 'Nonlinear Optical Dynamics of Glass-Embedded Silver Nanoparticles'. *Journal of Electronic Materials* 35(9):1715–21. doi: 10.1007/s11664-006-0224-8.
- Macioszczyk, Jan, Karol Malecha, Andrzej Stafiniak, and Leszek J. Golonka. 2015. 'Impact of Processing Parameters on the LTCC Channels Geometry'. *Materials Science-Poland* 33(4):816–25.
- Mahraz, Zahra Ashur Said, M. R. Sahar, S. K. Ghoshal, and M. Reza Dousti. 2013. 'Concentration Dependent Luminescence Quenching of Er³⁺-Doped Zinc Boro-Tellurite Glass'. *Journal of Luminescence* 144:139–45.
- Mallur, Saisudha B., Tyler Czarnecki, Ashish Adhikari, and Panakkattu K. Babu. 2015. 'Compositional Dependence of Optical Band Gap and Refractive Index in Lead and Bismuth Borate Glasses'. *Materials Research Bulletin* 68:27–34.

- Mandal, Nilrudra, B. Doloi, B. Mondal, and Reeta Das. 2011. 'Optimization of Flank Wear Using Zirconia Toughened Alumina (ZTA) Cutting Tool: Taguchi Method and Regression Analysis'. *Measurement* 44(10):2149–55. doi: 10.1016/j.measurement.2011.07.022.
- Mariselvam, K., R. Arun Kumar, and V. Rajeswara Rao. 2019. 'Concentration-Dependence and Luminescence Studies of Erbium Doped Barium Lithium Fluoroborate Glasses'. *Optics & Laser Technology* 118:37–43.
- Mehtab, Sameena, M. G. H. Zaidi, and Tanveer Irshad Siddiqi. 2018. 'Designing Fructose Stabilized Silver Nanoparticles for Mercury (II) Detection and Potential Antibacterial Agents'. *Mater. Sci. Res. India* 15:241–49.
- Mohan, N. S., A. Ramachandra, and S. M. Kulkarni. 2005. 'Influence of Process Parameters on Cutting Force and Torque during Drilling of Glass–Fiber Polyester Reinforced Composites'. *Composite Structures* 71(3–4):407–13. doi: 10.1016/j.compstruct.2005.09.039.
- Montgomery, Douglas C. 2017. *Design and Analysis of Experiments*. John Wiley & Sons.
- Morse, David L., and Jeffrey W. Evenson. 2016. 'Welcome to the Glass Age'. *International Journal of Applied Glass Science* 7(4):409–12. doi: 10.1111/ijag.12242.
- Mountjoy, Gavin. 2022. 'Phosphate Glasses'. *Atomistic Simulations of Glasses: Fundamentals and Applications* 295–346.
- Mrabet, Hounaida, Mohamed Atef Cherbib, and Ismail Khattech. 2020. 'Barium Polyphosphate Glasses, from Structure to Thermochemistry'. *Materials Chemistry and Physics* 239:122087. doi: 10.1016/j.matchemphys.2019.122087.
- Murugasen, PRIYA, SURESH Sagadevan, and DEEPA Shajan. 2015. 'Preparation, Techniques and Tools Used for Investigating Glasses: An Overview'. *Int. J. Chem. Sci* 13:695.
- Narayanan, Manoj Kumar, and H. D. Shashikala. 2014. 'Optimization of Melt-Quenching Process Parameters for Refractive Index of Barium Phosphate Glasses Using Taguchi Method'. *Procedia Materials Science* 5:303–10. doi: 10.1016/j.mspro.2014.07.271.
- Narayanan, Manoj Kumar, and H. D. Shashikala. 2015a. 'Physical, Mechanical and Structural Properties of BaO–CaF₂–P₂O₅ Glasses'. *Journal of Non-Crystalline Solids* 430:79–86. doi: 10.1016/j.jnoncrysol.2015.10.006.
- Narayanan, Manoj Kumar, and H. D. Shashikala. 2015b. 'Physical, Mechanical and Structural Properties of BaO–CaF₂–P₂O₅ Glasses'. *Journal of Non-Crystalline Solids* 430:79–86. doi: 10.1016/j.jnoncrysol.2015.10.006.

- Narayanan, Manoj Kumar, and H. D. Shashikala. 2015c. 'Physical, Mechanical and Structural Properties of BaO–CaF₂–P₂O₅ Glasses'. *Journal of Non-Crystalline Solids* 430:79–86. doi: 10.1016/j.jnoncrysol.2015.10.006.
- Narayanan, Manoj Kumar, H. D. Shashikala, and M. Manjaiah. 2015. 'Statistical Optimization of Melt-Quenching Process Parameters for Multiple Properties of Ternary Barium Phosphate Glasses'. *Materials Chemistry and Physics* 152:127–34. doi: 10.1016/j.matchemphys.2014.12.024.
- Othman, H. A., G. M. Arzumanyan, and D. Möncke. 2016. 'The Influence of Different Alkaline Earth Oxides on the Structural and Optical Properties of Undoped, Ce-Doped, Sm-Doped, and Sm/Ce Co-Doped Lithium Alumino-Phosphate Glasses'. *Optical Materials* 62:689–96. doi: 10.1016/j.optmat.2016.10.051.
- Parsons, Andrew James. 2021. 'Phosphate Glasses'. Pp. 901–17 in *Encyclopedia of Glass Science, Technology, History, and Culture*, edited by P. Richet, R. Conradt, A. Takada, and J. Dyon. Wiley.
- Presti, Davide, Francesco Muniz-Miranda, Francesco Tavanti, and Alfonso Pedone. 2022. 'Structure Analysis and Properties Calculations'. *Atomistic Simulations of Glasses: Fundamentals and Applications* 89–122.
- Pugliese, Diego, Nadia G. Boetti, Joris Lousteau, Edoardo Ceci-Ginistrelli, Elisa Bertone, Francesco Geobaldo, and Daniel Milanese. 2016. 'Concentration Quenching in an Er-Doped Phosphate Glass for Compact Optical Lasers and Amplifiers'. *Journal of Alloys and Compounds* 657:678–83. doi: 10.1016/j.jallcom.2015.10.126.
- Qian, Bin, Xiaofeng Liang, Shiyuan Yang, Shu He, and Long Gao. 2012a. 'Effects of Lanthanum Addition on the Structure and Properties of Iron Phosphate Glasses'. *Journal of Molecular Structure* 1027:31–35. doi: 10.1016/j.molstruc.2012.05.078.
- Qian, Bin, Xiaofeng Liang, Shiyuan Yang, Shu He, and Long Gao. 2012b. 'Effects of Lanthanum Addition on the Structure and Properties of Iron Phosphate Glasses'. *Journal of Molecular Structure* 1027:31–35. doi: 10.1016/j.molstruc.2012.05.078.
- Qian, Bin, Shiyuan Yang, Xiaofeng Liang, Yuanming Lai, Long Gao, and Guangfu Yin. 2012. 'Structural and Thermal Properties of La₂O₃Fe₂O₃P₂O₅ Glasses'. *Journal of Molecular Structure* 1011:153–57.
- Rai, V. N., B. N. Raja Sekhar, P. Tiwari, R. J. Kshirsagar, and S. K. Deb. 2011. 'Spectroscopic Studies of Gamma Irradiated Nd Doped Phosphate Glasses'. *Journal of Non-Crystalline Solids* 357(22–23):3757–64. doi: 10.1016/j.jnoncrysol.2011.07.036.

- Rao, G. Venkateswara, and H. D. Shashikala. 2014a. 'Optical, Dielectric and Mechanical Properties of Silver Nanoparticle Embedded Calcium Phosphate Glass'. *Journal of Non-Crystalline Solids* 402:204–9. doi: 10.1016/j.jnoncrysol.2014.06.007.
- Rao, G. Venkateswara, and H. D. Shashikala. 2014b. 'Optical, Dielectric and Mechanical Properties of Silver Nanoparticle Embedded Calcium Phosphate Glass'. *Journal of Non-Crystalline Solids* 402:204–9. doi: 10.1016/j.jnoncrysol.2014.06.007.
- Reddy, A. Amarnath, S. Surendra Babu, K. Pradeesh, C. J. Otton, and G. Vijaya Prakash. 2011. 'Optical Properties of Highly Er³⁺-Doped Sodium–Aluminium–Phosphate Glasses for Broadband 1.5 μ m Emission'. *Journal of Alloys and Compounds* 509(9):4047–52. doi: 10.1016/j.jallcom.2011.01.016.
- Reddy, R. R., Y. Nazeer Ahammed, P. Abdul Azeem, K. Rama Gopal, and T. V. R. Rao. 2001. 'Electronic Polarizability and Optical Basicity Properties of Oxide Glasses through Average Electronegativity'. *Journal of Non-Crystalline Solids* 286(3):169–80. doi: 10.1016/S0022-3093(01)00481-1.
- Righini, Giancarlo C., and Maurizio Ferrari. 2005. 'Photoluminescence of Rare-Earth—Doped Glasses'. *La Rivista Del Nuovo Cimento* 28(12):1–53.
- Robinson, Richard, Virginia Krause, Shan Wang, Shan Yan, Guojun Shang, Justine Gordon, Serena Tycko, and Chuan-Jian Zhong. 2022. 'Silver–Copper Alloy Nanoinks for Ambient Temperature Sintering'. *Langmuir*.
- Saad, Moufida, Wissal Stambouli, Shaimaa A. Mohamed, and Habib Elhouichet. 2017. 'Ag Nanoparticles Induced Luminescence Enhancement of Eu³⁺ Doped Phosphate Glasses'. *Journal of Alloys and Compounds* 705:550–58.
- Saddeek, Yasser B., A. A. El-Maaref, K. A. Aly, M. M. ElOkr, and A. A. showahy. 2017. 'Investigations on Spectroscopic and Elasticity Studies of Nd₂O₃ Doped CANP Phosphate Glasses'. *Journal of Alloys and Compounds* 694:325–32. doi: 10.1016/j.jallcom.2016.09.272.
- Saddeek, Yasser B., A. A. El-Maaref, M. G. Moustafa, M. M. El-Okr, and A. A. Showahy. 2018. 'A Comprehensive Study of Electrical and Optical Properties of Phosphate Oxide-Based Glasses Doped with Er₂O₃'. *Journal of Materials Science: Materials in Electronics* 29(12):9994–10007. doi: 10.1007/s10854-018-9043-y.
- Shakhgildyan, Georgiy, Veniamin Durymanov, Mariam Ziyatdinova, Grigoriy Atroshchenko, Nikita Golubev, Alexey Trifonov, Olga Chereuta, Leon Avakyan, Lusegen Bugaev, and Vladimir Sigaev. 2022. 'Effect of Gold Nanoparticles on the Crystallization and Optical Properties of Glass in ZnO–MgO–Al₂O₃–SiO₂ System'. *Crystals* 12(2):287.

- Shelby, James E. 2000. 'Properties of Alkali–Alkaline Earth Metaphosphate Glasses'. *Journal of Non-Crystalline Solids* 263–264:271–76. doi: 10.1016/S0022-3093(99)00639-0.
- Shelby, James E. 2007. *Introduction to Glass Science and Technology*. 2nd ed. Royal Society of Chemistry.
- Shelby, James E. 2020. *Introduction to Glass Science and Technology*. Royal society of chemistry.
- Shi, Qingshun, Yunlong Yue, Ya Qu, Shiquan Liu, G. A. Khater, Lulu Zhang, Jiling Zhao, and Junfeng Kang. 2019. 'Structure and Chemical Durability of Calcium Iron Phosphate Glasses Doped with La₂O₃ and CeO₂'. *Journal of Non-Crystalline Solids* 516:50–55. doi: 10.1016/j.jnoncrysol.2019.04.029.
- Soltani, I., S. Hraiech, K. Horchani-Naifer, H. Elhouichet, B. Gelloz, and M. Férid. 2016. 'Growth of Silver Nanoparticles Stimulate Spectroscopic Properties of Er³⁺ Doped Phosphate Glasses: Heat Treatment Effect'. *Journal of Alloys and Compounds* 686:556–63. doi: 10.1016/j.jallcom.2016.06.027.
- Soltani, I., S. Hraiech, K. Horchani-Naifer, J. Massera, L. Petit, and M. Férid. 2016. 'Thermal, Structural and Optical Properties of Er³⁺ Doped Phosphate Glasses Containing Silver Nanoparticles'. *Journal of Non-Crystalline Solids* 438:67–73. doi: 10.1016/j.jnoncrysol.2015.12.022.
- Tauc, J., and A. Menth. 1972. 'States in the Gap'. *Journal of Non-Crystalline Solids* 8–10:569–85. doi: 10.1016/0022-3093(72)90194-9.
- Taylor, John. 1997. *Introduction to Error Analysis, the Study of Uncertainties in Physical Measurements*.
- Uchida, K., S. Kaneko, S. Omi, C. Hata, H. Tanji, Y. Asahara, A. J. Ikushima, T. Tokizaki, and A. Nakamura. 1994. 'Optical Nonlinearities of a High Concentration of Small Metal Particles Dispersed in Glass: Copper and Silver Particles'. *Journal of the Optical Society of America B* 11(7):1236. doi: 10.1364/JOSAB.11.001236.
- Varshneya, Arun K. 2013. *Fundamentals of Inorganic Glasses*. Elsevier.
- Varshneya, Arun K., and John C. Mauro. 2019a. 'Density and Molar Volume'. Pp. 173–86 in *Fundamentals of Inorganic Glasses*. Elsevier.
- Varshneya, Arun K., and John C. Mauro. 2019b. 'Emerging Applications of Glass'. Pp. 687–701 in *Fundamentals of Inorganic Glasses*. Elsevier.
- Varshneya, Arun K., and John C. Mauro. 2019c. 'Glass Transition Range Behavior'. Pp. 293–382 in *Fundamentals of Inorganic Glasses*. Elsevier.

- Varshneya, Arun K., and John C. Mauro. 2019d. 'Introduction'. Pp. 1–18 in *Fundamentals of Inorganic Glasses*. Elsevier.
- Velli, L. L., Cristos-Platon E. Varsamis, E. I. Kamitsos, D. Möncke, and D. Ehrh. 2005. 'Structural Investigation of Metaphosphate Glasses'. *Physics and Chemistry of Glasses* 46(2):178–81.
- Venkateswara Rao, G., and H. D. Shashikala. 2014a. 'Optical and Mechanical Properties of Calcium Phosphate Glasses'. *Glass Physics and Chemistry* 40(3):303–9. doi: 10.1134/S1087659614030249.
- Venkateswara Rao, G., and H. D. Shashikala. 2014b. 'Optical and Mechanical Properties of Calcium Phosphate Glasses'. *Glass Physics and Chemistry* 40(3):303–9. doi: 10.1134/S1087659614030249.
- Venkateswara Rao, G., and H. D. Shashikala. 2014c. 'Structural, Optical and Mechanical Properties of Ternary CaO-CaF₂-P₂O₅ Glasses'. *Journal of Advanced Ceramics* 3(2):109–16. doi: 10.1007/s40145-014-0099-8.
- Venkateswara Rao, G., and H. D. Shashikala. 2015. 'Effect of Heat Treatment on Optical, Dielectric and Mechanical Properties of Silver Nanoparticle Embedded CaOCaF₂P₂O₅ Glass'. *Journal of Alloys and Compounds* 622:108–14. doi: 10.1016/j.jallcom.2014.09.156.
- Wen, Hongli, Shengjie Xie, Jiangtao Cui, Sile Mao, Li Luo, and Mikhail G. Brik. 2019. 'Optical Properties of 3d Transition Metal Ion-Doped Aluminophosphate Glasses'. *Journal of Luminescence* 213:263–72. doi: 10.1016/j.jlumin.2019.05.016.
- Yamane, Masayuki, and Yoshiyuki Asahara. 2000. *Glasses for Photonics*. Cambridge University Press.
- Zachariasen, W. H. 1932. 'THE ATOMIC ARRANGEMENT IN GLASS'. *Journal of the American Chemical Society* 54(10):3841–51. doi: 10.1021/ja01349a006.
- Zaman, F., G. Rooh, N. Chanthima, S. U. Khan, H. J. Kim, S. Kothan, N. Chanlek, M. Arshad, and J. Kaewkhao. 2022. 'Investigation of Spectroscopic and Photoluminescence Properties of Erbium Doped Phosphate (P₂O₅-K₂O₃-Al₂O₃) Glasses'. *Journal of Alloys and Compounds* 893:162215.
- Zanotto, Edgar D., and John C. Mauro. 2017a. 'The Glassy State of Matter: Its Definition and Ultimate Fate'. *Journal of Non-Crystalline Solids* 471:490–95. doi: 10.1016/j.jnoncrysol.2017.05.019.
- Zanotto, Edgar D., and John C. Mauro. 2017b. 'The Glassy State of Matter: Its Definition and Ultimate Fate'. *Journal of Non-Crystalline Solids* 471:490–95. doi: 10.1016/j.jnoncrysol.2017.05.019.

CURRICULUM VITAE (CV)



Name: **MATHEWOS TULORE DUTEBO**

HOSSANA, SNNPR, Ethiopia

Phone: +251-911855258/ P.O.Box: 667

E-mail: mathewostulore47@gmail.com

1) **PERSONAL PROFILE**

Date of Birth: February 02, 1984

Place of Birth: HOSSANA, SNNPR, ETHIOPIA

Nationality: Ethiopian

Marital Status: Married to Lydia Mathewos

2) **EDUCATIONAL DETAILS**

PhD Courses Completed: 8.33/10

Master of Science (in Physics) : with 1st Class (89%)

Addis Ababa University, P.O.Box, 1176, Addis Ababa, Ethiopia

Bachelor of Science (PHYSICS (Major) and Mathematics (Minor))

with 1st Class(77.5%)

Haramaya University (P.O.Box 138, Dire Dawa, Ethiopia)

High school: with First Class (90%)

Gimbichu Senior secondary School from grade 9-12, Gimbichu, Hossana/Ethiopia)

3) **REFERENCES**

Habtamu Abebe Agisho (Ph.D)

(Associate professor and president in charge of Wachemo University)

P.O. Box: 667 Mobile: +2519

Fax: +251 46 555 1930

Email: habtamuabebe83@gmail.com